PARAMETRIC STUDY OF STRESSES IN COOLING-TOWER SHELLS

AJAYI OLUGBENGA OLUMIDE

December 2002

Submitted to the Faculty of Engineering and Built Environment of the University of Cape Town in partial fulfillment of the requirements for the degree of Masters of Science in Civil Engineering.

Department of Civil Engineering
University of Cape Town
Private Bag, Rondebosch, 7700, South Africa.

DECLARATION

I Ajayi Olugbenga Olumide, hereby declare that this dissertation is my own, unaided work. It is being submitted for the degree of Masters of Science in Engineering in the University of Cape Town. It has not been submitted for any degree or examination in any other university.

Signed by candidate

Ajayi O.O.A

Dated this 2nd day of December 2002.

ACKNOWLEDGEMENTS

I wish to express my thanks to the following people for their valuable contributions:

Prof. A. Zingoni, my supervisor, for all his advice, assistance and constant encouragement during the formulation of this thesis.

Mrs Sheryldene Ajayi, my wife, for her moral support and patience throughout my years of studies. This work is dedicated to you and our son Akin.

Mr Victor Balden of CERECAM for his advice regarding finite element modelling problems.

Retired Wing Commander and Mrs. Ajayi, my parents, for their constant encouragement, discipline and morals they taught me, which I am grateful.

Members of the Department of Civil Engineering for their friendship during my Masters programme.

Mrs Pat Dykin and Regine Heuschneider for proofreading my thesis.

In entirety, my Lord and Saviour, Jesus Christ, for what my life has become.

ABSTRACT

Many attempts have been made in studying the structural behaviour of cooling tower shells, focusing more on the effect of wind on the structure and shape imperfections. However, little has been investigated on the most basic loading condition, i.e. self-weight load.

This thesis focuses on a cooling tower with uniform thickness where several geometric parameters like the hyperbolic axis ratio (b/a), top opening angle (ϕ_0), offset parameters (A), and scale of the structure are varied one at a time, to investigate the effect these parameters have on the meridional and hoop stresses.

A general-purpose finite element programme, ABAQUS, was used to create models of the cooling tower structure. The model results were verified using closed-form analytical membrane solutions as reported by Zingoni[41]. The model considers constraining the base against rotation in all directions while the top is made to be free.

The predicted numeric meridional and hoop stresses compare favourably well with the closed-form analytical results, except at the critically stressed zone near the base that exhibits some bending disturbances.

Parametric investigation shows that an increase in the hyperbolic axis ratio, the top opening angle, and offset parameters also increases meridional and hoop stresses.

It is concluded that lower b/a, ϕ_0, and zero offset parameters be adopted for preliminary design purposes. Finally, recommendations are made on the need for further investigations.

TABLES OF CONTENTS

LIST OF FIGURES

LIST OF TABLES

Tables **Pages**

CHAPTER ONE

INTRODUCTION

1.1 HISTORICAL BACKGROUND

Shells, as the name implies, occur in nature in different forms. Egg shells, shells of nuts, plants and leaves of various types, snails, many insect forms – all represent nature's attempt at efficient use of materials, possibly because of the relatively few factors affecting the growth of a given plant or species. The natural forms of shells have been known to man from time immemorial and must have influenced his design choices, even if not consciously.

Man has built shell-like structures since antiquity, when the curved form of Roman architecture was extended into three dimensions. The materials used were masonry and concrete, probably developed from the "pise" system of construction through the addition of the "wonderful dusky-red pozolana" natural cement[1]. The shell form used by the Romans was the hemispherical dome, as in the roof of the Pantheon completed in the middle of the second century, or the semi-circular barrel vault, as used in the roofs of the Termea[1]. While the Roman examples of domes and vaults do not constitute thin shells in the modern sense, they certainly represent a tremendous engineering achievement when considered in the context of the day. Notable examples of the domed roof are the church of St. Sophia built in Istanbul in the first half of the sixth century and later converted into a mosque, the Church of San Vitale in Ravenna, noted for its use of pottery as the material for the shell, the Baroque dome of St. Peter's designed by Michaelangelo and built in 1590, St. Paul's Cathedral in London designed by Sir Christopher Wren in 1710, and the Taj Mahal built in the seventeenth century.[1]

Broadly speaking, shells built until the 1900's share a common trend: the methods of construction remained essentially static through the ages. Further progress could not be achieved without basic improvement in the technology of construction, in the quality of construction materials, and in the understanding of the laws of mechanics.

Following the discovery of cement and its application in obtaining concrete, a new material was created by the addition of steel, namely reinforced concrete. Unlike the Roman masonry

of the past, reinforced concrete was capable of transferring tensions and was mouldable into any desired shape. The development of prestressing in the twentieth century brought additional relief to the designers. The volume of reinforced-concrete construction grew rapidly following the discovery of an effective process for the manufacture of iron and steel. In the second half of the nineteenth century, structural mechanics reached maturity. The theory of arches was worked out by Bresce in 1859. Kirchhoff's re-examination of the Lagrangian plate theory dates back to 1849, while the first theory of shells was proposed by Aron in 1874. The oldest form of shells is probably a cylindrical barrel vault which was developed from Roman architecture. In modern days, the shape of the cylindrical vaults remains the same, but some new variations have been added, i.e. the profiles are not only circular, but parabolic and elliptic. The first modern shell, designed and built with the knowledge of structural mechanics, was the roof of an experimental planetarium (in Iena) completed in 1923. This was hemispherical, corresponding to the functional shape of the project.

A great number of aircraft hangars, covered markets, factories, stadia, exhibition buildings and railroad terminals have been erected with roofs of shell construction.

1.2 DEFINITIONS

A thin shell is a body that is bounded by two closely spaced curved surfaces. It can thus be considered as the "materialisation" of a curved surface, just as the beam and flat plate can be considered as the "materialisation" of a line and a flat surface[2].

A shell has three fundamental identifying features: its reference surface, its thickness, and its edges. Of these, the reference surface is the most significant, because it defines the shape of the shell. Generally, if the shell is composed of a single homogeneous material, the middle surface (that is, the locus of points that are equidistant from the bounding surfaces) is selected as the reference surface. If the shell is of layered or other non-homogeneous construction, it is usually more convenient to use as the reference surface, one of the bounding surfaces or a so-called neutral surface that is analogous to the neutral axis of a beam.

The thickness t of the shell at a given point, defined as the distance between its bounding surfaces as measured along and normal to the reference surface that passes through the point, may vary over the shell. Furthermore, the edges of the shell are designated by appropriate

values of co-ordinates that are established on the reference surface. Shell edges are formed by curved surfaces whose normal are perpendicular to the normal of the reference surface along the intersections of the edge surfaces with the reference surface. There are cases where the shell might have no edges at all. In such cases, the shell is referred to as a closed shell; an example is an egg-shape sludge digester. Shells can be composed of any type of material. However, considerations in this thesis are restricted to linear elastic shells which obey Hook's law, and whose displacements at a point are small in comparison with the thickness.

Assuming a permissible error of 5% for ordinary engineering computations, Novozhilov[3] cites the cut-off point between thin and thick shells as corresponding to the ratio $\frac{t}{r_{min}} \leq \frac{1}{20}$ (where $r_{min.}$ is the minimum radius of curvature of the middle surface). He notes that a large number of shells encountered in practice are classified as thin if they lie in the range $\frac{1}{1000} \leq \frac{t}{r_{min}} \leq \frac{1}{50}$. Vlasov[5] adopts a more stringent criterion ($\frac{t}{r_{min}} \leq \frac{1}{30}$).

1.3 DEVELOPMENT OF THEORIES OF SHELLS

1.3.1 Historical Developments in Linear Shell Theory

An investigation of the general theory of shells, based on Kirchhoff's re-examination of the Lagrangian plate theory, dates back to 1849, while the first theory of shells founded on the hypothesis of Kirchhoff was proposed by Aron in 1874. In 1888, Love derived the basic equations which describe the behaviour of thin elastic shells[2]. These equations, together with the assumption upon which they are based, form the theory of thin elastic shells referred to as Love's first approximation.

1.3.2 The Love-Kirchhoff Assumptions and Love's Approximation

The simplifying assumptions first adopted by Kirchhoff for plates, and later extended to shells by Love, are sometimes referred to as the Love-Kirchhoff assumptions. These assumptions may be stated as follows:

(a) The shell thickness is negligibly small in comparison with the least radius of curvature of the shell middle surface.

(b) Strains and displacements that arise within the shell are small.

(c) Straight lines that are normal to the middle surface before deformation remain straight and normal to the middle surface during deformation, and undergo no change in length.

(d) The direct stress acting in the direction normal to the shell middle surface is negligible.

1.3.3 Shells of Revolution and Solution Approaches

Shells of revolution are generated by rotating a plane curve though 360^0 about a straight line in the plane of the curve. These include cylindrical, spherical and hyperbolic shells. In 1912, H. Reissner[4] reduced the differential equations for symmetrical deformations of such shells to a convenient form, and then applied the asymptotic method for the integration. He also discovered the possibility of reducing the order of the differential equations of this problem by means of complex transformation. The problem of spherical shells under symmetrical loading was found to reduce to the integration of a single second-order differential equation[3]. Meissner was later able to generalise H. Reissner's results to the problem of the symmetrical deformation of shells of revolution of arbitrary shape. In this way, the difficulty arising in the analysis of shells of revolution under symmetrical loading was largely overcome, since the asymptotic method was shown to be a simple and sufficiently accurate process for the integration of the relevant differential equations. However, these results were not suitable for practical application since one has to retain a lot of terms in the analysis of spherical shells using hypergeometric series.[3]

Shtaerman[4] in 1924 gave a very clear deduction of the equations of the problems by establishing the analogy between the problems of the symmetrical deformation of shells of revolution and of the bending of arches on elastic foundations.

In 1926, Geckeler[4] obtained a more simplified approximation for the integration of the equations for the symmetrical deformation of shells of revolution. He achieved this by omitting terms in the two dependent variables Q_ϕ and V (Q_ϕ is the transverse shear per unit length of shell element, V is the rotation of the meridian), and terms in the first derivatives of these variables, from the Reissner-Meissner pair of equations for arbitrary shells of revolution subjected to symmetric loading. From the point of view of simplicity, and the rapidity with which a stress analysis can be performed, the Geckeler approximation is undoubtedly the most convenient analytical tool for obtaining edge-zone stresses in axisymmetrically loaded spherical shells. It is most suited to such shells if they are sufficiently thin and of constant thickness.

Novozhilov[3] argues that, in the derivation of the Reissner-Meissner pair of reduced equations for the spherical shell, errors of order *t/a* (spherical shell's thickness to radius ratio) in comparison with unity are involved, so that there is no point in retaining in the solution to the equations terms of order smaller than *t/a*. He concluded that the simplifying asymptotic series method must, therefore, be employed irrespective of the difference between the solutions obtained by this method and the hypergeometric series, especially as the convergence problems associated with the mathematically-exact hypergeometric solution hamper the use of that solution for practical engineering calculations.

Timoshenko and Woinosky-Krieger[5] point out that, for an a/t =30, as many as ten terms are required in order to obtain sufficient accuracy for the hypergeometric-series solution. Flugge[4] also reports problems with the convergence of the hypergeometric series.

In 1944, Vlasov[4] independently developed a bending theory applicable to shallow shells. According to Vlasov, a shell is considered to be shallow if the ratio of the shorter side (for shells of rectangular plan) or to the diameter (for shells of circular plan) is less than 1/5. Such a criterion for shallowness corresponds to a ϕ value at the shell edge of approximately 44° in the case of spherical shells whose plan shape is circular.

1.4 COOLING TOWERS

1.4.1 General Considerations and Historical Developments

The advent of the natural draught cooling tower dates back to the beginning of the twentieth century. The first paper published in Britain on the theory of natural draught cooling towers was that of Robins[6] in 1907, which during its time was a remarkable work. In 1910, Prof. Van Iterson of the Dutch State mine first started exploring the use of reinforced concrete shells for natural draught cooling towers[7]. In 1916, he designed the first hyperbolic natural draught concrete cooling tower. It then became common practice to build cooling towers next to power stations.

It was during the Second World War (1939–45) that extensive and serious efforts were made to develop industrial cooling towers. Numerous towers were built in Europe during this period, and only in the late 1950s did the Americans start exploring their use. Cooling towers

only emerged in Africa in the 1960s with South Africa being the first country to adopt their use.

Fig. 1 Layout of Cooling Tower

As described by Rish and Steel[7], natural draught cooling towers are structures used to reduce the temperature of water in the cooling circuit of thermal power plants. Most of the structure is an empty shell. The lower portion contains the cooling stack over which the warm water is distributed by a pipe and nozzle system. The lower portion of the structure is open to allow air

access to the cooling stack. Beneath the tower is a pond that is constructed to catch the falling water and return it to the circulating water system. A typical layout of a hyperbolic cooling tower is shown in Figure 1. The function of the cooling stack is to increase the surface area between the water and the cooling air, either by breaking the water up into droplets or by spreading it over a large area in the form of films. As the warm water falls through the stack, it gives up its heat to the air. The air leaving the stack inside the shell is lighter than the ambient air and a draught is created by the chimney effect. Above the distribution pipes, a spray eliminator screen is constructed to catch the fine droplets of water that would otherwise be picked up by the rising air–stream. As the plume of vapour is discharged at a great height, there is no risk of the performance of the tower being affected by the re-circulation of air leaving the top of the tower. The draught through the tower results from a number of inter-related effects: the atmospheric air-pressure difference due to chimney height; induced draught due to wind velocity differentials; temperature difference of the air heated by the water; an increase in volatility due to vaporization.[6]

The earliest towers were built of wood, which comprises staked fagots over which water is dropped. Refinements were made by housing, which prevents the water from being polluted by the atmosphere, and extending it into a chimney shape to increase the draught. Metal towers were also explored, but unfortunately these were not so popular and most are now extinct[6]. Attempts were also made using other materials like aluminium and asbestos cement sheathing on a structural steel frame.

The final choice for constructing natural draught shells came from reinforced concrete which with its strength, flexibility in design and low maintenance expenditure has advantages over other materials. Furthermore, the possibility of utilising a single or double-curved surface enabled lightweight structures to be erected. The cooling tower is a huge double-curved thin shell structure with a negative Gaussian curvature. The shell of a cooling tower is a hyperboloid of revolution with a throat-radius-to-shell-thickness ratio in the range 125–400[8]. The slender shell is supported above the ground on a lattice of inclined columns forming a V, X or A pattern around the bottom opening of the shell. This type of support is a continuation of the membrane shell into the foundation, i.e. the columns meet the shell along the tangent plane of the mid-surface, and are cast into a ring-beam foundation. The shell is the most important part of the cooling tower, both in technical and financial terms. It is also the most

sensitive since its collapse would put all or part of the power station out of action for a considerable period of time. For this reason, the shell is the most fundamental factor influencing the life of the cooling tower.

According to Harte[9], natural draught cooling towers play a significant role as power plant components: they balance the technical requirements of an efficient energy supply with appropriate means for protecting the environment. Even in the most efficient nuclear power units, only 45% of the generating heat is converted into electric energy. The remaining 55% is discharged into the environment, mainly through the smokestack and the cooling water. To avoid thermal pollution of the rivers, lakes and seashores by using the water for cooling, natural draught cooling towers are the most effective measure for minimising the need for water. Thus they are able to balance the environmental factors, investment and operating costs with the demands of a reliable energy supply.

In the first quarter of the twentieth century, the size of towers was moderate, and did not exceed 80m in height. In this range, the structural safety and stability were not of primary concern because the minimum wall thickness and reinforcement were sufficient to provide the required safety. Nevertheless, several techniques developed during that period, pertaining to the computation of forces and stresses in the shell.

During the mid-fifties when cooling towers were becoming more and more common, the increase in size of these structures made it mandatory to carry out a thorough and accurate analysis to cater for both safety and economy. Analysis was then carried out using only the membrane theory,[7] which assumes:

i. The thickness of the shell is very small compared with its diameter.

ii. Bending moments are negligible throughout the shell, and this approach is adopted in cooling-tower theory even though the ring beam is likely to introduce moments in its vicinity.

iii. Applied loads (including wind forces) are resisted only by direct tension, compression, and shearing forces in the plane of the shell itself.

During this period, the analysis of cooling towers was done considering a "cone-cylinder-cone" model since the equations of membrane equilibrium for the constituent parts are well known and simple in form. However, Rish and Steel[7] developed equations describing the

effect of wind on a shell structure utilising the membrane theory. A major set-back with this model is the change of form of the equations at the junctions of the cylinder with the cones. Another disadvantage is that the resulting stresses depend explicitly upon derivatives of an empirically determined function, which represents the distribution of the wind pressure around the tower. These derivatives have to be calculated by approximate methods, and the use of such quantities is not desirable in general since inaccuracies in measured values of a function lead to larger errors in estimates of derivatives.[10]

The distribution of wind pressure on a cooling tower exposed to a steady wind of constant direction has been the subject of many investigations. There is general agreement on the overall shape of the wind-pressure distribution curve, but some differences of opinion remain concerning the peak values, and whether allowance should be made for internal suction. [10]

In recent times, probably due to the higher cooling demand of power stations and an increased understanding of the dynamics and mechanics of cooling towers, the heights have increased from 75m–200m. Such an increase of about 100% in dimensions needs a high degree of accuracy in both design and construction. The optimization of the wall-thickness distribution (from the bottom up to the top) becomes more important[11]. Locally in South Africa, there are six cooling towers at Kendal power station, each having a height of 166m, a base diameter of 163m and a capacity of 672MW[6]. The largest tower built to date (1999) is in Niederaussem, Germany, which measures 200m in height and 154.5m in base diameter, with wall thickness varying from 220 to 240mm in a wide region of the shell[9].

1.4.2 Developments in Theory, Analysis and Design

Most of the earlier work on hyperboloids of revolution dealt with various aspects of the application of the membrane theory of thin shells of revolution to this particular type of shell. Vlasov[17] showed that for hyperboloids of revolution with certain combinations of geometric parameters and edge loading, the membrane theory may lead to an indeterminate solution resulting in infinite values for the stresses. He concluded that the membrane theory must be applied only to shells of zero Gaussian curvature for which the solution of the governing equations leads to completely defined finite values for the internal forces. Novozhilov[3] elaborated on these observations by reference to arbitrary shells with negative Gaussian curvature, and showed that certain boundary conditions lead to the presence of modes of pure

bending under edge loads. He concluded that fixing the shell against displacement in both the meridional and tangential directions at either end might eliminate these pure bending modes. If these boundary conditions are enforced, then the membrane theory leads to a realistic solution. Flugge[13] discussed a membrane-theory solution for a hyperboloid subjected to arbitrary loading at one end. He later observed that the edge loading may be resolved along the characteristic lines of the shell, and thus propagates to the other edge that must be restrained against movement in the meridional and circumferential directions, to resist these forces.

As mentioned earlier, Rish and Steel[7] discussed the treatment of the hyperboloid as a combination of frusta of cones and a cylinder. Martin and Scriven[10], and Martin, Muddock and Scriven[14] presented numerical solutions for dead-load and wind-load stresses and displacements in a particular shell, and Billington[15] gave a solution for dead-load stresses. The membrane solution for the stress resultants and displacements in hyperbolic cooling towers subjected to dead load, earthquake load and wind load were presented by Gould and Lee.[16]

Although most of the early writers wrote extensively about the use of the membrane theory, they acknowledged the fact that at points of discontinuity due to a change in geometry, the membrane theory will fail, and the bending theory must be used instead. These early researchers maintained that the membrane theory was nevertheless sufficient to analyse the hyperboloid of revolution. Only in 1967 did Gould and Lee[17] publish expressions for the stress resultants for a hyperboloid of revolution based on Novozhilov's treatment of the bending theory of shells of revolution, which utilises an approximate analytical solution rather than a numerical solution to the governing equation.

In 1969, Gould[18] suggested some specifications, grouping various geometric combinations and some governing ranges of shell parameters for determining the minimum-weight design of cooling towers with respect to a "duty performance coefficient". He concluded that the weight factor was inversely proportional to the parameter k (k being a measure of the slope of the asymptote of the generating hyperbola), i.e. for a constant duty performance coefficient, it appears that towers with higher values of k are lighter than those with other configurations.

The collapse of three large towers (117m high) at Ferribridge, England, on 1 November 1965, prompted authorities to recognise that an extensive investigation, both experimentally and

analytically, was necessary to prevent similar collapse from occurring in the future. The investigation of this catastrophe revealed the following flaws: that inappropriately low wind forces had been assumed in the design, that minimum constant wall thickness and levels of reinforcement had been employed, that top stiffening rings had been omitted, and that wind turbulence had inadvertently been created as a result of the layout of the towers[19]. A few years later, in 1973, another collapse occurred at Ardeer, Scotland. This was attributed to the occurrence of vertical cracks and the meridional curvature imperfections in the tower, which had induced high circumferential tensile stresses[20].

After these two mishaps, attention in subsequent years was focused on the effects of wind (since it is one of the most important loading), and of meridional imperfections on cooling towers. For example, Al-Dabbagh and Gupta[21] investigated the effects of meridional imperfections on cooling towers. They concluded that the primary effect of an imperfection is to cause a significant increase in the hoop forces and meridional moments. Approximate expressions were developed to calculate the effect of the imperfection hoop force, and the effect of the imperfection meridional moment.

In 1979, Mungan[22] investigated buckling stresses in stiffened hyperboloidal shells. He modelled a series of cooling towers and compared the experimental results with theoretical values, and concluded that by suitably arranging the stiffening rings, the buckling behaviour of these shells could be improved, and that the buckling stresses in the circumferential direction could be increased. He proposed having at least four equidistant stiffening rings below the throat, which would have a beneficial effect by reducing both the wall thickness and the meridional stresses due to self-weight at the lower part of the tower shell.

When the tower height increased beyond 120m, it was felt that the dynamic action of the wind had to be considered in more detail. A number of researchers have conducted investigations relating the effect of wind on this type of structure.

Davenport[24] developed a comprehensive statistical approach to predict structural response and applied it to several structures whose behaviour is governed by height and span. A gust load factor was also proposed by Davenport[25] to account for the dynamic effect of wind.

Cooling tower response is governed by both vertical and circumferential wind distribution. Experimental results on cooling tower models have shown that dynamic stresses are of the same order as static stresses[23]. The vertical reinforcement in cooling towers is usually governed by the difference in tensile wind stresses and compressive dead load stresses. This difference is very sensitive to small changes in wind stresses.

A convenient way of dealing with wind stresses is to divide them into static stresses, which are based on the reference value of hourly mean wind speed, and dynamic stresses, which take into account fluctuating wind components and the tower's structural properties and configuration. The static wind pressure distribution depends largely on the Reynolds number and the surface roughness, both of which have been studied experimentally by Davenport & Isyumov[23].

Niemann[23] measured the pressure distribution for a particular full-scale tower and for various wind tunnel models with different surface roughness. He found that full-scale results indicate significantly smaller suction than wind tunnel models due to the difference in Reynolds number. Panduart[27] conducted extensive wind-tunnel experiments on smooth and rough surfaces using plexiglass models.

Isyumov, Abu-Shitta and Davenport[26] reported a wind tunnel study of dynamic behaviour in which an aero-elastic model was subject to a wind with about 11% turbulence intensity. They found that the "static (mean) wind stresses conformed closely to those calculated from membrane theory and that the maximum root-mean-square dynamics stresses were about one-third the mean stresses in the meridional direction near the base of the tower on the windward side". Further work by Abu-Shitta and Hashish[23] distinguishes between two types of dynamic responses to wind: quasi-steady and resonant. The resonant response is significant only when the lower natural frequencies of the structure are close to the dominant frequencies of the turbulence, while both the quasi-static analysis and the resonant effect must employ gust factors. They further presented a non-deterministic analysis approach to predict dynamic stresses, firstly where the resonant contribution is negligible[23] and, secondly, where it is significant[28]. Their method of analysis produces predictions that agree significantly with the actual measured responses of the aero-elastic wind-tunnel model.

Steinmetz and Billington[29] adopted two principal approaches namely: a deterministic analysis using specific wind records from an existing tower, and a stochastic analysis employing spectra of wind pressure. These two approaches were used to gain insight into the possible influence of resonance effects on the dynamic responses of towers subjected to very high wind pressure. They observed a large difference between the natural frequencies of the tower and the frequency of turbulence, and concluded that resonance does not play a major role in the response of cooling towers under a particular measured load.

Armitt[30] developed a wind tunnel technique by using an aero-elastic tower model to determine the stresses directly in cooling towers under realistic simulated conditions. He compared the results obtained from his model with full-scale wind pressure distribution, and concluded that the technique adopted was accurate.

Niemann[31] developed a design for wind effect for a reinforced concrete cooling tower which was based on the distribution of the mean pressures. He considered the influence of wind shear and surface roughness on the mean pressures, based on experimental results from full-scale investigations and test models using wind tunnel testing.

In January 1984, almost two decades after the collapse of the towers in Ferrybridge, a single tower at Fiddler Ferry power station collapsed. This failure was a full-scale demonstration of the effect which small dimensional errors in the shape of the shell can have on the stresses and ultimately on the stability of the structure[32]. The committee of inquiry into the incident found that "the most contributory factor in the failure of the tower was the presence of the outward circumferential bulge above the ring beam which would have caused a major vertical cracking of the concrete". This in turn caused the collapse. As a result, the Central Electricity Generating Board (CEGB) decided that it needed urgently to assess the likelihood of further collapses of the 139 cooling towers that it operated.

During 1985–1987[32], a programme of dimensional and material condition surveys was undertaken to collect the data required for stress analysis. The survey methods employed were able to detect dimensional inaccuracies of the surface of the shells of the cooling towers as small as 25mm, i.e. 20% of the shell thickness of the largest towers. These surveying methods

were not only sufficiently accurate to detect small shape errors but were also cost effective. Two surveying methods were used:

a. The method of triangulation using theodolites to make a large number of observations of the external surface of the tower shell, and
b. "Structural condition survey" where a comprehensive physical investigation of the structural damages is conducted, i.e. concrete samples are taken to test for strength and carbonation, and a covertometer used to determine the depth of cover to the reinforcement.

Calculation methods were also developed to determine the structural effects of dimensional errors detected, and these were used in estimating the possibility of structural damage leading to failure. The investigation concluded that dimensional errors as a result of constructional errors were dominant on the cooling towers. This, in effect, causes meridional cracks which produces high circumferential bending stresses.

In recent times, Gould, Hare and Koto[33] investigated the load-deflection behaviour of reinforced concrete cooling-tower shells under various conditions. They suggested that when geometric imperfection is considered, a minimum percentage of reinforcement (0.3–0.4%) must be used to allow for redistribution of stresses and a global deformation.

1.5 STATEMENT OF RESEARCH AND SUMMARY OF THESIS

While many investigations have been carried out on the behaviour, analysis and design of hyperbolic cooling-tower shells, there appears to be a gap in the literature regarding the availability of parametric data on the structural response of cooling towers, when design parameters (such as overall height of tower, throat radius, angle of opening, shell-thickness variation) are altered. Even for the most basic loading condition of self-weight, such data appears to be missing, or is taken for granted. This study seeks to investigate how the stresses in thin hyperbolic cooling-tower shells vary with respect to a number of geometric design parameters, and to make appropriate design recommendations on the basis of the observations made. The study is confined to the axisymmetric loading conditions of self-weight only, and makes use of both analytical and numerical methods to determine the stress distributions in the shell.

With a literature review having been presented in the opening chapter, Chapter Two presents the membrane theory for thin shells of revolution, after a discussion of its validity and limitations. This is followed in Chapter Three by a presentation of the general bending theory of shells of revolution, and a discussion on how the membrane analysis and the bending analysis, when performed separately, may be brought together through a flexibility-type approach. Much of this presentation is based on the work of Zingoni[4], and forms the basis of the analytical results that will be given in this thesis.

Chapter Four introduces the governing geometric parameters of the cooling-tower problem, and develops the membrane solution for the general self-weight loading situation. Explicit results are presented for the case of uniform shell thickness, and one other case of gradual variation in shell thickness.

A general description of the finite-element modelling of axisymmetric shells of revolution, with specific reference to cooling-tower shells, is presented in Chapter Five. The implementation of ABAQUS, the finite-element programme used in the numerical work, is also explained. The treatment covers the theoretical basis of the programme, types of elements used in cooling-tower analysis, choice of appropriate elements for the various regions of the structure, discretization strategies, modelling of geometry and support conditions, output results, and extraction of relevant stress components.

Chapter Six adopts a cooling tower of typical proportions as a "standard", and presents comparative analytical and finite-element stress results for the case of self-weight loading. This work serves to validate the finite-element modelling, and the results form a "benchmark" for the intended parametric investigations. The chapter also presents the stress distributions that are obtained when the parameters b/a (hyperbolic axes ratio), A (rotation axis offset parameter), ϕ_o (top angle of opening), ϕ_b (bottom angle of opening), H (overall height of tower) and t (shell thickness) are varied in a controlled manner, one at a time. These results are mostly obtained on the basis of the finite-element method, with the analytical expressions used to check the finite-element results. The presentations take the form of both tables and illustrative plots.

Chapter Seven discusses these results in detail, one parameter at a time, and makes conclusions as appropriate.

In Chapter Eight, an overview of the results of Chapter Six is made, and the parameters that have the most influence on design stresses are identified. Overall conclusions and design recommendations are summarized, and directions for future research are pointed out.

A listing of references at the end, and an appendix, conclude the thesis.

CHAPTER TWO

THE MEMBRANE THEORY OF SHELLS OF REVOLUTION

2.1 THE MEMBRANE HYPOTHESIS

The origin of the membrane theory of shells goes back to the work of Lame and Clapeyron who, in 1828, had considered shells of revolution loaded symmetrically with respect to their axes[5]. Beltrami and Lecornu are generally credited with having first established the general form of the equations of the membrane theory in the second half of the nineteeth century[3].

The theory is applicable to either completely flexible membranes (inflated tyre tube, toy balloon), which have negligible bending stiffness, or shells with finite bending rigidity but in which the moments developed are so small that they can be neglected, owing to the geometry of the shell, the nature of the boundary conditions at the shell edges, and the manner in which the applied loading is distributed.

The membrane theory, otherwise called the "momentless" theory, requires that bending actions be neglected, so that the external load acting on the structure is assumed to be equilibrated by in-plane forces only. As is well known, such an approach results in a spectacular simplification of the equations of thin shell theory, enabling many interesting and important problems to be tackled by relatively simple computations.

The often-used term "membrane theory" is quite misleading. As Calladine[34] points out, the approach is essentially a "hypothesis", in the sense that one can assume that bending actions can be neglected, and then carry out an eventual check on the validity of the hypothesis. This will either confirm the validity of the membrane calculations, or will show these to be inadequate, necessitating a better and more realistic analysis. Few authors spell out explicitly the necessity for such a check. Instead, most attempt to provide broad guidelines for the validity of the membrane hypothesis. According to Calladine, one could argue that such guidelines are helpful in developing an intuitive feeling for identifying shell structures for which the membrane calculations may be valid. On the other hand, there is a definite tendency to take these guidelines as rules of general validity, thus ignoring the fact that exceptions can always be found to each and every such 'rule'. However, the only reliable way in which

membrane solutions can be checked with certainty is to compute the displacements due to the membrane stress resultants; the membrane hypothesis will be valid if the deformation pattern thus obtained is compatible with a negligible curvature-change field throughout the whole shell[34]. Zingoni [36,37] has suggested a procedure for checking the validity of the membrane hypothesis in interior regions of shells of revolution loaded symmetrically with respect to their axes of rotation. Unlike previous standard procedures, Zingoni adopts a more direct method that does not involve the explicit determination of displacements, which would require a knowledge of the kinematic boundary conditions of the shell in order to evaluate the constant of integration associated with the general solution for one of the displacement components.

The existence of the momentless state of stress in shells is subject to the provision of suitable boundary conditions, as well as the fulfilment of certain smoothness conditions regarding shell geometry and loading distribution. These locations include external supports, discontinuities in loading and/or shell geometry, and concentrated line loadings. All these locations at which there is a breakdown in the membrane solution (manifested by its failure to satisfy the boundary conditions) may be conceptualised as 'edges'. At such edges, Zingoni[4] points out that transverse shearing forces, bending moments and twisting moments are, in general, required in order to satisfy the boundary conditions, so that, quite clearly, a momentless state of stress cannot exist in their vicinity.

Novozhilov[3] and Nielsen[3] in their considerations of the axisymmetric deformation of shells of revolution, discussed the conditions for the validity of the membrane hypothesis from a more practical point of view. Novozhilov indicates that at certain locations in the interior of the shell, the continuity of the middle surface appears to be violated when one uses the membrane hypothesis alone. However, since the middle surface is in reality continuous, there must exist at these locations transverse shearing forces and moments to satisfy the conditions of continuity. For axisymmetric shells of revolution, locations at which such phenomena occur are those where the following quantities are discontinuous along a meridian:[3,4]

- meridional loading component, radial loading component, and the first derivative of the radial loading component with respect to distance along the meridian;
- shell thickness, and the first derivative of the shell thickness with respect to distance along the meridian;

- meridional radius of curvature, and its first derivative with respect to distance along the meridian.

2.2 GENERAL SHELL OF REVOLUTION UNDER AXISYMMETRIC LOADING

2.2.1 Introduction

A surface of revolution is generated by rotating a plane curve through 360^0 about an axis in its own plane. The generating curve is called the meridian. It is convenient to regard the axis of revolution of the shell mid-surface as vertical, so that the parallel 'circles of latitude' of the shell, which are the intersections of the shell mid-surface with planes perpendicular to the axis of revolution, lie in horizontal planes. Meridians lie in vertical planes all containing the axis of revolution, and such planes will be referred to as meridional planes. The tangent to the meridian at a given point defines the meridional direction. The circles of latitude will be referred to as hoop circles, while the direction of the tangent to a hoop circle is referred to as the hoop direction.

Shells of revolution find application in the design of roof domes, cooling towers, egg-shaped sludge digesters, pressure vessels and liquid-filled tanks. The principal loading conditions for these structures are usually axisymmetric, meaning that the meridians will deform in the same manner, with no relative transverse shearing between adjacent portions of the shell. The theoretical treatment in the rest of this chapter follows that given by Zingoni[4].

Consider a shell element cut out by two meridians and two circles of latitude, each pair being infinitesimally close together. Since our geometry is curvilinear, we shall adopt the angular co-ordinate system with ϕ (called the meridional angle) measured between a normal to the shell mid-surface and the axis of revolution of the shell, and θ (called the hoop angle) measured in the horizontal plane from a datum meridian.

As shown in Fig. 2.1, r_1 is the principal radius of curvature of the shell mid-surface at a given point as seen in the meridional plane, r_2 is the second principal radius of curvature of the shell midsurface, given by the distance between the point (of the shell midsurface) in question and the intercept of the normal to the shell midsurface at the point and the axis of revolution of the shell, while r is the radius of the horizontal circle of latitude through a given point. The two radii r and r_2 are related as follows:

$$r = r_2 \sin\phi$$

It follows that the sides of the curvilinear elements are of lengths

$$L_{AC} = rd\theta = r_2 \sin\phi d\theta$$

$$L_{CD} = r_1 d\phi$$

It is assumed in the above description that the principal radii of curvature of the shell r_1 and r_2 are known. In the case of radii of curvature that vary from point to point, the radii are computed from the equation that defines the shell shape, along with various relationships of differential geometry.

When considering shells of revolution subjected to axisymmetric loading and boundary conditions, in-plane shearing-force stress resultants cannot exist. There are only two unknown internal membrane stress resultants acting on the shell element, which are the meridional stress resultant N_ϕ (force per unit length in the meridional direction), and the hoop stress resultant N_θ (force per unit length in the hoop direction). The external loading components are P_ϕ (load per unit area of shell surface in the meridional direction) and P_r (load per unit area of shell surface in the normal direction); P_θ (load per unit area of shell surface in the hoop direction) is zero under axisymmetric loading conditions.

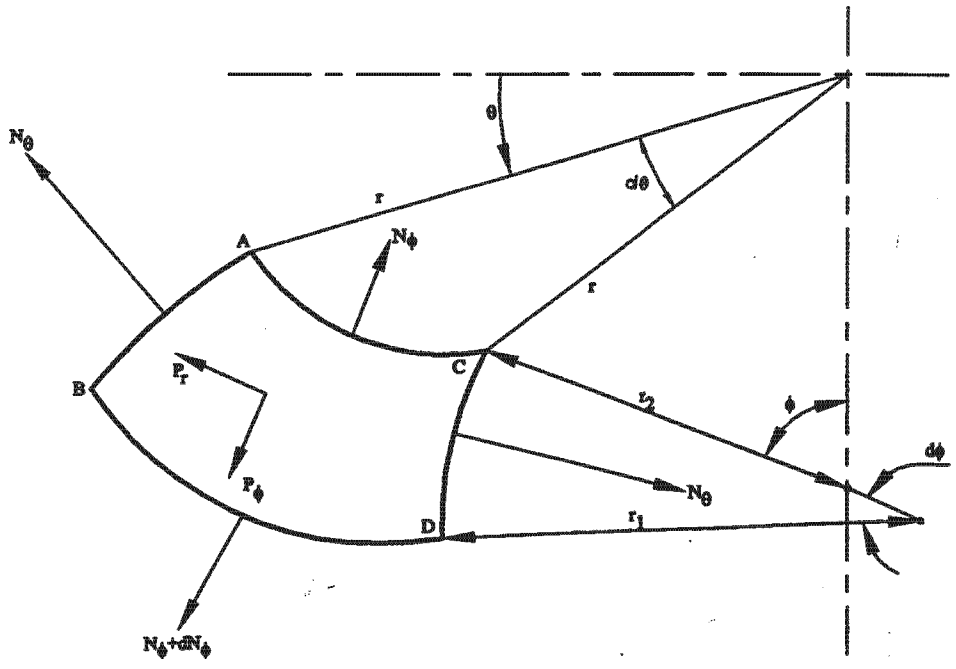

Fig. 2.1: Element of axisymmetrically loaded shell of revolution

2.2.2 Equilibrium of Shell Element

The shell element is in equilibrium under the external applied loading (P_ϕ and P_r) and the internal stress resultants (N_ϕ and N_θ). Force equilibrium requires that the sum of the forces acting on the shell element, resolved in the direction of the tangent to a meridian and in the direction of the normal to the shell mid-surface, must be zero.

Following Zingoni[4], consider the components of all the forces acting on the shell element, in the positive direction (i.e. the direction of increasing ϕ) of the tangent to a meridian. Each of the stress resultant N_ϕ and N_θ and the external loading component P_ϕ, contributes a force in this direction.

Figure 2.2(a) shows the section of an element in the horizontal plane of a circle of latitude, the forces acting at the ends of the element equal $N_\theta . r_1 d\phi$. The resultant of these two forces is a horizontal force F_1 directed towards the axis of revolution, and given by

$$F_1 = N_\theta . r_1 d\phi \left(\sin \frac{d\theta}{2} \right) + N_\theta . r_1 d\phi \left(\sin \frac{d\theta}{2} \right) \qquad (2.1)$$

$$\approx N_\theta r_1 d\phi d\theta$$

since for very small angle α, $\sin \alpha \approx \alpha$.

Figure 2.2(b) shows a section of the element in the vertical plane of a meridian. Resolving F_1 along OT, the positive meridional direction, one obtains the contribution of N_θ to the force resultant along OT as

$$-F_1 \cos\phi$$

which, on substitution of the equation (2.1), becomes

$$-N_\theta . r_1 \cos\phi d\phi d\theta \qquad (2.2)$$

Figure 2.2(c) depicts a section of the element in the vertical plane of a meridian, but this time the meridional end forces are shown. The total meridional force acting at the upper edge is $N_\phi r d\theta$. The total meridional force acting at the lower edge is

$$(N_\phi + dN_\phi)(r + dr)d\theta \qquad (2.3)$$

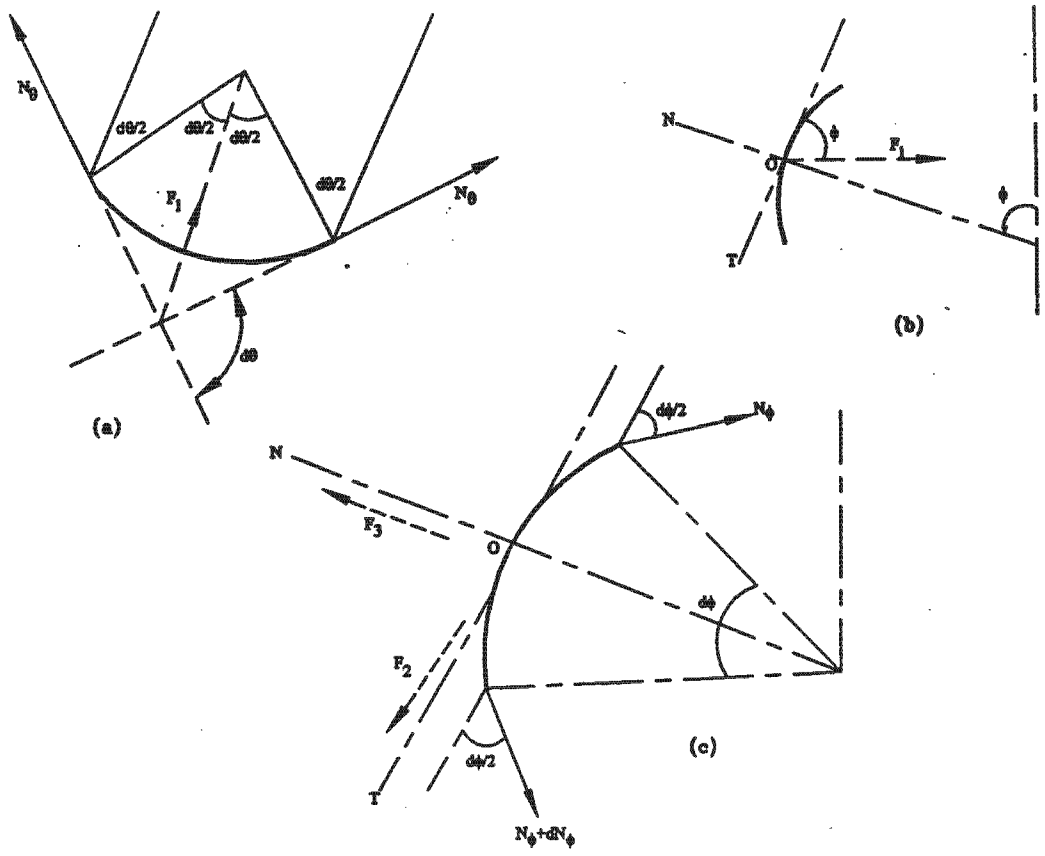

Fig. 2.2 Derivation of the governing equations of equilibrium for an element of an axisymmetrically loaded shell of revolution.

Resolving these two forces along OT, the resultant F_2 is obtained as

$$F_2 = (N_\phi + dN_\phi)(r + dr)d\theta.\cos\frac{d\phi}{2} - N_\phi.rd\theta.\cos\frac{d\phi}{2}$$

$$\approx N_\phi.drd\theta + rdN_\phi d\theta \qquad (2.4)$$

$$= d(rN_\phi)d\theta$$

As indicated earlier, for very small value of angle α, $\cos\alpha \approx 1$

Finally, the contribution of the external loading to the force resultant along OT is given by P_ϕ x surface area i.e.

$$P_\phi.r_1 rd\phi d\theta \qquad (2.5)$$

Summation of (2.2)–(2.5) yields

$$d(rN_\phi).d\theta - N_\theta.r_1\cos\phi.d\phi d\theta + P_\phi.r_1 rd\phi d\theta = 0$$

which, upon dividing throughout by $d\theta$, yields

$$d(rN_\phi) - r_1 N_\theta\cos\phi d\phi = -r_1 rP_\phi d\phi \qquad (2.6)$$

The next step is to find the component of all the forces in the direction ON, which is the positive direction of the normal to the shell mid-surface. With reference to Fig. 2.2(b), F_1 has the component

$$-F_1 \sin\phi$$

Which, on substitution of the expression for F_1, becomes

$$-r_1 N_\theta \sin\phi d\phi d\theta \tag{2.7}$$

From Fig. 2.2(c), the resultant of the N_ϕ forces along ON, denoted by F_3, is given by

$$F_3 = -N_\phi . r d\theta . \sin\frac{d\phi}{2} - (N_\phi + dN_\phi)(r + dr) d\theta . \sin\frac{d\phi}{2} \tag{2.8}$$

$$\approx -rN_\phi . d\theta d\phi$$

Note that $\sin(\frac{d\phi}{2}) = (\frac{d\phi}{2})$, and ignoring the relatively small quantities

$$N_\phi . dr . d\theta . \frac{d\phi}{2};\ \ r . dN_\phi . d\theta \frac{d\phi}{2};\ \ dN_\phi . dr . d\theta \frac{d\phi}{2}$$

The resultant of the external loading along the direction ON is

$$P_r . r_1 r d\phi d\theta \tag{2.9}$$

Summation of equations (2.7)–(2.9) yields

$$-r_1 \sin\phi N_\theta d\phi d\theta - rN_\phi d\phi d\theta + r_1 r P_r d\phi d\theta = 0$$

Dividing throughout by $d\theta d\phi$, replacing r with $r_2 \sin\phi$, dividing throughout by $\sin\phi$ and rearranging yields

$$r_2 N_\phi + r_1 N_\theta = r_1 r_2 P_r \tag{2.10}$$

Dividing throughout by $r_1 r_2$, one of the basic relations for the axisymmetrically loaded shell is found as follows

$$\frac{N_\phi}{r_1} + \frac{N_\theta}{r_2} = P_r \tag{2.11}$$

This equation is valid not only for a shell in the form of a surface of revolution, but may be applied to all shells when the co-ordinate lines ϕ and θ = constant are the lines of principal curvature of the surface.

2.2.3 General Solution

From equation 2.11

$$N_\theta = r_2 P_r - \frac{r_2}{r_1} N_\phi \tag{2.12}$$

which when substituted into equation (2.6), yields

$$d(rN_\phi) - r_1\left(r_2 P_r - \frac{r_2}{r_1}N_\phi\right)\cos\phi d\phi = -r_1 r P_\phi d\phi$$

dividing throughout by $d\phi$ leads to

$$\frac{d(rN_\phi)}{d\phi} + r_2 N_\phi \cos\phi = r_1 r_2 P_r \cos\phi - r_1 r P_\phi$$

which, on multiplication throughout by sin ϕ, becomes

$$\left[\frac{d(rN_\phi)}{d\phi}\right]\sin\phi + (r_2 \sin\phi)N_\phi \cos\phi$$

$$= r_1 r_2 P_r \cos\phi \sin\phi - r_1 r P_\phi \sin\phi \qquad (2.13)$$

Replacing ($r_2$sinϕ) in the second term of the left–hand side of equation (2.13) by r, we may then write the left–hand side as

$$\left[\frac{d(rN_\phi)}{d\phi}\right]\sin\phi + rN_\phi \cos\phi$$

On application of the product rule of differential calculus in reverse, this reduces to

$$\frac{d}{d\phi}(rN_\phi \sin\phi)$$

Hence, equation (2.13) may be written as

$$\frac{d}{d\phi}(rN_\phi \sin\phi) = r_1 r_2 P_r \cos\phi \sin\phi - r_1 r P_\phi \sin\phi \qquad (2.14)$$

Integrating both sides of equation (2.14) with respect to ϕ yields

$$rN_\phi \sin\phi = \left[\int (r_1 r_2 P_r \cos\phi \sin\phi - r_1 r P_\phi \sin\phi)d\phi + c\right]$$

Replacing r with $r_2$sinϕ, we obtain

$$(r_2 \sin^2\phi)N_\phi = \left[\int (r_1 r_2 (P_r \cos\phi - P_\phi \sin\phi)\sin\phi d\phi + c\right]$$

The general solution for N_ϕ can be written as

$$N_\phi = \frac{1}{r_2 \sin^2\phi}\left[\int (r_1 r_2 (P_r \cos\phi - P_\phi \sin\phi)\sin\phi d\phi + c\right] \qquad (2.15)$$

The constant of integration c is obtained from an appropriate boundary condition. Equation (2.12) is sufficient to determine the hoop force N_θ from which the stresses are readily determined. Negative algebraic results indicate compressive stresses.

Flugge[13] noted that because of the freedom of motion in the z-direction, for the axisymmetrically loaded shells of revolution considered, strains are produced which assure consistency with the field of stress and compatibility with one another. This action demonstrates the basic difference between the problem of a shell membrane and one of plane stress. In the later case, a compatibility equation is required. However, it is clear that when a shell is subjected to the action of concentrated surface loadings or is constrained at its boundaries, membrane theory cannot everywhere fulfil the conditions of deformation. The complete solution is obtained by application of the bending theory[38].

2.2.4 Deformations

No stress problem is complete until the corresponding deformations have been determined. The basic displacements in axisymmetrically loaded shells of revolution are v (tangential to the meridian, and considered positive when pointing in the direction of increasing ϕ) and w (in the direction normal to the shell mid-surface, considered positive when pointing away from the meridional centre of curvature).

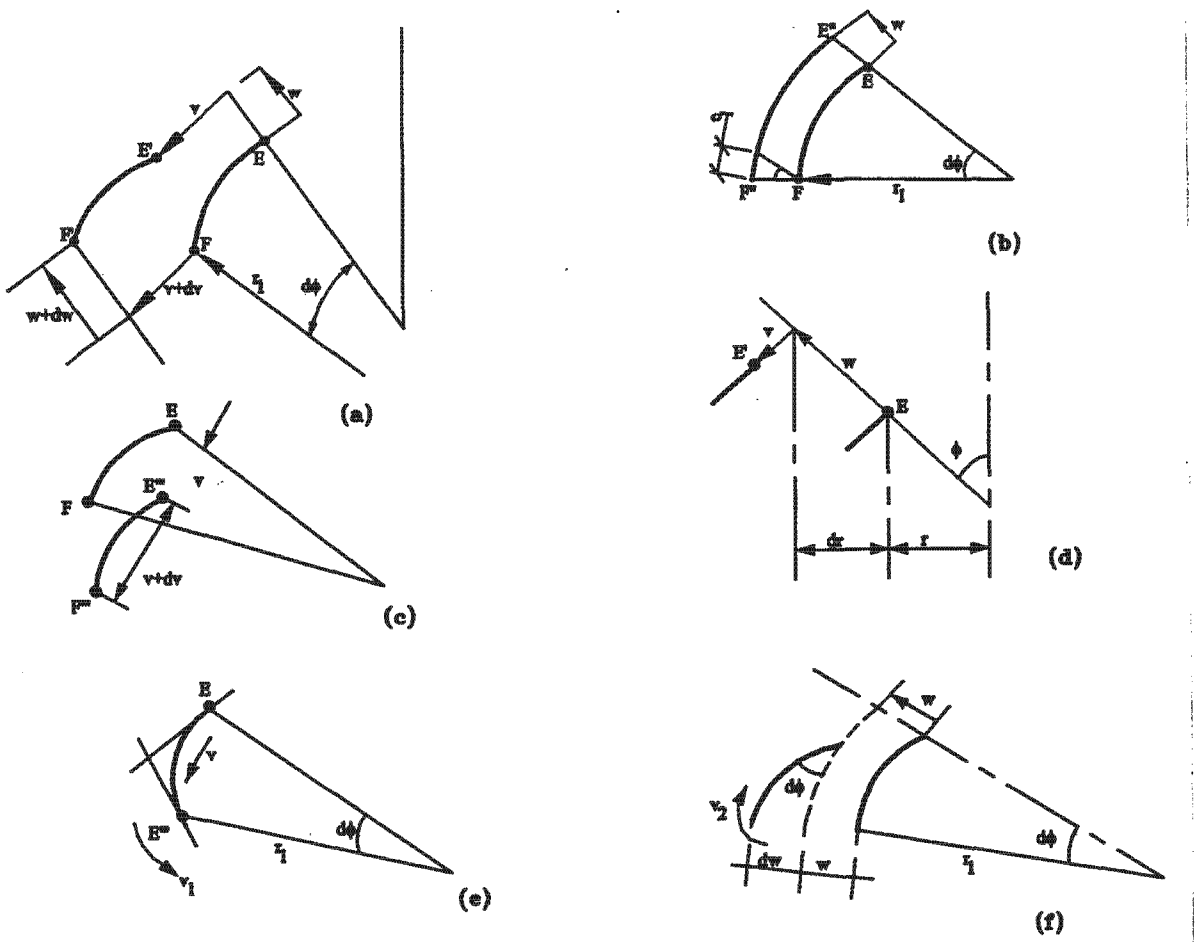

Fig. 2.3 Deformations of a line element of an axisymmetrically-loaded shell of revolution

The deformation of a shell element consists of the elongation of line element EF in Fig. 2.3(a), consists of a component e_1 due to the purely radial movement w, equal to $wd\phi$ in Fig. 2.3(b), and a component e_2 due to the difference in the purely tangential movements of ends E and F, equal to dv in Fig. 2.3(c). Therefore, the total elongation of the line element EF, is given by

$$e_\phi = dv + wd\phi \tag{2.16}$$

The original length of the element was $r_1 d\phi$, the meridional strain ε_ϕ of the element is given by

$$\varepsilon_\phi = \frac{1}{r_1 d\phi}(dv + wd\phi) = \frac{1}{r_1}\left(\frac{dv}{d\phi} + w\right) \tag{2.17}$$

By reference to Fig. 2.3(d), the radius of the circle of latitude at point E increases from r to $r+dr$ as a result of the movement of the point to E'. Thus hoop strain ε_θ is defined as,

$$\varepsilon_\theta = \frac{2\pi(r+dr) - 2\pi r}{2\pi r} = \frac{dr}{r} \tag{2.18}$$

By reference to Fig. 2.3(d),

$$dr = v\cos\phi + w\sin\phi \tag{2.19}$$

Therefore,

$$\varepsilon_\theta = \frac{1}{r}(v\cos\phi + w\sin\phi) \tag{2.20}$$

$$= \frac{1}{r_2}(v\cot\phi + w)$$

since $r = r_2 \sin\phi$.

From equations (2.17) and (2.20)

$$\frac{dv}{d\phi} + w = r_1\varepsilon_\phi \tag{2.21}$$

$$v\cot\phi + w = r_2\varepsilon_\theta \tag{2.22}$$

Subtraction of equation (2.22) from equation (2.21) yields,

$$\frac{dv}{d\phi} - v\cot\phi = r_1\varepsilon_\phi - r_2\varepsilon_\theta \tag{2.23}$$

Between this strain and stress resultants exists an empirical relation, the elastic law, which depends on the material of the shell. In the mathematical treatment of structural problems, Hooke's law is of importance. Some structural materials, such as steel, follow this law perfectly within the limits of the usual stresses; for others like concrete, a linear

approximation generally leads to satisfactory results. Solving for the stresses using Hooke's law

$$\sigma_\phi = \frac{E}{1-\nu^2}\left[\varepsilon_\phi - \nu\varepsilon_\theta\right] \tag{2.24}$$

$$\sigma_\theta = \frac{E}{1-\nu^2}\left[\varepsilon_\theta - \nu\varepsilon_\phi\right] \tag{2.25}$$

Introducing the normal forces instead of the stresses, we then obtain,

$$\varepsilon_\phi = \frac{1}{E}\left(\sigma_\phi - \nu\sigma_\theta\right) = \frac{1}{Et}\left(N_\phi - \nu N_\theta\right) \tag{2.26}$$

$$\varepsilon_\theta = \frac{1}{E}\left(\sigma_\theta - \nu\sigma_\phi\right) = \frac{1}{Et}\left(N_\theta - \nu N_\phi\right) \tag{2.27}$$

Using these results in equation (2.23), yields

$$\frac{dv}{d\phi} - v\cot\phi = \frac{1}{Et}\left[r_1\left(N_\phi - \nu N_\theta\right) - r_2\left(N_\theta - \nu N_\phi\right)\right]$$

$$= \frac{1}{Et}\left[\left(r_1 + \nu r_2\right)N_\phi - \left(r_2 + \nu r_1\right)N_\theta\right] \tag{2.28}$$

Integrating equation (2.28) by standard procedures yields

$$v = \sin\phi\left[\int\left(\frac{1}{\sin\phi}\right)\frac{1}{Et}\left[\left(r_1 + \nu r_2\right)N_\phi - \left(r_2 + \nu r_1\right)N_\theta\right]d\phi + c\right] \tag{2.29}$$

Where c is a constant of integration to be determined from a boundary condition.

Once this has been determined, w follows from equation (2.22) and (2.27)

$$w = r_2\varepsilon_\theta - v\cot\phi = \frac{r_2}{Et}\left(N_\theta - \nu N_\phi\right) - v\cot\phi \tag{2.30}$$

In practical calculations, only the horizontal displacement dr, henceforth denoted by δ, and the rotation V of the meridian, need to be known. The flexibility procedure for evaluating bending redundants M_e and H_e at the edge, involves superimposing the membrane solution deformation parameter δ and V with their counterparts associated with the application of arbitrary values of M_e and H_e, so that the net values of δ and V at a given shell edge are consistent with the actual boundary conditions at the edge, thereby allowing the redundant actions M_e and H_e to be solved[4]. The edge effect can then be quantified once M_e and H_e have been evaluated. The addition of their stresses to those steaming from the membrane solution yields the net stresses in the shell.

Since $\varepsilon_\theta = \frac{dr}{r} = \frac{\delta}{r}$, it follows that

$$\delta = r\varepsilon_\theta = (r_2 \sin\phi)\varepsilon_\theta \tag{2.31}$$

Eliminating ε_θ with equation (2.27), finally yields

$$\delta = \frac{1}{Et}(r_2 \sin\phi)(N_\theta - \nu N_\phi) \tag{2.32}$$

To obtain the meridional rotation V, consider Fig. 2.3 (e) and (f). As a result of the movement by v of E to E''' (Fig. 2.3(e)), the tangent at E rotates anticlockwise by $V_1 = d\phi = v/r_1$. As a result of the difference dw in the radial movement of the two ends of the line element (Fig. 2.3(f)), the line element rotates clockwise by $V_2 = d\phi = dw/(r_1 d\phi)$. Thus the net anticlockwise rotation V is obtained as

$$V = \frac{1}{r_1}\left(v - \frac{dw}{d\phi}\right) \tag{2.33}$$

Differentiation of equation (2.22) yields

$$\frac{dv}{d\phi}\cot\phi - \frac{v}{\sin^2\phi} + \frac{dw}{d\phi} = \frac{d}{d\phi}(r_2\varepsilon_\theta) = \frac{d}{d\phi}\left[\frac{r_2}{Et}(N_\theta - \nu N_\phi)\right] \tag{2.34}$$

Multiplying equation (2.28) by cot ϕ, yields

$$\frac{dv}{d\phi}\cot\phi - v\cot^2\phi = \frac{\cot\phi}{Et}[(r_1 + \nu r_2)N_\phi - (r_2 + \nu r_1)N_\theta] \tag{2.35}$$

Subtracting equation (2.34) from equation (2.35) yields

$$v - \frac{dw}{d\phi} = \frac{\cot\phi}{Et}[(r_1 + \nu r_2)N_\phi - (r_2 + \nu r_1)N_\theta] - \frac{d}{d\phi}\left[\frac{r_2}{Et}(N_\theta - \nu N_\phi)\right] \tag{2.36}$$

Substituting this result into equation (2.33) yields

$$V = \frac{1}{r_1}\left[\frac{\cot\phi}{Et}\{(r_1 + \nu r_2)N_\phi - (r_2 + \nu r_1)N_\theta\} - \frac{d}{d\phi}\left\{\frac{r_2}{Et}(N_\theta - \nu N_\phi)\right\}\right] \tag{2.37}$$

Thus δ and V at any point on the shell can be computed, once the stress resultants N_ϕ and N_θ of a problem have been obtained.

2.3 CONCLUDING REMARKS

Having examined the membrane solution for axisymmetrically loaded shells of revolution, and acknowledging that the membrane theory will fail at the edge-zones and point of discontinuity, the bending theory becomes of primary importance in such locations. This will be discussed in Chapter Three.

CHAPTER THREE

BENDING THEORY OF SHELLS OF REVOLUTION

3.1 INTRODUCTION

Many shells may achieve equilibrium through membrane action alone, provided the actual shells closely approach the conditions for membrane behaviour. For such shells, the bending is a secondary phenomenon often confined to narrow regions near boundaries, geometric discontinuities and concentrated loads. On the other hand, there are shells for which the membrane theory solution is grossly violated by the physical situation. The bending behaviour may alter the stress pattern from that computed by membrane theory in two ways. First and the most obvious, significant transverse shearing forces, and also bending and twisting moments can develop. Also, the pattern of the in-plane stress resultants may be altered markedly by the bending deformations. It is this latter possibility, whereby the transverse loading is resisted by a combination of in-plane forces and transverse shearing forces, which distinguishes the bending theory of plates. Although a shell may seriously violate the membrane theory requirements, there still remains the mechanism of resisting transverse loading primarily with in-plane forces, which is the basic initial attraction of this structural form[39].

According to Zingoni[4], the approach will be to consider the membrane solution as the particular integral of the general bending-theory equations, so solutions need only be found for the homogeneous bending-theory equations. These equations, with an adequate number of constants of integration, make the total solution adaptable to arbitrary axisymmetric boundary conditions prevailing at the shell edges, and account for the general localised edge effects. For the homogeneous solution, the surface-loading components P_ϕ and P_r are assumed to be zero (P_θ already being zero owing to axisymmetry), and the solution is found for the edge-loaded shell.

3.2 EQUILIBRIUM CONSIDERATIONS

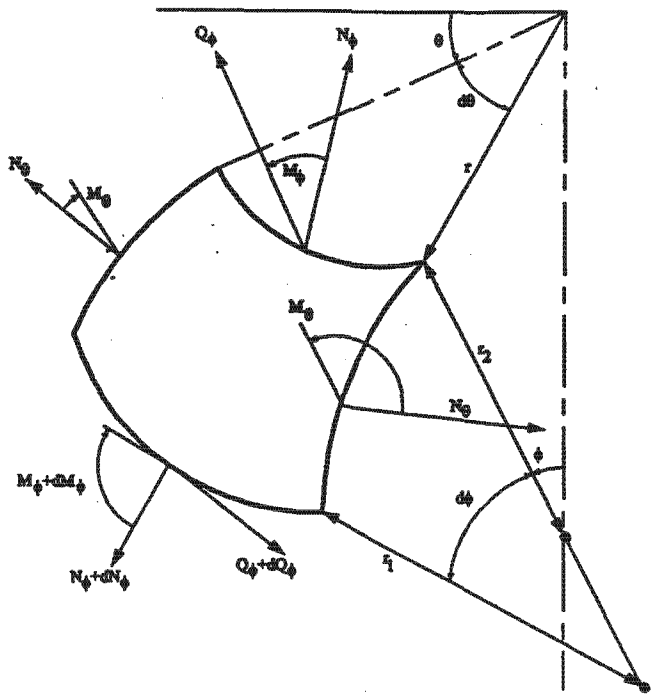

Fig. 3.1 Bending element of axisymmetrically-loaded shell of revolution

Figure 3.1 shows a shell element, which is cut out by two adjacent co-ordinates lines. Condition of symmetry dictates that only the resultants Q_ϕ, M_ϕ, Q_θ, M_θ, N_θ, N_ϕ exist, and that the normal forces N_θ and the bending moments M_θ cannot vary with θ. The notation for the radii of curvature and the angular orientation are identical with those of the membrane theory. The derivations that follow in the rest of this chapter are due to Zingoni[4].

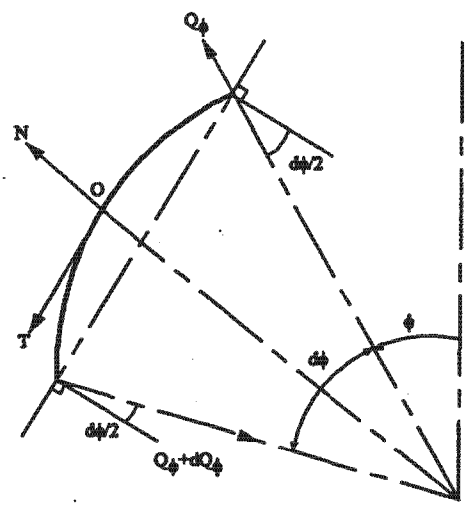

Fig. 3.2 Contributions of Q_ϕ to net forces in the directions OT & ON. Section of the element in the vertical plane of a meridian, showing transverse shears at upper & lower ends.

From Fig. 3.2, the resultant of the transverse shears in the direction OT is

$$-Q_\phi \cdot rd\theta \cdot \sin\frac{d\phi}{2} - (Q_\phi + dQ_\phi)(r+dr)d\theta \cdot \sin\frac{d\phi}{2} \approx -rQ_\phi \cdot d\theta d\phi$$

Summation of the contributions of the N_ϕ, N_θ and Q_ϕ actions in the direction of the tangent to a meridian (see section 2.2.2 for the contributions of N_ϕ *and* N_θ) yields

$$d(rN_\phi)\cdot d\theta - N_\theta \cdot r_1 \cos\phi \cdot d\phi d\theta - rQ_\phi \cdot d\phi d\theta = 0$$

Dividing throughout by $d\phi d\theta$ yields

$$\frac{d(rN_\phi)}{d\phi} - r_1 N_\theta \cos\phi - rQ_\phi = 0 \qquad (3.1)$$

Consider equilibrium of the shell element in the direction of the normal to the shell mid-surface. From Fig. 3.2, the resultant of the transverse shear in the direction ON is

$$Q_\phi \cdot rd\theta \cdot \cos\frac{d\phi}{2} - (Q_\phi + dQ_\phi)(r+dr)d\theta \cdot \cos\frac{d\phi}{2}$$

$$\approx -(Q_\phi \cdot dr + r \cdot dQ_\phi)d\theta = -d(rQ_\phi)d\theta$$

Summation of the contributions of the N_ϕ, N_θ and Q_ϕ actions in the direction of the normal to the shell mid-surface (in Chapter Two) yields

$$-rN_\phi \cdot d\phi d\theta - r_1 \sin\phi \cdot N_\theta \cdot d\phi d\theta - d(rQ_\phi)d\theta = 0$$

which, on dividing throughout by $d\phi d\theta$, becomes

$$rN_\phi + r_1 N_\theta \sin\phi + \frac{d(rQ_\phi)}{d\phi} = 0 \qquad (3.2)$$

Finally consider moment equilibrium of the shell element in the vertical meridional plane. Taking clockwise moments as positive (see Fig. 3.1 and 3.2), the net moment of the M_ϕ and Q_ϕ actions is approximately

$$(M_\phi + dM_\phi)\cdot(r+dr)d\theta - M_\phi \cdot rd\theta - Q_\phi \cdot rd\theta \cdot r_1 d\phi$$

$$\approx (M_\phi \cdot dr + r \cdot dM_\phi)d\theta - r_1 rQ_\phi d\phi d\theta$$

$$= d(rM_\phi)d\theta - r_1 rQ_\phi d\phi d\theta$$

The contribution of the resultant moment M_θ vectors in the direction of the (M_ϕ+dM_ϕ) vector is clearly

$$-2M_\theta \cdot r_1 d\phi \cdot \sin\frac{\gamma}{2} \approx -r_1 M_\theta \cdot \gamma d\phi$$

The length of the edges over which M_θ acts is $r_1 d\phi$, and since these sides are not parallel, the

angle γ is equal to $\cos\phi \cdot d\theta$. Therefore, the contribution of M_θ becomes

$$-r_1 M_\theta \cdot \cos\phi \cdot d\theta d\phi$$

Summation of the contribution of the M_ϕ, Q_ϕ and M_θ actions in the meridional plane yields

$$d(rM_\phi)d\theta - r_1 r Q_\phi d\phi d\theta - r_1 M_\theta \cos\phi d\phi d\theta = 0$$

dividing throughout by $d\phi d\theta$ *yields,*

$$\frac{d(rM_\phi)}{d\phi} - r_1 M_\theta \cos\phi - r_1 r Q_\phi = 0 \qquad (3.3)$$

Thus the equilibrium considerations yield three equations (3.1)–(3.3) in five unknowns N_ϕ, N_θ, M_ϕ, M_θ, Q_ϕ. In order to determine a solution, one will need to utilize the strain-displacement relations and Hooke's law.

3.3 STRAIN-DISPLACEMENT RELATIONS AND HOOK'S LAW

The parameters v and w are the displacements as defined in section 2.2.4, with the strain-displacement relations defined as

$$\varepsilon_\phi = \frac{1}{r_1}\left(\frac{dv}{d\phi} + w\right) \qquad (3.4a)$$

$$\varepsilon_\theta = \frac{1}{r_2}(v\cot\phi + w) \qquad (3.4b)$$

The relationship between direct stress and strain is given by

$$\varepsilon_\phi = \frac{1}{E}(\sigma_\phi - \nu\sigma_\theta) \qquad (3.5a)$$

$$\varepsilon_\theta = \frac{1}{E}(\sigma_\theta - \nu\sigma_\phi) \qquad (3.5b)$$

On rearranging

$$\sigma_\phi = \frac{E}{1-\nu^2}(\varepsilon_\phi - \nu\varepsilon_\theta) \qquad (3.6a)$$

$$\sigma_\theta = \frac{E}{1-\nu^2}(\varepsilon_\theta - \nu\varepsilon_\phi) \qquad (3.6b)$$

from which the stress resultants follow as

$$N_\phi = \sigma_\phi t = \frac{Et}{1-\nu^2}\left\{\frac{1}{r_1}\left(\frac{dv}{d\phi} + w\right) + \frac{\nu}{r_2}(v\cot\phi + w)\right\} \qquad (3.7a)$$

$$N_\theta = \sigma_\theta t = \frac{Et}{1-\nu^2}\left\{\frac{1}{r_2}(\nu\cot\phi + w) + \frac{\nu}{r_1}\left(\frac{dv}{d\phi} + w\right)\right\} \qquad (3.7b)$$

The bending moments M_ϕ and M_θ can be expressed in terms of the basic displacements v and w. Chapter Two defines the meridional rotation V at a point as

$$V = \frac{1}{r_1}\left(v - \frac{dw}{d\phi}\right) \qquad (3.8)$$

Now the change in the meridional curvature χ_ϕ is given approximately by the rate of change of meridional rotation with distance along the meridian, i.e. $|\chi_\phi| = \left|\frac{dV}{ds_\phi}\right|$. To deduce the correct sign of χ_ϕ relative to dV/ds_ϕ, consider Fig. 3.3, which shows a positive V (i.e. an anticlockwise rotation on the left side of the axis of revolution, in the meridional section of the shell of revolution) prescribed at the edges of shell caps closed over the top (ϕ=0) and over the bottom (ϕ=180^0). For the upper cap and in accordance with Saint Venant's principle, V tends to diminish in magnitude with increasing distance from the shell edge, i.e. with decreasing ϕ. Therefore $dV/d\phi$ is positive. However, the associated change of curvature χ_ϕ, which, by definition has the same sign as M_ϕ, is clearly negative at the upper diagram. For the lower cap, V also tends to diminish with increasing distance from the shell edge, i.e. with increasing ϕ, so that $dV/d\phi$ is negative.

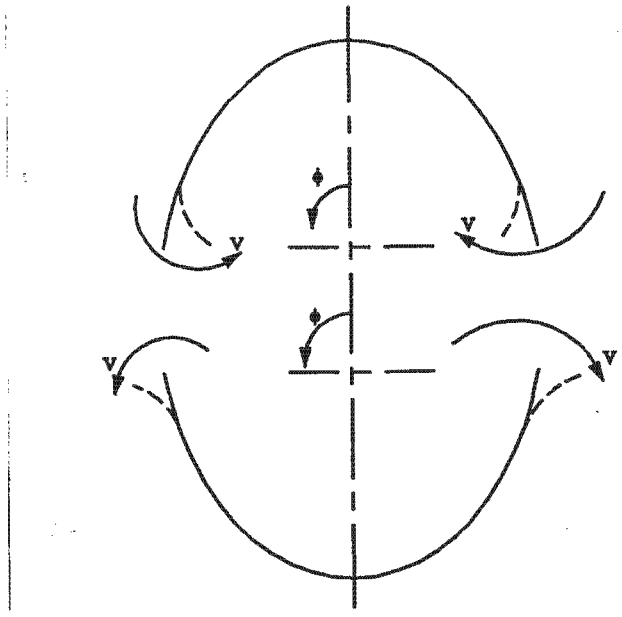

Fig. 3.3 Effect of V on the meridional curvature χ_ϕ

The associated change of curvature χ_ϕ that is of the same sign as would be produced by a positive moment M_ϕ applied at the edge, is positive in the lower diagram. In both cases, it has been established that the sign of $dV/d\phi$ in the vicinity of the shell edge is opposite to that of the associated χ_ϕ. Thus, the relationship between χ_ϕ and V, taking proper account of the positive sign conventions, must read

$$\chi_\phi \approx -\frac{dV}{ds_\phi} \tag{3.9}$$

But $ds_\phi = r_1 d\phi$. Therefore

$$\chi_\phi \approx -\frac{dV}{r_1 d\phi} = -\frac{1}{r_1}\frac{dV}{d\phi} = -\frac{1}{r_1}\frac{d}{d\phi}\left\{\frac{1}{r_1}\left(v - \frac{dw}{d\phi}\right)\right\} \tag{3.10}$$

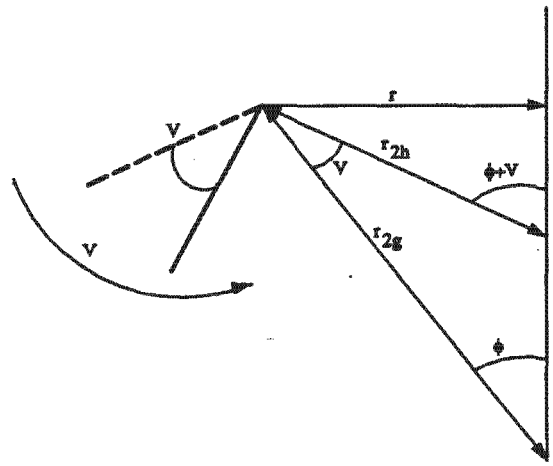

Fig. 3.4 Line element of shell in the meridional section, showing change of the second principal radius of curvature r_2 due to meridional rotation V.

As a result of the rotation V, the second principal radius of curvature r_2 changes, from an initial value of r_{2g} to r_{2h} Fig. 3.4. Therefore,

$$r_{2_g} \sin\phi = r_{2_h} \sin(\phi + V)$$

Now $$\sin(\phi + V) = \sin\phi\cos V + \cos\phi\sin V \approx \sin\phi + V\cos\phi$$

The last approximation being valid for small rotations V, $\cos V \approx 1$ and $\sin V \approx V$. Therefore

$$r_{2_g} \sin\phi = r_{2_h}(\sin\phi + V\cos\phi)$$

from which

$$r_{2h} = \frac{r_{2g} \sin\phi}{\sin\phi + V\cos\phi}$$

Hence

$$\frac{1}{r_{2h}} = \frac{\sin\phi + V\cos\phi}{r_{2g}\sin\phi} = \frac{1}{r_{2g}} + \frac{1}{r_{2g}} V\cot\phi$$

The change in second principal curvature χ_θ is given by

$$\begin{aligned}\chi_\theta &= -\left(\frac{1}{r_{2h}} - \frac{1}{r_{2g}}\right) \\ &= -\left(\frac{1}{r_{2g}} + \frac{1}{r_{2g}} v\cot\phi - \frac{1}{r_{2g}}\right) \\ &= -\frac{1}{r_{2g}} V\cot\phi\end{aligned} \tag{3.11}$$

Eliminating V from the above expression (using equation (3.8)), and dropping the subscript g of r_{2g} in order to return to the original notation, one may now write

$$\chi_\theta = -\frac{1}{r_1 r_2}\left(v - \frac{dw}{d\phi}\right)\cot\phi \tag{3.12}$$

For direct strains caused by bending, the following relations, similar to that for cylindrical shell, are,

$$\varepsilon_\phi = z\chi_\phi \tag{3.13a}$$

$$\varepsilon_\theta = z\chi_\theta \tag{3.13b}$$

Insert equation (3.13) into equation (3.6) yields

$$\sigma_\phi = \frac{Ez}{1-v^2}\left(\chi_\phi + v\chi_\theta\right) \tag{3.14a}$$

$$\sigma_\theta = \frac{Ez}{1-v^2}\left(\chi_\theta + v\chi_\phi\right) \tag{3.14b}$$

The bending moments M_ϕ and M_θ are given by the following expressions

$$M_\phi = \int_{-\frac{t}{2}}^{+\frac{t}{2}} \sigma_\phi \cdot z \cdot dz \tag{3.15a}$$

$$M_\theta = \int_{-\frac{t}{2}}^{+\frac{t}{2}} \sigma_\theta \cdot z \cdot dz \tag{3.15b}$$

where t is the shell thickness. Substituting σ_ϕ and σ_θ as given by equation (3.14), and performing the integration, these expressions become

$$M_\phi = D(\chi_\phi + \nu\chi_\theta) \tag{3.16a}$$

$$M_\theta = D(\chi_\theta + \nu\chi_\phi) \tag{3.16b}$$

where D is the flexural rigidity defined as

$$D = \frac{Et^3}{12(1-\nu^2)} \tag{3.17}$$

Substitution of the results for χ_ϕ and χ_θ, as given in equations (3.10) and (3.12) respectively, yields

$$M_\phi = -\frac{D}{r_1}\left[\frac{d}{d\phi}\left\{\frac{1}{r_1}\left(v - \frac{dw}{d\phi}\right)\right\} + \frac{\nu}{r_2}\left(v - \frac{dw}{d\phi}\right)\cot\phi\right] \tag{3.18a}$$

$$M_\theta = -\frac{D}{r_1}\left[\frac{1}{r_2}\left(v - \frac{dw}{d\phi}\right)\cot\phi + \nu\frac{d}{d\phi}\left\{\frac{1}{r_1}\left(v - \frac{dw}{d\phi}\right)\right\}\right] \tag{3.18b}$$

3.4 REDUCTION OF THE THREE EQUILIBRIUM EQUATIONS TO TWO DIFFERENTIAL EQUATIONS IN THE VARIABLE V AND Q_ϕ

Substitution of the expressions for the stress resultants N_ϕ and N_θ (equation (3.7)) and those for M_ϕ and M_θ (equation (3.18)) into the equilibrium equations (3.1)–(3.3) yields three equations in three unknowns, v, w and Q_ϕ, which, in principle, may then be solved in terms of these three variables. A simpler approach involves reducing equations (3.1)–(3.3) to two ordinary differential equations of second order, in the variables V and Q_ϕ, as follows. Expressions (3.18) are written as

$$M_\phi = -D\left\{\frac{1}{r_1}\frac{dV}{d\phi} + \frac{\nu}{r_2}V\cot\phi\right\} \tag{3.19a}$$

$$M_\theta = -D\left\{\frac{1}{r_2}V\cot\phi + \frac{\nu}{r_1}\frac{dV}{d\phi}\right\} \tag{3.19b}$$

V is as defined in expression (3.8). Substitution of these expressions for M_ϕ and M_θ into equation (3.3) yields, with r replaced by $r_2\sin\phi$

$$\frac{d}{d\phi}\left[(r_2\sin\phi)D\left\{\frac{1}{r_1}\frac{dV}{d\phi} + \frac{\nu}{r_2}V\cot\phi\right\}\right] - r_1 D\left\{\frac{1}{r_2}V\cot\phi + \frac{\nu}{r_1}\frac{dV}{d\phi}\right\}\cos\phi = -r_1 r_2(\sin\phi)Q_\phi$$

which, on simplification, becomes

$$\left[D\left(\frac{r_2}{r_1}\right)\sin\phi\right]\frac{d^2V}{d\phi^2}+\left[D\left(\frac{r_2}{r_1}\right)\cos\phi+\sin\phi\frac{d}{d\phi}\left(D\frac{r_2}{r_1}\right)\right]\frac{dV}{d\phi}+\left[\nu\left(\cos\phi\frac{dD}{d\phi}-D\sin\phi\right)-D\left(\frac{r_1}{r_2}\right)\frac{\cos^2\phi}{\sin\phi}\right]V$$

$$=-r_1r_2(\sin\phi)Q_\phi \qquad (3.20)$$

This second-order differential equation in V, with Q_ϕ appearing on the right-hand side only as a non-derivative term, is the first of the required governing equations. To obtain the second, we begin by establishing a relationship between N_ϕ and Q_ϕ. A comparison of equation (3.1) and (3.2) shows that N_θ may be eliminated between the two expressions by multiplying the first equation by *sin* ϕ and the second equation by *cos* ϕ, and then adding the expressions. The result becomes,

$$(\sin\phi)\frac{d(rN_\phi)}{d\phi}+(\cos\phi)rN_\phi-(\sin\phi)rQ_\phi+(\cos\phi)\frac{d(rQ_\phi)}{d\phi}=0$$

This may be written as

$$\frac{d}{d\phi}(rN_\phi\sin\phi)+\frac{d}{d\phi}(rQ_\phi\cos\phi)=0$$

implying that

$$rN_\phi\sin\phi=-rQ_\phi\cos\phi$$

i.e. $$N_\phi=-Q_\phi\cot\phi \qquad (3.21)$$

Substituting this result into equation (3.2) and rearranging, yields

$$N_\theta=\frac{1}{r_1\sin\phi}\left[rQ_\phi\cot\phi-\frac{d(rQ_\phi)}{d\phi}\right]=-\left(\frac{r_2}{r_1}\frac{dQ_\phi}{d\phi}+\frac{1}{r_1}\frac{dr_2}{d\phi}Q_\phi\right) \qquad (3.22)$$

The above expressions for N_ϕ and N_θ (equation (3.21) and (3.22) are substituted into the expression for V in terms of N_ϕ and N_θ in equation (2.37) to obtain an expression for V in terms of Q_ϕ

Thus the result is as follows

$$\frac{{r_2}^2}{tr_1}\frac{d^2Q_\phi}{d\phi^2}+\left[\frac{{r_2}^2}{tr_1}\cot\phi+\frac{r_2}{tr_1}\frac{dr_2}{d\phi}+\frac{d}{d\phi}\left(\frac{{r_2}^2}{tr_1}\right)\right]\frac{dQ_\phi}{d\phi}+$$

$$\left[\frac{r_2}{tr_1}\frac{d^2r_2}{d\phi^2}+\left\{\frac{d}{d\phi}\left(\frac{r_2}{tr_1}\right)\right\}\frac{dr_2}{d\phi}+\left\{\left(\frac{r_2+\nu r_1}{r_1}\right)\frac{dr_2}{d\phi}-(r_1+\nu r_2)\cot\phi\right\}\frac{\cot\phi}{t}-\nu\left\{(\cot\phi)\frac{d}{d\phi}\left(\frac{r_2}{t}\right)-\left(\frac{r_2}{t}\right)\frac{1}{\sin^2\phi}\right\}\right]Q_\phi$$

$$=r_1EV \qquad (3.23)$$

where E and ν are the material properties which are assumed to be constant throughout the shell.

Equations (3.20) and (3.23) are the required governing differential equations for axisymmetric bending of shells of revolution. Due to the complexity of the coefficients of the differential terms, it would be extremely difficult to find a general solution for these equations. Only for special geometries like sphere, circular torus, circular cylinder and circular cone can a solution be obtained.

3.5 CONCLUDING REMARKS

After considering the membrane theory in Chapter Two and the governing equations for axisymmetric bending of shells of revolution in Chapter Three, it is imperative to use the membrane theory to derive closed-form analytical results for cooling towers subjected to axisymmetric loading. This will be done in the next chapter.

CHAPTER FOUR

SELF-WEIGHT STRESSES IN COOLING TOWERS

4.1 INTRODUCTION

Generally in evaluating the ultimate strength of cooling tower shells, the dead weight and wind load are considered as the primary load. Numerous researchers have worked tirelessly aiming at gathering accurate data as well as quantifying the effects of wind load on the structure[23,24,26]. Regardless of whether it is self-weight, wind load or a combination of the two which is being considered, the choice of cooling tower thickness is governed by buckling rather than material strength considerations. In this regard, it may be noted that the local buckling occurs when the combination of membrane hoop and meridional stresses at a given point, regardless of the actual loading on the cooling tower, becomes critical. [22,40]

However, self-weight remains the most basic loading for cooling towers, effective from the moment of construction. Being axisymmetric in distribution, and invariant with time, self-weight is clearly more amenable to closed-form analytical study than the generally non-axisymmetric and time-dependant wind loading. In this respect, stresses associated with self-weight can be quickly computed to form the basis of initial proportioning of the cooling tower and other preliminary design considerations.[41] Self-weight has also been shown to be the predominant cause of shape distortion observed in old cooling towers.

The present chapter focuses on self-weight, and presents explicit closed-form results for membrane stresses in hyperbolic cooling towers as developed by Zingoni,[41] for arbitrary geometry incorporating an offset parameter A, for a number of different patterns of shell-thickness variation along the meridian of the cooling tower. The derivational details and closed-form analytical results, which will form the basis of the parametric studies of this thesis and are thus of crucial importance, are reproduced here (for convenience) from the paper by Zingoni,[41] with the kind permission of the author and the publisher.

4.2 GEOMETRIC PARAMETERS

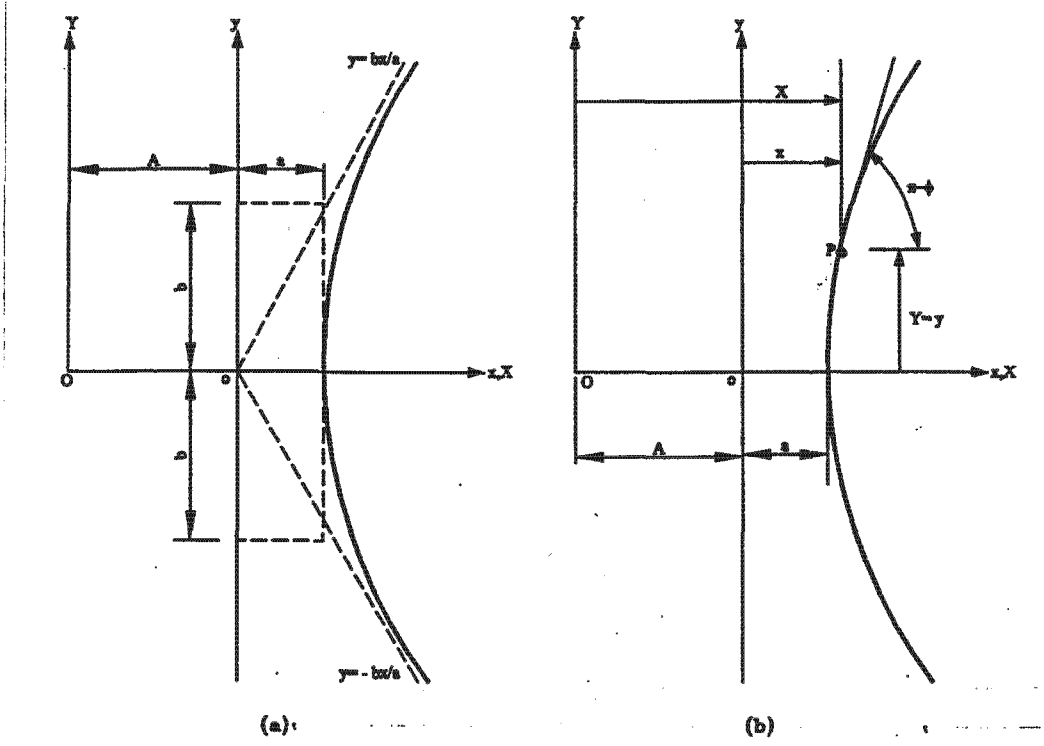

Fig. 4.1 Generating meridian of general hyperbolic cooling tower, showing:
(a) Offset parameters a, b, A in the (x,y) and (X,Y) Cartesian coordinate systems;
(b) The coordinate distances x, y, X and Y, and angular parameter (π-ϕ), corresponding to a given point P on the meridian.

Figure 4.1 shows a portion of the meridian of a hyperboloid of revolution of any vertical plane containing the axis of revolution of the cooling tower, with the Y axis being the (vertical) axis of revolution of the cooling tower, and the y axis being the vertical axis of the hyperbola comprising the shell meridian; the distance between the Y and y axes is the offset parameter A. The horizontal axes x and X are coincident, and located at the level corresponding to the "waist" (that is, the horizontal cross-section of smallest diameter) of the cooling tower; their intercept with the Y and y axes are the origins O and o of the (X,Y) and (x,y) Cartesian coordinate systems respectively. If the horizontal and vertical semi-axes of the generating hyperbola of the cooling tower are a and b respectively, as depicted in the figure, then the equation of this hyperbola in terms of the coordinate x and y is

$$\frac{x^2}{a^2} - \frac{y^2}{b^2} = 1 \qquad (4.1)$$

From Fig 4.1(b)

$$x = X - A \tag{4.2a}$$

$$y = Y \tag{4.2b}$$

Therefore we may rewrite equation (4.1) as

$$\frac{(X-A)^2}{a^2} - \frac{Y^2}{b^2} = 1 \tag{4.3}$$

giving

$$Y = \pm \frac{b}{a}\left[(X-A)^2 - a^2\right]^{\frac{1}{2}} \tag{4.4}$$

Differentiating equation (4.3) with respect to X, we obtain,

$$\frac{dY}{dX} = \pm \frac{b}{a} \frac{X-A}{\left[(X-A)^2 - a^2\right]^{1/2}} = -\tan\phi \tag{4.5}$$

Where ϕ is the meridional angle at any given point P defined by the Cartesian coordinates $\{X,Y\}$, ϕ is measured clockwise around point Q from the upward branch of the axis of revolution to the normal of the shell midsurface through point P (Fig. 4.2). It may be noted that ϕ decreases in magnitude from the top to bottom of the meridian of the cooling tower.

From equation (4.5), we have

$$\tan^2\phi = \frac{b^2}{a^2} \frac{(X-A)^2}{\left[(X-A)^2 - a^2\right]} \tag{4.6}$$

which upon solving gives

$$(X-A)^2 = \frac{a^4 \tan^2\phi}{a^2\tan^2\phi - b^2} \tag{4.7}$$

that is, for the meridian in the positive x domain

$$X - A = \frac{a^2\tan\phi}{\left(a^2\tan^2\phi - b^2\right)^{1/2}} = \frac{a^2\sin\phi}{\left(a^2\sin^2\phi - b^2\cos^2\phi\right)^{1/2}} \tag{4.8}$$

This solution is real and finite if

$$a^2\sin^2\phi > b^2\cos^2\phi \tag{4.9}$$

That is, if

$$\tan^2\phi > \frac{b^2}{a^2} \tag{4.10}$$

which, from equation (4.6), is always so for a hyperbolic meridian.

From equation (4.8), we can write

$$X = A + \frac{a^2 \sin\phi}{\left(a^2 \sin^2\phi - b^2 \cos^2\phi\right)^{1/2}} \tag{4.11}$$

Substitute equation (4.8) into equation (4.4), and we obtain

$$Y = \pm\frac{b}{a}\left[\frac{a^4 \sin^2\phi}{\left(a^2 \sin^2\phi - b^2 \cos^2\phi\right)} - a^2\right]^{1/2} \tag{4.12}$$

This then simplifies to

$$Y = \pm\frac{b^2 \cos\phi}{\left(a^2 \sin^2\phi - b^2 \cos^2\phi\right)^{1/2}} \tag{4.13}$$

The first principal radius of curvature r_1 at a given point P of the shell of revolution is the radius of curvature of the meridian at point P, that is, the distance between P and the centre of curvature C of the infinitesimal portion of meridian adjoining point P (Fig 4.2), and can be derived from a well-known result from plane-curve geometry. For example

$$r_1 = \frac{\left[1 + \left(\frac{dY}{dX}\right)^2\right]^{3/2}}{\frac{d^2Y}{d^2X}} \tag{4.14}$$

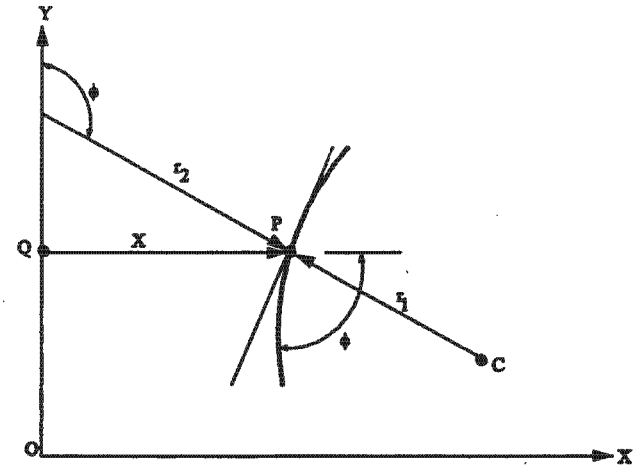

Fig. 4.2. Angular coordinate ϕ and principal radii of curvature r_1 and r_2 at point P on the meridian of the cooling tower.

From equation (4.5),

$$\frac{d^2Y}{dX^2} = \pm\frac{ab}{\left[(X - A)^2 - a^2\right]^{3/2}} \tag{4.15}$$

Substituting equations (4.5) and (4.15) into equation (4.14), we obtain

$$r_1 = \pm \frac{\left[\left(a^2 + b^2\right)(X - A)^2 - a^4\right]^{3/2}}{a^4 b} \tag{4.16}$$

Replacing $(X–A)$ in the above expression with the result in equation (4.8), we obtain, after further simplifications

$$r_1 = \pm \frac{a^2 b^2}{\left(a^2 \sin^2 \phi - b^2 \cos^2 \phi\right)^{3/2}} \tag{4.17}$$

Now, r_1, must be taken as negative being on the side of the shell mid-surface opposite to that, on which the axis of revolution lies, must be taken as negative, that is

$$r_1 = -\frac{a^2 b^2}{\left(a^2 \sin^2 \phi - b^2 \cos^2 \phi\right)^{3/2}} \tag{4.18}$$

The second principal radius of curvature r_2 at a given point P of a shell of revolution is given by the distance between P and the intercept Q of the normal to the shell mid-surface at P on the axis of revolution of the shell (Figure 4.2). Thus, and making use of result (4.11)

$$r_2 = \frac{X}{\sin \phi} = \frac{A}{\sin \phi} + \frac{a^2}{\left(a^2 \sin^2 \phi - b^2 \cos^2 \phi\right)^{1/2}} \tag{4.19}$$

4.3 LOADING COMPONENTS

Let q be the downward vertical loading per unit area of the shell mid-surface. If $t(\phi)$ is the shell thickness at any given point P defined by the coordinate ϕ, and γ is the weight per unit volume of the shell material, then q is the self-weight loading, given by

$$q = \gamma t(\phi) \tag{4.20}$$

Resolving this loading into two components: P_ϕ (tangential to the meridian, and always pointing downward the base of the cooling tower) and P_r (perpendicular to the shell mid-surface, and always pointing away from the axis of revolution of the cooling tower). These components are depicted in Fig. 4.3, from which we can see that

$$P_\phi = q \sin \phi = \{\gamma t(\phi)\} \sin \phi \tag{4.21a}$$

$$P_r = -q \cos \phi = -\{\gamma t(\phi)\} \sin \phi \tag{4.21b}$$

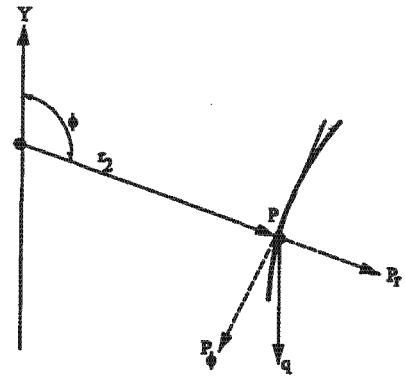

Fig. 4.3 Self-weight loading components P_ϕ and P_r at the point P on the meridian of the cooling tower.

4.4 GENERALISED SELF-WEIGHT STRESSES

For axisymmetrically loaded shells of revolution, the membrane-solution expressions for N_ϕ (meridional stress resultant) and N_θ (hoop stress resultant) have been dealt with in chapter Two (equation 2.11 and 2.15). For a cooling tower with a free top edge, for instance, the stress resultant N_ϕ, while generally being non-zero over the interior regions of the shell material, must vanish at the top edge of the cooling tower. The value of ϕ at the top opening of the cooling tower is denoted as ϕ_0, N_ϕ is set equal to zero when $\phi=\phi_0$, and the constant c is evaluated which may then be eliminated from equation (2.15) to yield an explicit analytical result for the stress resultant N_ϕ. The hoop stress resultants then follow from equation (2.11).

For a cooling tower with a ring beam around the top edge, we may impose the condition, as a way of evaluating the constant C, that the lateral/ horizontal displacement of the edge of the shell under membrane action stemming from the self-weight of the shell must match the lateral/horizontal displacement of the prescribed ring beam under the shell action N_ϕ and N_θ existing at the shell edges.

Once the membrane stress resultant N_ϕ and N_θ have been evaluated, they may be converted into actual stresses σ_ϕ (meridional) and σ_θ (hoop) within the shell material (and constant across the shell thickness at a given location on the cooling tower), by simply dividing by the shell thickness $t(\phi)$ at the location in question:

$$\sigma_\phi = \frac{N_\phi}{t(\phi)} \qquad (4.22a)$$

$$\sigma_\theta = \frac{N_\theta}{t(\phi)} \tag{4.22b}$$

Since all stresses in the shell can be considered fully determined once the stress resultant N_ϕ at any given point has been fully evaluated, there is need to recall the general solution for N_ϕ (equation 2.15), develop a general expression for N_ϕ due to self-weight in a general hyperbolic cooling tower, and then explore several different cases of shell-thickness variation along a meridian of the cooling tower. From equation (4.19)

$$r_2 \sin^2\phi = \frac{A\sin\phi\left(a^2\sin^2\phi - b^2\cos^2\phi\right)^{\frac{1}{2}} + a^2\sin^2\phi}{\left(a^2\sin^2\phi - b^2\cos^2\phi\right)^{\frac{1}{2}}} \tag{4.23}$$

Letting

$$F = \frac{1}{r_2\sin^2\phi} = \frac{\left(a^2\sin^2\phi - b^2\cos^2\right)^{\frac{1}{2}}}{A\sin\phi\left(a^2\sin^2\phi - b^2\cos^2\phi\right)^{\frac{1}{2}} + a^2\sin^2\phi} \tag{4.24}$$

and making use of expression (4.18), (4.19) and (4.21) to eliminate r_1, r_2 and (P_r, P_ϕ) from equation (2.15), we can reduce the expression for N_ϕ to

$$N_\phi = F\left[c_1\int\frac{t(\phi)}{\left(a^2\sin^2\phi - b^2\cos^2\phi\right)^{\frac{3}{2}}}d\phi + c_2\int\frac{(\sin\phi)t(\phi)}{(a^2\sin^2\phi - b^2\cos^2\phi)^2}d\phi + c\right] \tag{4.25}$$

Where

$$C_1 = \gamma A a^2 b^2 \tag{4.26a}$$

$$C_2 = \gamma a^4 b^2 \tag{4.26b}$$

4.5 VARIOUS CASES OF SHELL-THICKNESS VARIATION

This section shall consider various shell thickness variations as developed by Zingoni[41].

4.5.1 Generalised Stress Resultants

Case I: t constant

Expression (4.25) becomes

$$N_\phi = F\left[c_1 tI_1 + c_2 tI_2 + c\right] \tag{4.27}$$

Where c_1 and c_2 are as defined in equation (4.26), while I_1 and I_2 are the integrals

$$I_1 = \int\frac{1}{(a^2\sin^2\phi - b^2\cos^2\phi)^{\frac{3}{2}}}d\phi \tag{4.28}$$

$$I_2 = \int \frac{\sin\phi}{\left(a^2\sin^2\phi - b^2\cos^2\phi\right)^2} d\phi \tag{4.29}$$

Case II: t proportional to the horizontal distance X

Let

$$t(\phi) = kX = kA + \frac{ka^2\sin\phi}{\left(a^2\sin^2\phi - b^2\cos^2\phi\right)^{\frac{1}{2}}} \tag{4.30}$$

where k is a constant and X is given by equation (4.11). Expression (4.25) becomes

$$N_\phi = F\left[c_1\left(kA\int \frac{1}{(a^2\sin^2\phi - b^2\cos^2\phi)^{\frac{3}{2}}} d\phi + ka^2\int \frac{\sin\phi}{\left(a^2\sin^2\phi - b^2\cos^2\phi\right)^2} d\phi \right) \right.$$

$$\left. + c_2\left(kA\int \frac{\sin\phi}{\left(a^2\sin^2\phi - b^2\cos^2\phi\right)^2} d\phi + ka^2\int \frac{\sin^2\phi}{\left(a^2\sin^2\phi - b^2\cos^2\phi\right)^{\frac{5}{2}}} d\phi \right] + c \right)$$

$$= F\left[c_1\left(kAI_1 + ka^2I_2\right) + c_2\left(kAI_2 + ka^2I_3\right) + c\right]$$

$$= F\left[c_1kAI_1 + \left(c_1a^2 + c_2A\right)kI_2 + c_2ka^2I_3 + c\right] \tag{4.31}$$

where F, k, a, A, c, c_1, c_2, I_1, I_2 are as previously defined, and I_3 is given by

$$I_3 = \int \frac{\sin^2\phi}{\left(a^2\sin^2\phi - b^2\cos^2\phi\right)^{\frac{5}{2}}} d\phi \tag{4.32}$$

Case III: t proportional to X^2 (square of the horizontal radius X)

Let

$$t(\phi) = KX^2$$

$$= K\left[A^2 + \frac{2Aa^2\sin\phi}{\left(a^2\sin^2\phi - b^2\cos^2\phi\right)^{\frac{1}{2}}} + \frac{a^4\sin^2\phi}{\left(a^2\sin^2\phi - b^2\cos^2\phi\right)} \right]$$

$$= KA^2 + 2KAa^2\frac{\sin\phi}{\left(a^2\sin^2\phi - b^2\cos^2\phi\right)^{\frac{1}{2}}} + Ka^4\left(\frac{\sin^2\phi}{a^2\sin^2\phi - b^2\cos^2\phi}\right) \tag{4.33}$$

Using the function of the shell thickness in expression (4.25), we obtain

$$N_\phi = F\left[c_1\left(KA^2\int\frac{1}{\left(a^2\sin^2\phi - b^2\cos^2\phi\right)^{\frac{3}{2}}}d\phi + 2KAa^2\int\frac{\sin\phi}{\left(a^2\sin^2\phi - b^2\cos^2\phi\right)^{2}}d\phi\right.\right.$$

$$\left. + Ka^4\int\frac{\sin^2\phi}{\left(a^2\sin^2\phi - b^2\cos^2\phi\right)^{\frac{5}{2}}}d\phi\right) + c_2\left(KA^2\int\frac{\sin\phi}{\left(a^2\sin^2\phi - b^2\cos^2\phi\right)^{2}}d\phi\right.$$

$$\left.\left. + 2KAa^2\int\frac{\sin^2\phi}{\left(a^2\sin^2\phi - b^2\cos^2\phi\right)^{\frac{5}{2}}}d\phi + Ka^4\int\frac{\sin^3\phi}{\left(a^2\sin^2\phi - b^2\cos^2\phi\right)^{3}}d\phi\right) + c\right]$$

$$= F\left[c_1\left(KA^2I_1 + 2KAa^2I_2 + Ka^4I_3\right) + c_2\left(KA^2I_2 + 2KAa^2I_3 + Ka^4I_4\right) + c\right]$$

$$= F\left[c_1KA^2I_1 + \left(2c_1a^2 + c_2A\right)KAI_2 + \left(c_1a^2 + 2c_2A\right)Ka^2I_3 + c_2Ka^4I_4 + c\right] \qquad (4.34)$$

where F, k, a, A, c, c_1, c_2, I_2 and I_3 have previously been defined, and the integral I_4 is given by

$$I_4 = \int\frac{\sin^3\phi}{\left(a^2\sin^2\phi - b^2\cos^2\phi\right)^{3}}d\phi \qquad (4.35)$$

Case IV: t varying linearly with arc length s along the meridian

Let us define the arc length s as the distance from the top of the cooling tower (corresponding to $\phi = \phi_0$) along a meridian to the point in question (corresponding to the coordinate ϕ) as depicted in Fig. 4.4(a).

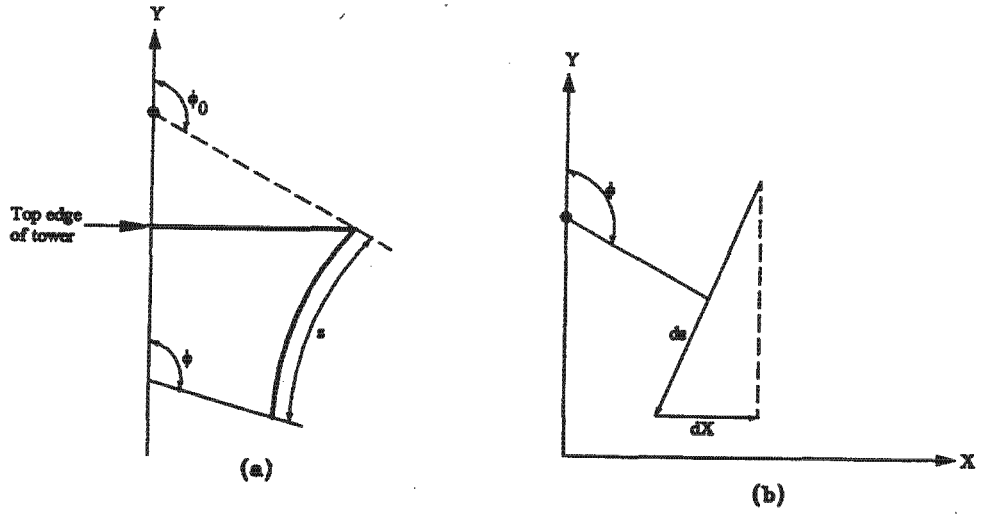

Fig. 4.4.Arc-length parameters along a meridian (a) measurement of arc lengths (b) arc-length element ds at coordinate ϕ

By reference to Figure 4.4(b), the relationship between an increment dX in the positive X direction is given by

$$ds = \frac{dX}{\cos\phi} \tag{4.36}$$

From equation (4.11), and after some simplifications, we obtain

$$dX = -a^2b^2 \frac{\cos\phi}{\left(a^2\sin^2\phi - b^2\cos^2\phi\right)^{\frac{3}{2}}} d\phi \tag{4.37}$$

Integrating both sides of equation (4.36), and making use of result (4.37), we obtain

$$s = \int \frac{dX}{\cos\phi} = -a^2b^2 \int_{\phi}^{\phi_0} \frac{1}{\left(a^2\sin^2\phi - b^2\cos^2\phi\right)^{\frac{3}{2}}} d\phi = a^2b^2 \left[I_1\right]_{\phi_0}^{\phi} \tag{4.38}$$

where $\left[I_1\right]_{\phi_0}^{\phi}$ is the magnitude of the integral I_1 evaluated as a definite integral between the limits ϕ_0 and ϕ. Note that $\left[I_1\right]_{\phi_0}^{\phi}$ is a function of ϕ.

Since the shell thickness t varies linearly with arc length s measured along a meridian from the top of the cooling tower, we may write

$$t(\phi) = t_0 + Cs = t_0 + Ca^2b^2\left[I_1\right]_{\phi_0}^{\phi} \tag{4.39}$$

where t_0 is the shell thickness at the top (s=0) and C is the constant.

Substituting the above expression for $t(\phi)$ into equation (4.25), we obtain

$$N_\phi = F\left[c_1\left(t_0 \int \frac{1}{\left(a^2\sin^2\phi - b^2\cos^2\phi\right)^{\frac{3}{2}}} d\phi + Ca^2b^2 \int \frac{\left[I_1\right]_{\phi_0}^{\phi}}{\left(a^2\sin^2\phi - b^2\cos^2\phi\right)^{\frac{3}{2}}} d\phi \right) \right.$$

$$\left. + c_2\left(t_0 \int \frac{\sin\phi}{\left(a^2\sin^2\phi - b^2\cos^2\phi\right)^{2}} d\phi + Ca^2b^2 \int \frac{(\sin\phi)\left[I_1\right]_{\phi_0}^{\phi}}{\left(a^2\sin^2\phi - b^2\cos^2\phi\right)^{2}} d\phi \right] + c \right)$$

$$= F\left[c_1\left(t_0 I_1 + Ca^2b^2 I_5\right) + c_2\left(t_0 I_2 + Ca^2b^2 I_6\right) + c\right]$$

$$= F\left[c_1 t_0 I_1 + c_2 t_0 I_2 + c_1 Ca^2b^2 I_5 + c_2 Ca^2b^2 I_6 + c\right] \tag{4.40}$$

where

$$I_5 = \int \frac{\left[I_1\right]_{\phi_0}^{\phi}}{\left(a^2\sin^2\phi - b^2\cos^2\phi\right)^{\frac{3}{2}}} d\phi \tag{4.41}$$

$$I_6 = \int \frac{(\sin\phi)\left[I_1\right]_{\phi_0}^{\phi}}{\left(a^2\sin^2\phi - b^2\cos^2\phi\right)^{2}} d\phi \tag{4.42}$$

For all the four cases of shell-thickness variation, the self-weight meridional stress resultant N_ϕ and the hoop stress resultant N_θ as well as the actual stress σ_ϕ and σ_θ can be evaluated analytically provided the integrals $I_1, I_2, I_3, I_4, I_5, I_6$ can be evaluated analytically.

4.5.2 Integrals I_1, I_2, I_3, I_4, I_5 and I_6

The evaluation of I_2 and I_4 yields the following explicit results:

$$I_2 = -\frac{1}{2a^2(a^2+b^2)}\left\{\frac{(a^2+b^2)\cos\phi}{a^2-(a^2+b^2)\cos^2\phi}+\frac{\sqrt{a^2+b^2}}{2a}\ln\left|\frac{a+\sqrt{a^2+b^2}\cos\phi}{a-\sqrt{a^2+b^2}\cos\phi}\right|\right\} \tag{4.43}$$

$$I_4 = -\frac{1}{a^2(a^2+b^2)^2}\left[\frac{b^2(a^2+b^2)\cos\phi}{4\left[a^2-(a^2+b^2)\cos^2\phi\right]^2}+\left(\frac{4a^2+3b^2}{8a^2}\right)\times\right.$$
$$\left.\left\{\frac{(a^2+b^2)\cos\phi}{a^2-(a^2+b^2)\cos^2\phi}+\frac{\sqrt{a^2+b^2}}{2a}\ln\left|\frac{a+\sqrt{a^2+b^2}\cos\phi}{a-\sqrt{a^2+b^2}\cos\phi}\right|\right\}\right] \tag{4.44}$$

The expressions for I_2 and I_4 are valid provided

$$\frac{a^2}{a^2+b^2} > \cos^2\phi \tag{4.45}$$

which is always satisfied for a hyperbolic cooling tower.

The integrals I_1 and I_3 may readily be shown to be elliptic integrals. Evaluating these, we obtain the results

$$I_1 = \frac{1}{b^3}\left[\left(\frac{1}{1-\beta^2}\right)\left\{\frac{1}{\beta}H\left(\varphi,\frac{\sqrt{\beta^2-1}}{\beta}\right)-\beta G\left(\varphi,\frac{\sqrt{\beta^2-1}}{\beta}\right)\right\}\right.$$
$$\left.+\left(\frac{\beta^2}{1-\beta^2}\right)\left\{\frac{\sin\phi\cos\phi}{(\beta^2\sin^2\phi-1)^{\frac{1}{2}}}\right\}\right] \tag{4.46}$$

$$I_3 = \frac{1}{b^5}\left[\left\{\frac{-2}{3\beta(1-\beta^2)^2}\right\}H\left(\varphi,\frac{\sqrt{\beta^2-1}}{\beta}\right)+\left\{\frac{\beta^2+1}{3\beta(1-\beta^2)^2}\right\}G\left(\varphi,\frac{\sqrt{\beta^2-1}}{\beta}\right)\right.$$
$$\left.-\left\{\frac{\beta^2(\beta^2+1)\sin^2\phi-2}{3(1-\beta)^2(\beta^2\sin^2\phi-1)^{\frac{3}{2}}}\right\}\sin\phi\cos\phi\right] \tag{4.47}$$

where

$$\beta^2 = \frac{a^2+b^2}{b^2} \qquad (>1) \tag{4.48a}$$

$$\varphi = \sin^{-1}\left(\frac{\beta\cos\phi}{\sqrt{\beta^2-1}}\right) \tag{4.48b}$$

with the functions $H(\theta,\lambda)$ and $G(\theta,\lambda)$ being elliptic integrals of the first and second kind respectively, defined as follows:

$$H(\theta,\lambda)=\int_0^{\theta}\frac{d\phi}{\sqrt{1-\lambda^2\sin^2\phi}}d\phi \tag{4.49a}$$

$$G(\theta,\lambda)=\int_0^{\theta}\sqrt{1-\lambda^2\sin^2\phi}d\phi \tag{4.49b}$$

For any given combination of parameters θ and λ, elliptic integrals $H(\theta,\lambda)$ and $G(\theta,\lambda)$ may be read from standard tables[42].

4.5.3 Special Case: A=0

When the offset parameter A is equal to zero, the axis of revolution (Y) of the cooling tower coincides with the axis y of the generating hyperbola. Consider the value of F when A=0 to be F_0. Equation (4.24) then becomes,

$$F_0=\frac{\left(a^2\sin^2\phi-b^2\cos^2\phi\right)^{\frac{1}{2}}}{a^2\sin^2\phi} \tag{4.50}$$

From equation (4.26a), the parameter c_1 also vanishes, i.e. c_1=0 when A=0.

Case I: t = constant

Inserting $c_1 = 0$ in expression (27), with F=F_0, we obtain

$$N_\phi = F_0\left[c_2 t I_2 + c\right] \tag{4.51}$$

Upon eliminating c_2, I_2, F_0, on the basis of expressions (4.26b), (4.43) and (4.50) respectively, we obtain

$$N_\phi=\frac{\left(a^2\sin^2\phi-b^2\cos^2\phi\right)^{\frac{1}{2}}}{a^2\sin^2\phi}\left[-\left\{\frac{\gamma a^2b^2t}{2\left(a^2+b^2\right)}\right\}\times\left\{\frac{\left(a^2+b^2\right)\cos\phi}{a^2-\left(a^2+b^2\right)\cos^2\phi}\right.\right.$$
$$\left.\left.+\frac{\sqrt{a^2+b^2}}{2a}\ln\left|\frac{a+\sqrt{a^2+b^2}\cos\phi}{a-\sqrt{a^2+b^2}\cos\phi}\right|\right\}+c\right] \tag{4.52}$$

Assuming the top of the cooling tower is free, the boundary condition N_ϕ=0 at ϕ=ϕ_0 yields the result

$$c=\frac{\gamma a^2b^2t}{2\left(a^2+b^2\right)}\left\{\frac{\left(a^2+b^2\right)\cos\phi_0}{a^2-\left(a^2+b^2\right)\cos\phi}+\frac{\sqrt{a^2+b^2}}{2a}\ln\left|\frac{a+\sqrt{a^2+b^2}\cos\phi_0}{a-\sqrt{a^2+b^2}\cos\phi_0}\right|\right\} \tag{4.53}$$

so that expression (4.52) finally becomes

$$N_\phi=\frac{\gamma b^2t\left(a^2\sin^2\phi-b^2\cos^2\phi\right)^{\frac{1}{2}}}{2\left(a^2+b^2\right)\sin^2\phi}\times\left[\left(a^2+b^2\right)\left\{\frac{\cos\phi_0}{a^2-\left(a^2+b^2\right)\cos^2\phi_0}\,\frac{\cos\phi}{a^2-\left(a^2+b^2\right)\cos^2\phi}\right\}\right.$$

$$\left.+\frac{\sqrt{a^2+b^2}}{2a}\ln\left|\left(\frac{a+\sqrt{a^2+b^2}\cos\phi_0}{a-\sqrt{a^2+b^2}\cos\phi_0}\right)\left(\frac{a-\sqrt{a^2+b^2}\cos\phi}{a+\sqrt{a^2+b^2}\cos\phi}\right)\right|\right] \tag{4.54}$$

When A=0, the expression for r_2 (equation 4.19) reduces to

$$r_2=\frac{a^2}{\left(a^2\sin^2\phi-b^2\cos^2\phi\right)^{\frac{1}{2}}} \tag{4.55}$$

Eliminating the geometric parameter r_1 and r_2 on the basis of equations (4.17) and (4.55) respectively, and the loading parameter P_r on the basis of equations (4.21b), we may write expression (2.11) for hoop stress resultant N_θ, for the special case of A=0, in the following general form:

$$N_\theta=r_2P_r-\frac{r_2}{r_1}N_\phi$$

$$=\left(\frac{a^2\sin^2\phi-b^2\cos^2\phi}{b^2}\right)N_\phi-\frac{\gamma a^2t(\phi)\cos\phi}{\left(a^2\sin^2\phi-b^2\cos^2\phi\right)^{\frac{1}{2}}} \tag{4.56}$$

For the present case where t is a constant, N_θ is therefore

$$N_\theta=\left(\frac{a^2\sin^2\phi+b^2\cos^2\phi}{b^2}\right)N_\phi-\frac{\gamma a^2t\cos\phi}{\left(a^2\sin^2\phi-b^2\cos^2\phi\right)^{\frac{1}{2}}} \tag{4.57}$$

Case II: t proportional to the horizontal distance X

With c_1=0, A=0 and F=F_0, expression (4.34) reduces to

$$N_\phi=F_0\left[c_2ka^2I_3+c\right] \tag{4.58}$$

where c_2, I_3 and F_0 are as defined by equation (4.26b), (4.47) and (4.50), while c is determined from the boundary condition for N_ϕ at the top of the cooling tower.

Case III: t is proportional to X^2

With c_1=0, A=0 and F=F_0, expression (4.34) reduces to.

$$N_\phi = F_0\left[c_2 K a^4 I_4 + c\right] \tag{4.59}$$

Upon eliminating c_2, I_4 and F_0 on the basis of expression (4.26b), (4.44) and (4.50) respectively, we obtain

$$N_\phi = \frac{\left(a^2\sin^2\phi - b^2\cos^2\phi\right)^{\frac{1}{2}}}{a^2\sin^2\phi}\times\left[-\frac{\gamma a^6 b^2 K}{(a^2+b^2)^2}\left\{\frac{b^2(a^2+b^2)\cos\phi}{4\left[a^2-(a^2+b^2)\cos^2\phi\right]^2}\right.\right.$$

$$\left.\left.+\left(\frac{4a^2+3b^2}{8a^2}\right)\times\left(\frac{(a^2+b^2)\cos\phi}{a^2-(a^2+b^2)\cos^2\phi}+\frac{\sqrt{a^2+b^2}}{2a}\ln\left|\frac{a+\sqrt{a^2+b^2}\cos\phi}{a-\sqrt{a^2+b^2}\cos\phi}\right|\right)\right\}+c\right] \tag{4.60}$$

Assuming the top of the cooling tower is a free edge, the boundary condition N_ϕ=0 at ϕ=ϕ_0 yields the result

$$c = \frac{\gamma a^6 b^2 K}{(a^2+b^2)^2}\left\{\frac{b^2(a^2+b^2)\cos\phi_0}{4\left[a^2-(a^2+b^2)\cos^2\phi_0\right]^2}+\left(\frac{4a^2+3b^2}{8a^2}\right)\right.$$

$$\left.\times\left(\frac{(a^2+b^2)\cos\phi_0}{a^2-(a^2+b^2)\cos^2\phi_0}+\frac{\sqrt{a^2+b^2}}{2a}\ln\left|\frac{a+\sqrt{a^2+b^2}\cos\phi_0}{a-\sqrt{a^2+b^2}\cos\phi_0}\right|\right)\right\} \tag{4.61}$$

so that expression (4.60) finally becomes

$$N_\phi = \frac{\gamma a^4 b^2 K\left(a^2\sin^2\phi - b^2\cos^2\phi\right)^{\frac{1}{2}}}{\left(a^2+b^2\right)^2\sin^2\phi}$$

$$\times\left[\frac{b^2(a^2+b^2)}{4}\left\{\frac{\cos\phi_0}{\left[a^2-(a^2+b^2)\cos^2\phi_0\right]^2}-\frac{\cos\phi}{\left[a^2-(a^2+b^2)\cos^2\phi\right]^2}\right\}\right.$$

$$+\left(\frac{4a^2+3b^2}{8a^2}\right)\left\{(a^2+b^2)+\left[\frac{\cos\phi_0}{\left[a^2-(a^2+b^2)\cos^2\phi_0\right]}-\frac{\cos\phi}{\left[a^2-(a^2+b^2)\cos^2\phi\right]}\right]\right.$$

$$\left.\left.+\frac{\sqrt{a^2+b^2}}{2a}\ln\left(\left|\frac{a+\sqrt{a^2+b^2}\cos\phi_0}{a-\sqrt{a^2+b^2}\cos\phi_0}\times\frac{a-\sqrt{a^2+b^2}\cos\phi}{a+\sqrt{a^2+b^2}\cos\phi}\right|\right)\right\}\right] \tag{4.62}$$

For the present case, and by reference to expression (4.33) with A=0,

$$t(\phi) = KX^2 = \frac{Ka^4\sin^2\phi}{a^2\sin^2\phi - b^2\cos^2\phi} \tag{4.63}$$

Using the function of $t(\phi)$ in equation (4.56), we obtain for the hoop stress resultant

$$N_\theta = \left(\frac{a^2\sin^2\phi - b^2\cos^2\phi}{b^2}\right)N_\phi - \frac{\gamma a^6 K\sin^2\phi\cos\phi}{\left(a^2\sin^2\phi - b^2\cos^2\phi\right)^{\frac{3}{2}}} \tag{4.64}$$

Case IV: t vary linearly with arc length s along the meridian

With c_1=0 (since A=0) and F=F_0, expression (4.40) reduces to

$$N_\phi = F\left[c_2\left(t_0 I_2 + Ca^2b^2 I_6\right) + c\right] \tag{4.65}$$

Where I_1, I_2, I_6 are as defined previously. As before, c is determined from the boundary condition for N_ϕ at the top of the cooling tower.

4.5.4 Final Stresses For Two of the Case Studies

Assuming that the top of the cooling-tower shell is free, the explicit results for stress resultants (N_ϕ, N_θ) for case I and III are given by equations (4.54, 4.57) and (4.62, 4.64) respectively. The actual direct stresses σ_ϕ and σ_θ in the cooling-tower shell follow by simply dividing the applicable values of N_ϕ and N_θ by the shell thickness $t(\phi)$ at the point in question, as indicated by equations (4.22). The results of interest are as follows:

Case I: t constant

$$\sigma_\phi = \frac{\gamma b^2\left(a^2\sin^2\phi - b^2\cos^2\phi\right)^{\frac{1}{2}}}{2\left(a^2+b^2\right)\sin^2\phi}\times$$

$$\left[\left(a^2+b^2\right)\left\{\frac{\cos\phi_0}{a^2-\left(a^2+b^2\right)\cos^2\phi_0} - \frac{\cos\phi}{a^2-\left(a^2+b^2\right)\cos^2\phi}\right\}\right.$$

$$\left. + \frac{\sqrt{a^2+b^2}}{2a}\ln\left|\left(\frac{a+\sqrt{a^2+b^2}\cos\phi_0}{a-\sqrt{a^2+b^2}\cos\phi_0}\right)\left(\frac{a-\sqrt{a^2+b^2}\cos\phi}{a+\sqrt{a^2+b^2}\cos\phi}\right)\right|\right] \tag{4.66a}$$

$$\sigma_\theta = \left(\frac{a^2\sin^2\phi - b^2\cos^2\phi}{b^2}\right)\sigma_\phi - \left(\frac{\gamma a^2\cos\phi}{\left(a^2\sin^2\phi - b^2\cos^2\phi\right)^{\frac{1}{2}}}\right) \tag{4.66b}$$

Case III: t proportional to X^2 (Square of the Horizontal Radius X)

$$\sigma_\phi = \frac{\gamma b^2\left(a^2\sin^2\phi - b^2\cos^2\phi\right)^{\frac{3}{2}}}{\left(a^2+b^2\right)^2\sin^4\phi}\times\left[\frac{b^2(a^2+b^2)}{4}\left\{\frac{\cos\phi_0}{\left[a^2-\left(a^2+b^2\right)\cos^2\phi_0\right]^2} - \frac{\cos\phi}{\left[a^2-\left(a^2+b^2\right)\cos^2\phi\right]^2}\right\}\right.$$

$$+\left(\frac{4a^2+3b^2}{8a^2}\right)\times\left\{\left(a^2+b^2\right)\left[\frac{\cos\phi_0}{a^2-\left(a^2+b^2\right)\cos^2\phi_0}-\frac{\cos\phi}{a^2-\left(a^2+b^2\right)\cos^2\phi}\right]\right.$$

$$\left.+\frac{\sqrt{a^2+b^2}}{2a}\ln\left[\left(\frac{a+\sqrt{a^2+b^2}\cos\phi_0}{a-\sqrt{a^2+b^2}\cos\phi_0}\right)\left(\frac{a-\sqrt{a^2+b^2}\cos\phi}{a+\sqrt{a^2+b^2}\cos\phi}\right)\right]\right\}\right] \tag{4.67a}$$

$$\sigma_\theta=\left(\frac{a^2\sin^2\phi-b^2\cos^2\phi}{b^2}\right)\sigma_\phi-\frac{\gamma a^2\cos\phi}{\left(a^2\sin^2-b^2\cos^2\phi\right)^{\frac{1}{2}}} \tag{4.67b}$$

4.6 CONCLUDING REMARKS

Closed-form analytical results for membrane stresses in cooling towers have been presented. These will be used in the subsequent chapters as a benchmark to check the validity of the finite-element model results.

CHAPTER FIVE

FINITE ELEMENT MODELLING

5.1 INTRODUCTION

This chapter outlines the finite element method, and describes the finite element modelling of a hyperbolic cooling tower. It also discusses the various options considered in the solution of the problem. The results presented in Chapter Four are used in the verification of the finite element model.

5.2 THE FINITE ELEMENT METHOD (FEM)

The finite element method (FEM) can be described as follows: "The FEM is a computer-aided mathematical technique for obtaining approximate numerical solutions to the abstract equations of calculus that predict the response of physical systems subjected to external influence"[43]. Problems that can be solved using FEM encompass solid mechanics (e.g. elasticity, plasticity, statics and dynamics), heat transfer (e.g. conduction, convection and radiation) and fluid mechanics. A finite element is derived by assuming a form of the equation for the internal strain[44]. There will be one equation for each degree of freedom of each node of element. These equations are most conveniently written in a matrix form for use in computer algorithms. The matrix of the coefficients becomes a "stiffness matrix" that relates forces to displacements as stated in the equation below.

$$[F]=[K]\times[d] \tag{5.1}$$

where F, K and d are the force vector, stiffness matrix and displacement vector respectively.

5.2.1 Isoparametric Element Formulation

Finite element methods are implemented in the computer code, not algebraically, but by procedures of numerical integration. To implement computer code-solving FEM problems, isoparametric elements are used for computational advantages[44]. The isoparametric formulation makes it possible to generate elements that are non-rectangular and have curved sides. The isoparametric formulation includes elements for solid, plates and shell problems. Features peculiar to isoparametric elements are:

- Isoparametric elements are defined on the ξ, η and ζ axes.

- Isoparametric elements are defined on the domain: $-1<\xi, \eta, \zeta<+1$.
- There exists a mapping from the isoparametric domain to the problem domain. The isoparametric mapping of the isoparametric element in the (ξ, η and ζ) domain to the (x, y, z) domain (3D), is achieved by the mapping:

$$x=\sum N_i x_i, \quad y=\sum N_i y_i, \quad z=\sum N_i z_i \tag{5.2}$$

  Where i ranges over the number of nodes in the element. The shape functions N_i (or trial function) are functions of the isoparametric co-ordinates ξ, η and ζ.
- The derivative of the mapping, the Jacobian, provides a numerical value to the local amount of expansion or contraction of the co-ordinates due to the isoparametric mapping[44].

$$J=(\xi,\eta,\varsigma)=\begin{bmatrix} \frac{\partial x}{\partial \xi} & \frac{\partial y}{\partial \xi} & \frac{\partial z}{\partial \xi} \\ \frac{\partial x}{\partial \eta} & \frac{\partial y}{\partial \eta} & \frac{\partial z}{\partial \eta} \\ \frac{\partial x}{\partial \varsigma} & \frac{\partial y}{\partial \varsigma} & \frac{\partial z}{\partial \varsigma} \end{bmatrix} \tag{5.3}$$

5.3 FINITE ELEMENT ANALYSIS OF SHELLS

The ease or difficulty in obtaining a solution for a shell problem is dependent on the geometry, loading and boundary conditions. Continuous geometry, smooth loading and idealised boundary conditions are generally required to obtain analytical solutions. Derivations from any of these proceedings result in complications that may prevent, or greatly complicate the attainment of an analytical solution, thereby directing the analyst to numerical techniques, the most prominent of which is the finite element method (FEM)[45]. One first critical decision that has to be decided upon early in the process is to evaluate how detailed and accurate the analysis needs to be.

When a numerical approach is pursued, it is productive to re-examine the assumptions of the corresponding analytical problem, with the thought that it may be possible to relax certain of the assumptions and possibly increase the generality of the numerical approach. In this case, there are two assumptions made; these are: the use of a "reference or middle surface" to achieve a two-dimensional shell theory; the enforcement of Kirchhoff's hypothesis to eliminate transverse shearing strain[45].

If the idealised structure is analysed by the FE methods, some differences from the real structure will arise from the assumptions embedded in the technique. Assumptions must be made so as to ensure that reasonable results are obtained at an acceptable cost. FEM analysis will generally always contain assumptions that will lead to errors in the predictions and stresses of a structure [46].

The purpose of FE modelling is to make a model that behaves mathematically like the structure that is modelled. Although the results may not be predicted accurately, it may be possible to assess within a few percentages the difference in the results between the real and the idealised structure. Boundary conditions are required to ensure that the behaviour of the model approximates the behaviour of the real structure. When it is not possible to establish an accurate representation of boundary conditions, it is advisable to use different sets of conditions that can be examined to investigate the sensitivity of the solution[46]. After the boundary conditions have been determined, the loading conditions are applied. Most FE codes have a large variety of loads applied; examples are: point, distributed, gravity, pressure and centrifugal loads. The next step is to define the material data for the shell elements in the model. This is normally straightforward.

5.3.1 Steps in FE Analysis

Finite element modelling consists of three steps [47]. These are:

1. Pre-processing
2. Simulation
3. Post-processing

Pre-processing:

This includes the entire process of constructing the geometry of the FE model, applying physical and material properties and describing the boundary and loading conditions. The first step involves deciding of the number of elements in the model [47]. The efficiency of the computational run time is related to the number of elements. The greater the number of elements, the longer the computational run time and this does not necessarily mean a more accurate result.

Simulation:

This is the stage in which the FEM solves the numerical problem defined in the model. For example, it involves determining all the local governing stiffness matrices for the elements and assembles all these into a global stiffness matrix, from where all the unknown degrees of freedom can be solved.

Post-processing:

The results are evaluated once the simulation has been completed and the displacements and stresses have been calculated. The evaluation is done interactively using a postprocessor which reads the binary files, thereafter, there are various options for displaying the results, including colour contour plots, animations, deformed shape plots, and x-y plots. The post-processing also includes checking for errors that might not have been detected while building the model.

5.3.2 Choice of Shell Element in Finite Element Analysis

The FE modelling used in this thesis is done exclusively using the general purpose finite element code ABAQUS/Standard version 6.2. An element's formulation refers to the mathematical theory used to define the element's behaviour. All the stress/displacement elements in ABAQUS are based on the theory that the elements deform with the material (Lagrangian behaviour). To accommodate different types of behaviour, there is a range of different element families. Each element family is suited for a certain application. Examples of element families in ABAQUS are shell elements, continuum elements, membrane elements, rigid elements and beam elements. For shells of revolution, the entire structure is modelled by exploiting axisymmetry. In the present investigation, the structure is idealised by an assembly of a 2-noded linear axisymmetric shell element (SAX1), with integration points averaged at the nodes.

5.3.3 Components of an ABAQUS Model

An ABAQUS model is composed of several different components that together describe the physical problem to be analysed and the results to be obtained. The analysis model consist the following: Discretized geometry, element section properties, material data, loads and boundary conditions, analysis type and output requests.

i. *Discretized Geometry*:

Finite elements and nodes define the basic geometry of the physical structure being modelled in ABAQUS. Each element in the model represents a discrete portion of the physical structure, which is, in turn, represented by many interconnected elements. Elements are connected together by shared nodes. The coordinates of the nodes and the connectivity of the elements–that is, which node belongs to which elements – comprise the model geometry. The collection of all the elements and nodes in a model is called the *mesh*. Generally the mesh is only an approximation of the actual geometry of the structure.

The element type, shape, and the location, as well as the overall number of elements used in the mesh, affect the results obtained from a simulation. As the mesh density increases, the analysis results converge to a unique solution, and the computer time required for the analysis increases. The solution obtained from numerical modelling is generally an approximation to the solution of the physical problem being simulated. The extent of the approximations made in the model's geometry, material behaviour, boundary conditions and loading determines how well the numerical simulation matches the physical problem.

ii. *Element Section Properties*

ABAQUS has a wide range of elements, many of which have geometry not defined completely by the coordinates of their nodes; for example, the layers of a shell or the dimensions of an I-beam section are not defined by the nodes of the element. Such additional geometric data are defined as physical properties of the element and are necessary to define the model geometry completely.

iii. *Material Data*

The material properties of all elements must be specified. The validity of the ABAQUS results is limited by the accuracy and extent of the material data.

iv. *Loads and Boundary conditions*

Loads distort the physical structure and thus create stress in it. Examples of the basic loading conditions are: point loads, pressure loads on surfaces, gravity loads and thermal loads.

Boundary conditions are used to constrain portions of the model to remain fixed (zero displacements) or to move by a prescribed amount (non-zero displacements). In either

situation the constraints are applied directly to the nodes of the model. The directions in which the nodes are able to move are called the degrees of freedom (dof). For a stress/displacement simulation the degrees of freedom are the translations and, for shell elements, the rotation at each node.

In a static analysis enough boundary conditions must be used to prevent the model from moving as a rigid body in any direction: otherwise a solver problem will occur during the solution stage and may cause the simulation to stop prematurely.

v. ***Analysis Type***

The most common type of simulation is a static analysis, where the long-term response of the structure to the applied loads is obtained. In other cases, the dynamic response of a structure to the loads may be of interest: for example; the effects of wind load on a structure.

vi. ***Output Request***

Finite element analyses have the ability to create very large amounts of output. Therefore, it is essential that the user manages this output so that only data required to interpret the results of the simulation are produced. Three types of output are available in ABAQUS:

- Restart data, used as a database to continue the analysis;
- Printed tables of results;
- Results stored in binary files for subsequent post-processing.

5.3.4 Modelling the Cooling Tower

The ABAQUS input file is the means of communication between the pre-processor, and the solver. It contains a complete description of the numerical model. A complete ABAQUS input file is split into two distinct parts. The first section contains *model data* and includes all the information required to define the structure being analyzed. The second section contains *history data* that define what happens to the model: the sequence of loading or events for which the response of the structure is required. This history is divided into a sequence of steps, each defining a separate part of the simulation. For example, the first step may define a static loading while the second step may define a dynamic loading. The input file is composed of option blocks that contain data describing a part of the model.

Since the configuration of the cooling tower as well as the external conditions is symmetric, an axisymmetric 2-dimensional (2D) modelling of the cooling tower is adopted by discritizing the meridional line alone. This is preferable because it requires the least number of elements and will result in the smallest computational run time (i.e. the computational time is about one/tenth of a three-dimensional (3D) analysis).

Units

Before a model is built, a decision on the system of units must be agreed because ABAQUS will only process the output based on the consistency of the units used. The SI system of units is used throughout this thesis, which are: length in metre (m), force in Newton (N), mass in kilograms (kg), stress in Pascal (N/m^2) and density in (Kg/m^3).

Nodal Coordinates

The global coordinate system in ABAQUS is a right-handed, rectangular Cartesian system. As a result of the type of model, (i.e.axisymmetric 2-dimensional model), the coordinates of the nodes are given in the radial and axial positions. For example, the *r*- and *z*-directions coincide with global *X*- and *Y*-directions (see Fig. 5.1). The *NODE option is used to define the coordinates of the nodes. For example

*NODE

100, 40, 50

The first column in the data line indicates the node number and the second and third columns define the nodal coordinate in the *r*- and *z*-directions.

Node numbering

The nodes are numbered in an ascending order from the bottom of the tower to the top (see Fig. 5.1). These nodes are grouped into a node set called "tower", which is used as a cross-reference when defining loads, constraints and the material properties (see Appendix A2).

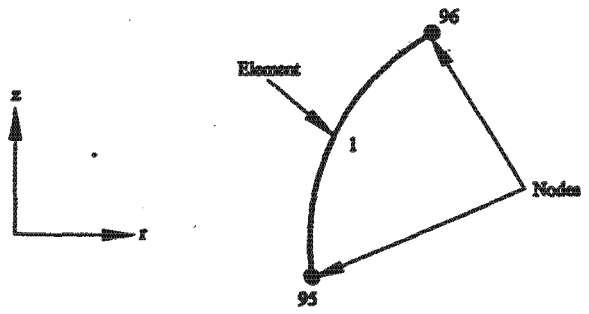

Fig. 5.1 Schematic drawing of an SAX1 element, showing coordinate system, node and element numbers.

Element Numbering

The *ELEMENT option defines individual elements in the model. However, individual elements are grouped into element sets for convenience. The format of each data line for a shell element is

<element number>, <node 1>, <node 2>

where node1 and node 2 are at the ends of the element (see Fig. 5.1); for example, element 1 connects nodes 95 and 96, so that the data line defining this element is

1, 95, 96

The TYPE parameter on the *ELEMENT option is used to specify the kind of element being defined. For the present analysis, the meridional line is discretized by means of a two nodded elements SAX1 (i.e.2-node thin linear shell element).

In finite element method the solution approaches the exact solution of the governing equations as the number of elements approaches infinity (i.e. the smaller the elements, the more accurate are the solution). It is therefore necessary for sufficient elements to be used in the model so that a satisfactory representation of the exact solution is found. In order to optimize the number of elements to capture the results in the least possible time, a total of 119 elements and 120 nodes along the meridional direction is adopted. Each element having an arch length of 1000mm. Fig. 5.2 shows a half symmetry finite element mesh.

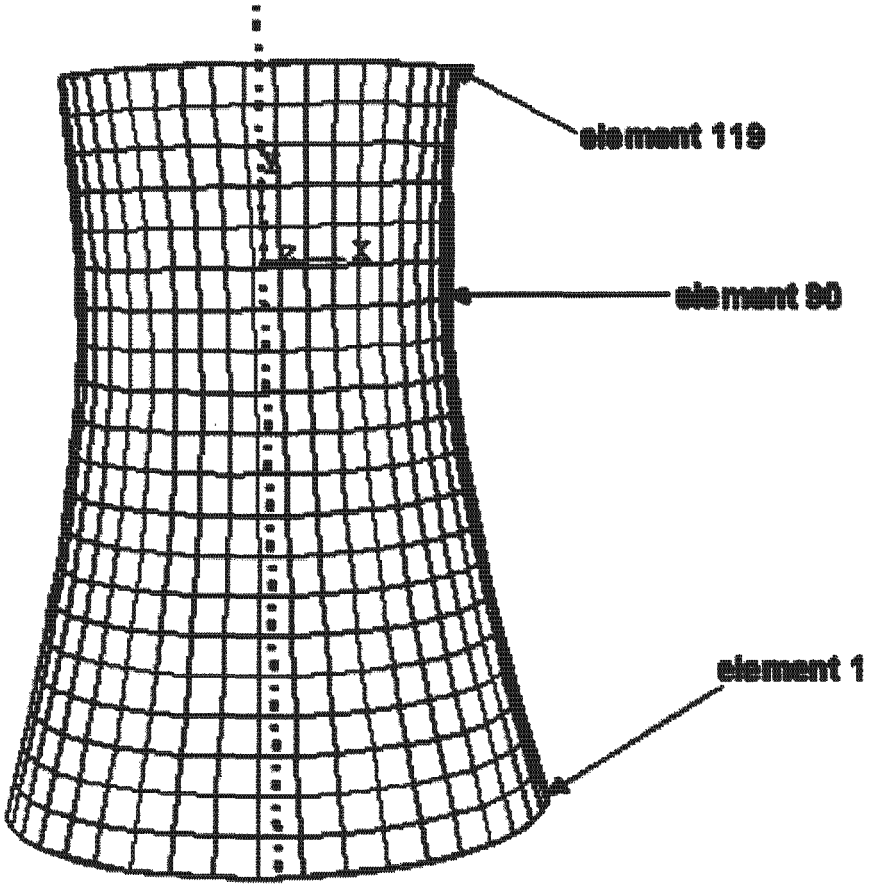

Fig. 5.2 Finite element mesh of cooling tower (half symmetry) showing elements

Section/ Material Properties

As the structure is made of a single material with constant thickness, the section properties will be the same for all the elements. Therefore, the element set "tower" can be used to assign the physical and material properties to the elements. Since it is assumed that the shell is linear elastic, the *SHELL SECTION option is adopted, which uses numerical integration to calculate the behaviour at each section point through the thickness of the shell.

The shell is made of an Isotropic, homogeneous, linear elastic material having a concrete grade of 40Mpa, Young's Modulus of 28×10^9 Pascal and a Poisson's ratio of 0.15. The linear elastic material model has been considered because this simulation is undertaken within the material's linear elastic zone. Beyond this zone, failure mechanisms such as concrete cracking and steel reinforcement yielding occur. Modelling of this failure mechanism is beyond the scope of this work. However it is suggested that such mechanism may be modelled by the use of appropriate failure criteria.

Boundary Conditions

Constraints on nodes are defined using the *BOUNDARY option and specifying the constrained degree of freedom. Each data line is of the form:

<node number>, <constrained degree of freedom>, <magnitude of displacement>

For the purpose of the finite-element modelling, it is assumed that at the soffit of the structure, the boundary is fully constrained (i.e. Encastre) while at the top the shell is freely supported. The supporting column is not included in this analysis. In order to simulate this action, the shell is assumed to rotate freely in the radial direction, but constrained in the vertical and tangential directions. This latter form of boundary condition would not significantly change the magnitude of the bending stresses at the soffit of the structure (See Fig. 5.3).

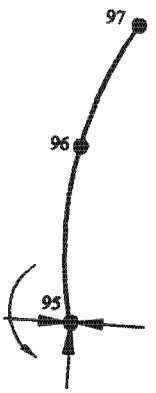

Fig. 5.3 Schematic drawing illustrating a node constrained in all direction.

Loading

For the purpose of this modelling, a distributed gravity load is applied to the shell structure. The *DLOAD option is used to define distributed loads on element faces and bodies. The data line for this option has the form:

<element set or element numbers>, <distributed load type label>, <magnitude>

Gravity load is specified by using the distributed load type GRAV and giving the gravity constant as the magnitude of the load. The direction of the gravity field is specified by giving the component of the gravity vector on the data line (see Appendix A2). Fig.5.4 shows the direction of gravity loading.

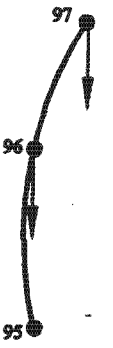

Fig. 5.4 Schematic drawing showing the direction of loading.

Output Request

ABAQUS generates a large output request file which allows the user to specify the parameter to be processed when running the analysis. In this case, the meridional stresses (S_{22}) and the hoop stresses (S_{11}) are requested to be averaged at nodes for the purpose of this analysis. Contour plots of meridional and hoop stresses are shown in Appendix A3.

Once the output file is saved, the analysis is run interactively. The table of stresses can be obtained from the dat. File after running the simulation successfully.

5.4 CONCLUDING REMARKS

After proper modelling of the cooling tower is complete, using the FE tool ABAQUS, it becomes apparent that the results obtained are to be compared to closed-form analytical results to verify the validity of the numeric modelling, before adopting this as the basis of the parametric studies undertaken in this thesis.

CHAPTER SIX

PARAMETRIC STUDIES

6.1 STANDARD/BENCHMARK COOLING TOWER

6.1.1 Introduction

Cooling towers come in different sizes and dimensions, varying from 80m to 200m in height. For the purposes of this study, a standard-size cooling tower is assumed to have the dimensions furnished below. The author's choice of this standard size is based on a series of investigations and assessments of existing cooling towers built to date. The reason why this size has been chosen is to give an appropriate idea of the static behavior of cooling towers with regard to the self-weight stresses.

The cooling tower has an overall height of 120m, with a base diameter of 89.80m. The throat of the tower is 60m, in diameter; and is, located 30m from the top of the shell. The material used is concrete with a constant thickness of 150mm from the top to the bottom. The physical and material properties of the cooling tower are summarised in Table 6.1, and a detailed geometry is shown in Fig 6.1.

Parameter	Symbol (unit)	Value
Height	H (m)	120.0
Throat radius	a (m)	60.00
Thickness	t (m)	0.150
Poisson's ratio	ν	0.150
Young's Modulus	E_c (GPa)	28×10^9
Density	γ (KN/m^3)	24.00
Angle of opening at top	ϕ_0	97.36^0
Angle of opening at bottom	ϕ_b	74.56^0

Table 6.1, Physical and material properties of standard size cooling tower.

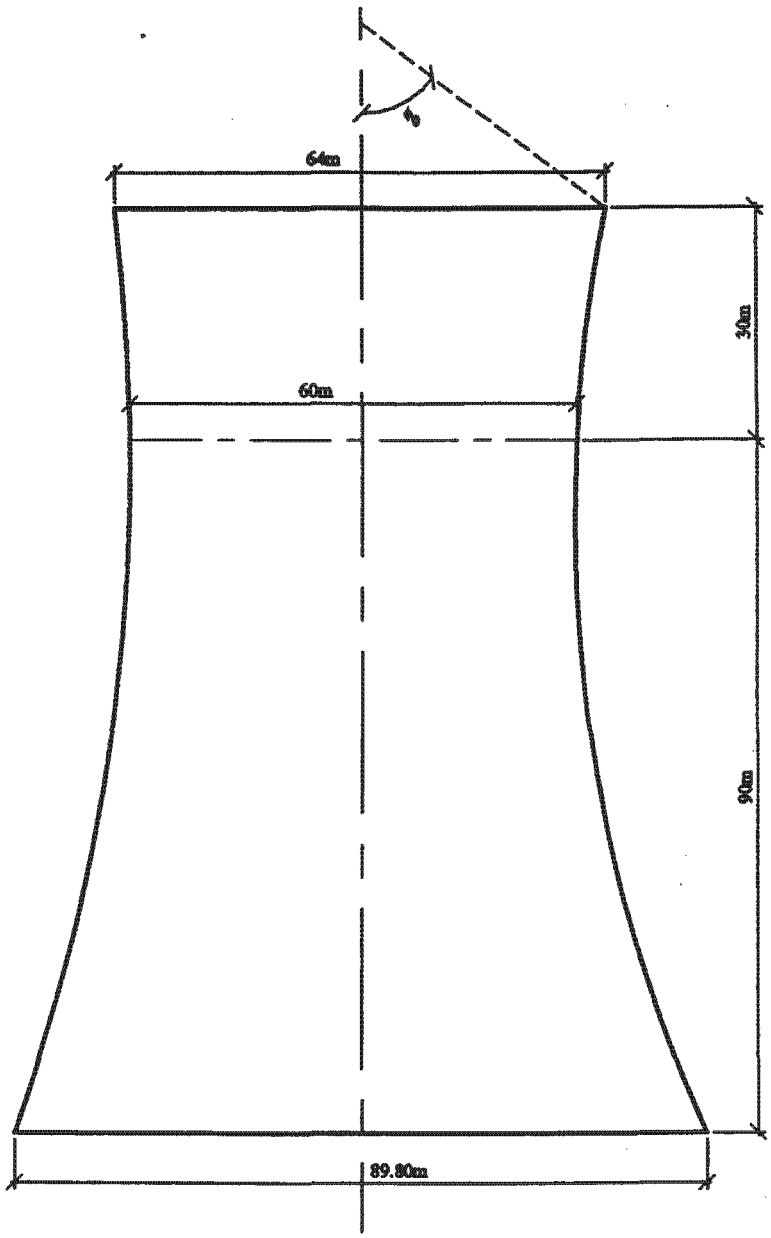

Figure 6.1 Geometry of Cooling tower

6.1.2 Verification of Present Analysis

To check the validity of the analytical results, the finite element method is used to model the behavior of meridional and hoop stresses over the entire height of the shell with the application of a gravity load. A multi-purpose FE program ABAQUS/Standard version 6.2 is used and a 2-noded axisymmetric shell element is adopted throughout the entire meridian having a $\phi_0 = 97.36^0$ at the top and a $\phi_b = 74.56^0$ at the base of the shell.

The profiles predicted by the analytical result illustrated in Figure 6.2, corresponds well with the FE model profiles. These profiles predict the correctly shaped profile for all cases of stresses. With regards to the meridional stress, for instance, it is observed that the profile that uses the FE model, under-predicts the analytical profile from the throat to approximately 12-15m above the base of the tower, while beyond the throat the profile is more or less the same. However, the profiles for the analytical and FEM model for the hoop stresses arrive at the same result from the top to approximately 20m above the soffit of the structure.

Tables 6.2 compares the results obtained using the analytical membrane solution with the results obtained with the FEM for meridional and hoop stresses at the inner and outer surfaces. From Table 6.2, it is evident that the results obtained using the analytical solution in the case of the standard cooling tower is in line with those obtained using the FE method, with discrepancies not exceeding 3%. The difference between the numeric and analytical results is attributed to the fact that the analytical closed-form results consider only the membrane solution while the numerical result takes into account both the membrane and bending effect. This suggests that the FEM solutions are indeed valid for this present study. Further parametric studies in this thesis will thus be based on the FE method.

Table 6.2 Comparison Between Analytical Membrane vs FEM for Self-Weight Loading, Uniform Thickness, b/a=2.694

Y (m)	ϕ	Meridional stress σ_ϕ (N/mm^2)				hoop stress σ_θ (N/mm^2)			
		ANALYTIC	FEM		Variance	ANALYTIC	FEM		Variance
			Inner sect.	Outer sect.			Inner sect.	Outer sect.	
-90	74.56	-2.310	-2.133	-2.384	0.004	-0.430	-0.322	-0.360	0.008
-70	76.34	-2.049	-2.011	-2.001	0.003	-0.384	-0.378	-0.378	-0.002
-50	78.95	-1.751	-1.712	-1.723	0.002	-0.333	-0.325	-0.326	-0.002
-30	82.64	-1.396	-1.368	-1.371	0.001	-0.266	-0.261	-0.261	-0.002
-10	87.39	-0.973	-0.956	-0.952	0.000	-0.165	-0.162	-0.161	-0.003
0	90.00	-0.738	-0.725	-0.724	-0.001	-0.102	-0.101	-0.101	-0.003
10	92.61	-0.494	-0.486	-0.485	-0.002	-0.034	-0.033	-0.033	-0.003
15	93.88	-0.371	-0.367	-0.361	-0.002	0.001	-0.001	0.000	-0.003
30	97.36	0.000	-0.012	-0.012	-0.004	0.099	0.095	0.095	0.009

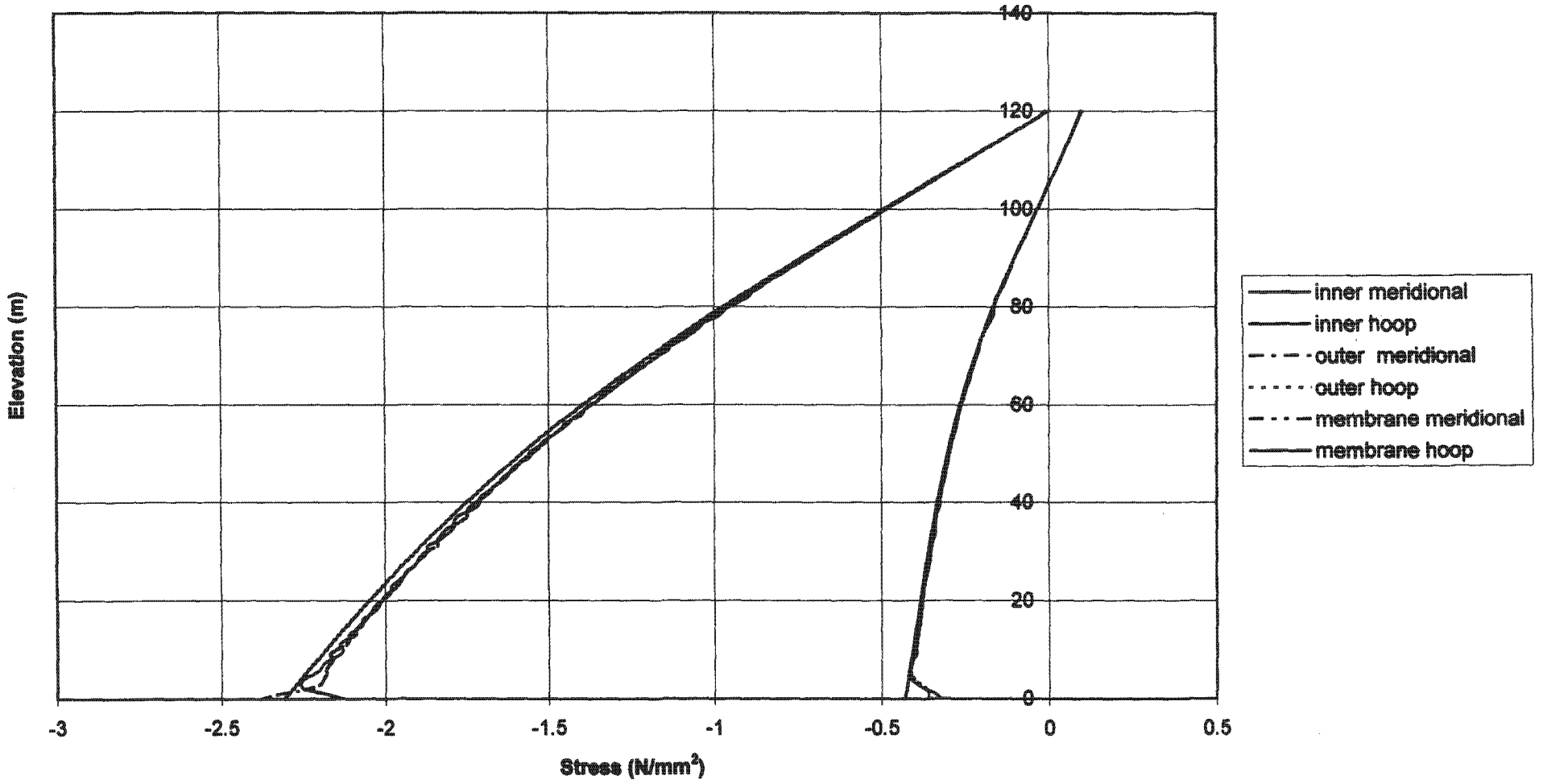

Fig. 6.2 Comparison Between Analytic vs FEM Stresses for Uniform Thickness, b/a=2.694

6.2 DESCRIPTION OF PARAMETRIC STUDY AND PRESENTATION OF RESULTS

6.2.1 Introduction

The parametric study carried out investigates the behaviour of the meridional and hoop stresses of a standard size concrete cooling tower, where several geometric parameters like the hyperbolic axis ratio (b/a), top edge angle (ϕ_0), offset parameter (A) and scale of the structure are varied one at a time. The cases considered are briefly described below.

6.2.1.1 Case I

Most hyperbolic cooling towers built to date have a hyperbolic axis ratio (b/a) of between 2.2–2.8, with 2.5 being a typical value. For the purpose of the parametric study, we shall change the hyperbolic axis ratio from 2.2 to 2.5 and 2.8 (i.e. the lower end, middle range, and the higher end) to study the effect of the variation on stress. The results obtained are presented in Tables 6.4–6.6 (Appendix A1) and plotted in Figures 6.3–6.5 respectively. An ABAQUS input deck for the model can be found in Appendix A2.

6.2.1.2 Case II

The top edge angle (ϕ_0) of most cooling towers ranges from 95^0-100^0 with $\phi_0=97^0$ being a typical value. To illustrate the range of ϕ_0, two extreme cases are chosen, i.e. $\phi_0=95^0$ and $\phi_0=100^0$, while the bottom edge angle (ϕ_b) is kept constant at $\phi_b=75^0$. The results are shown in Tables 6.7–6.14 (Appendix A1) and plotted in Figures 6.6–6.13.

6.2.1.3 Case III

In order to obtain a feel for the effect of the offset parameter "A" over the stress variations, A is varied at every 10m interval (i.e. 10, 20, 40m). The results are shown in Tables 6.15–6.17 (Appendix A1) and plotted in Figures 6.14–6.16.

6.2.1.4 Case IV

In the fourth and final scenario, the scale of the standard size cooling tower is first reduced and then increased by a scale factor of 0.5 and 1.666 respectively to see the

effect of this scales on the stresses experienced by the tower. The results obtained are presented in Tables 6.18–6.19 (Appendix A1) and plotted in Figures 6.17–6.18.

6.3 CONCLUDING REMARKS

Having defined the standard/benchmark cooling tower, a number of different models were created and results presented. Chapter Seven will discuss and analyze these results.

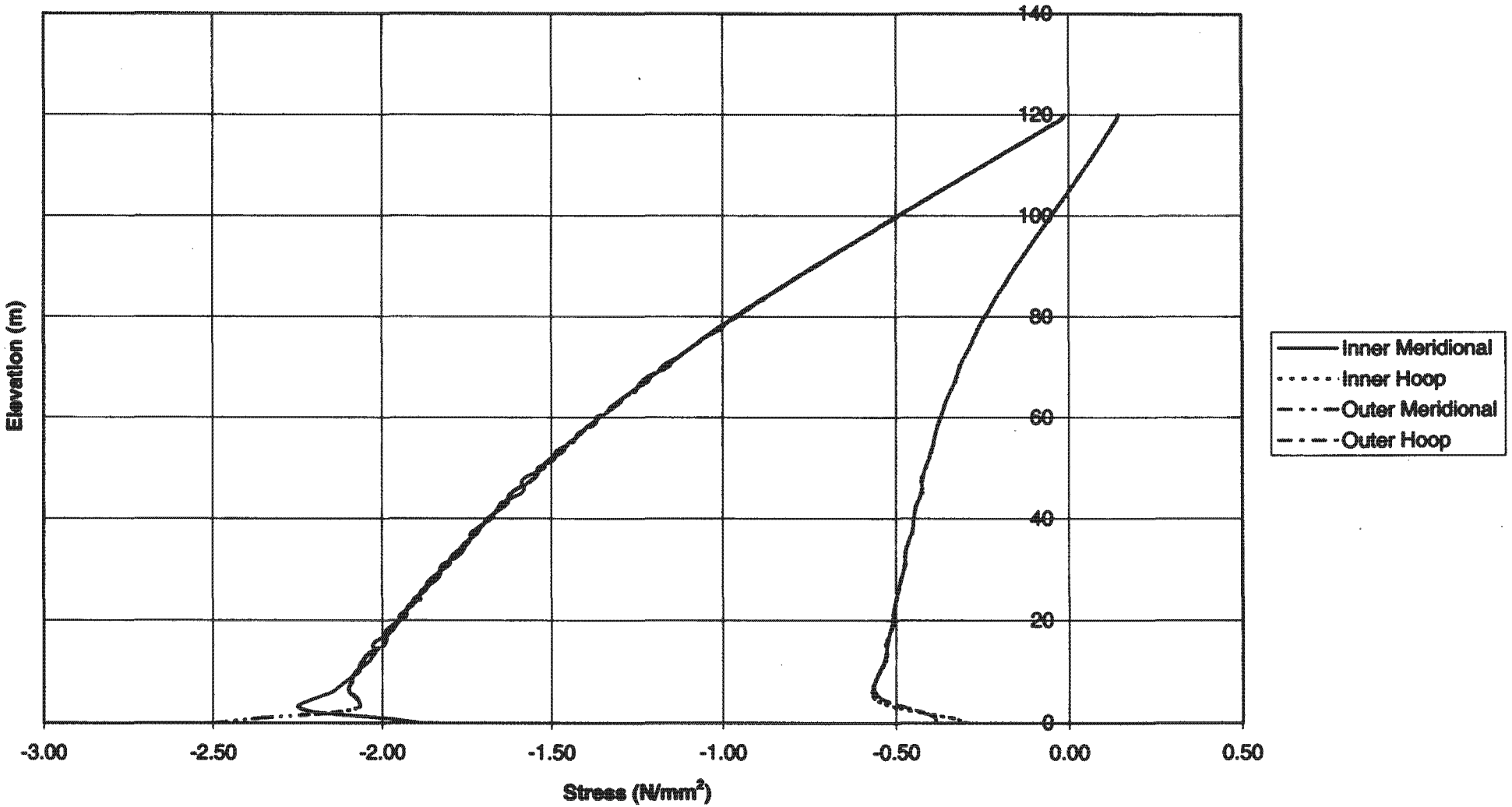

Fig. 6.3 Self-Weight Loading Consideration, b/a=2.2

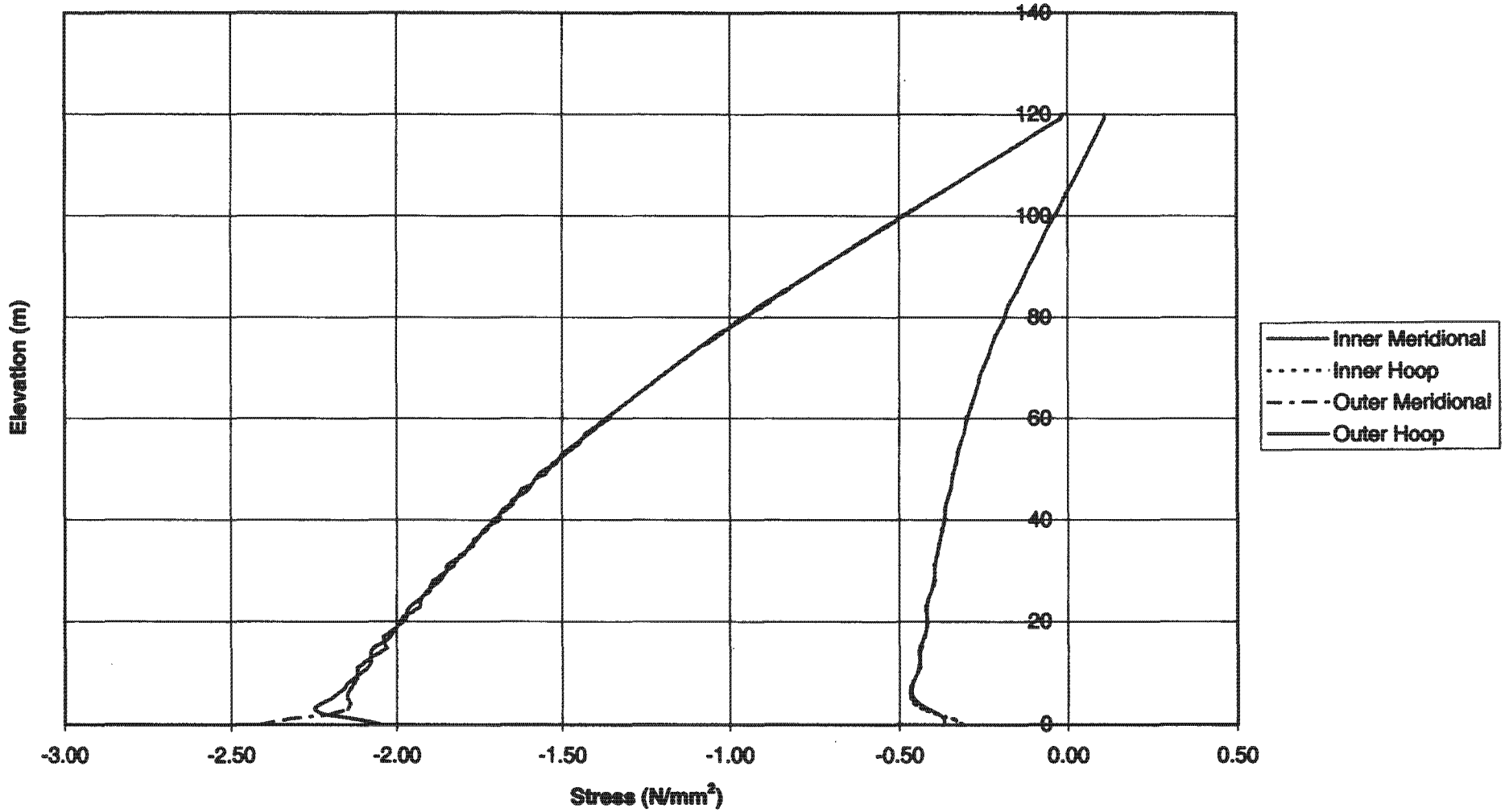

Fig. 6.4 Self-Weight Loading Consideration, b/a=2.5

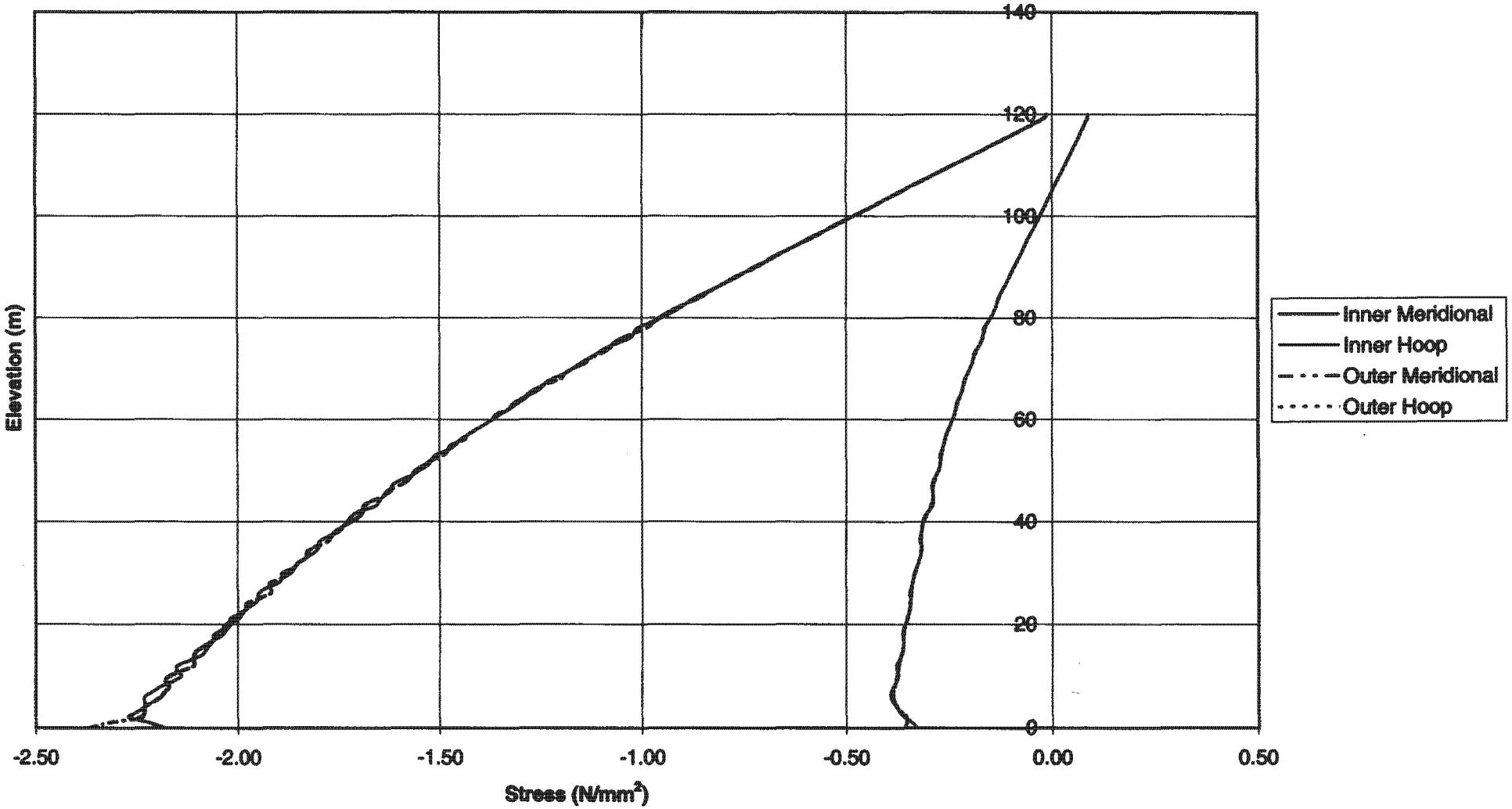

Fig. 6.5 Self-Weight Loading Consideration, b/a=2.8

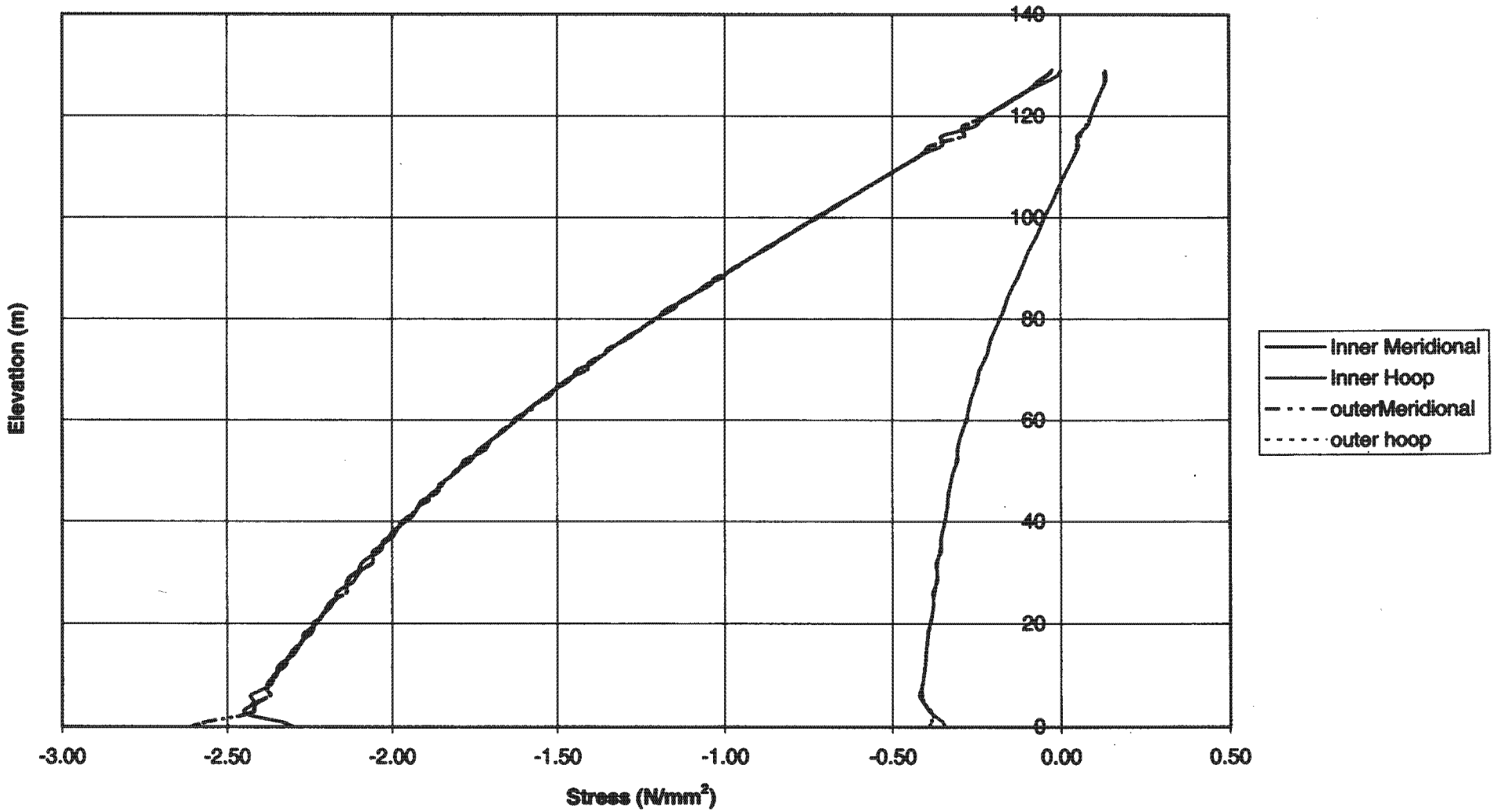

Fig. 6.6 Self-Weight Loading Consideration, b/a=2.694, $\phi_0=100^0$

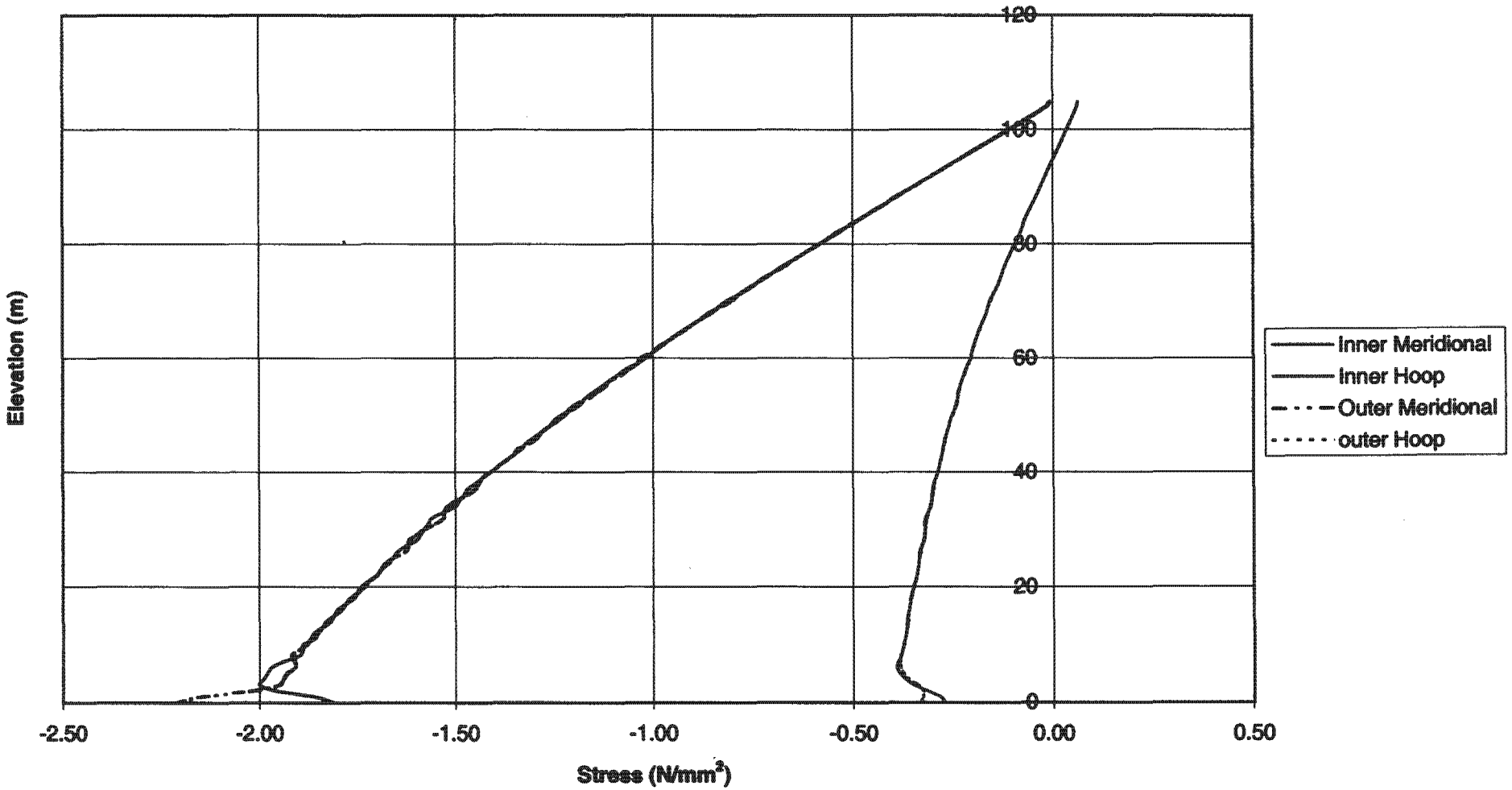

Fig. 6.7 Self-Weight Loading Consideration, b/a=2.694, $\phi_0=95^0$

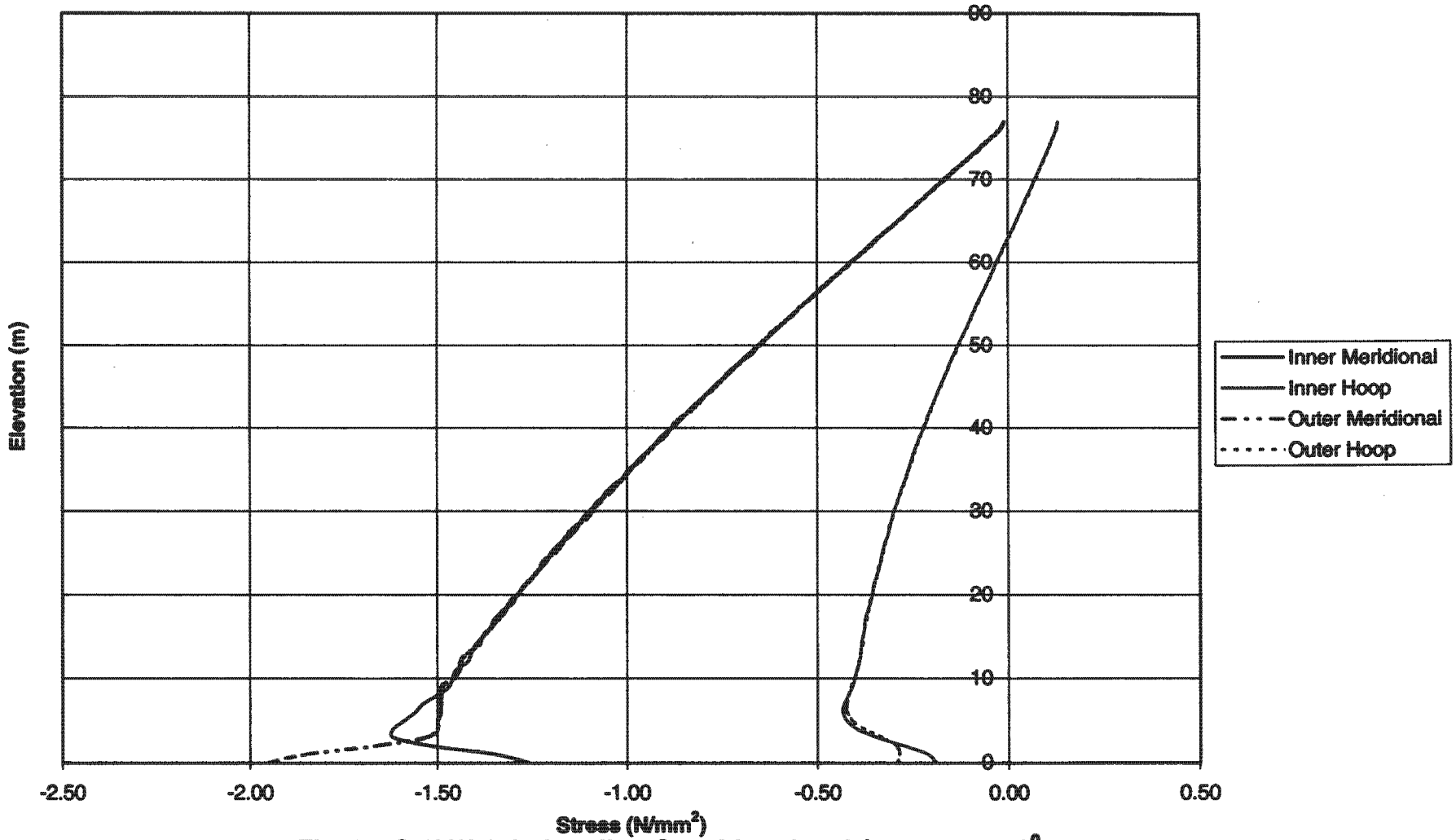

Fig. 6.8 Self-Weight Loading Consideration, b/a=2.2, $\phi_0=100^0$

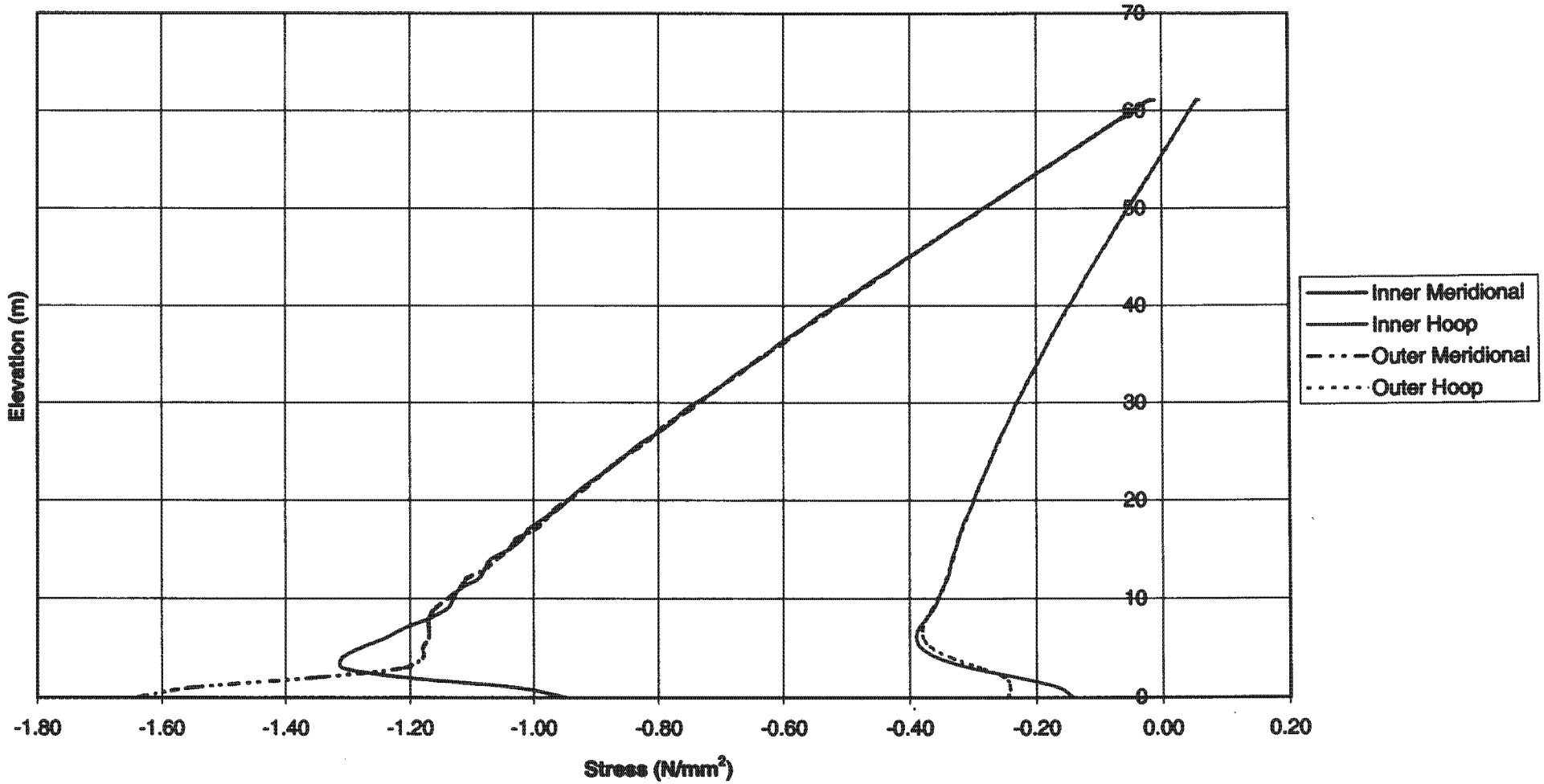

Fig. 6.9 Self-Weight Loading Consideration, b/a=2.2, $\phi_0=95^0$

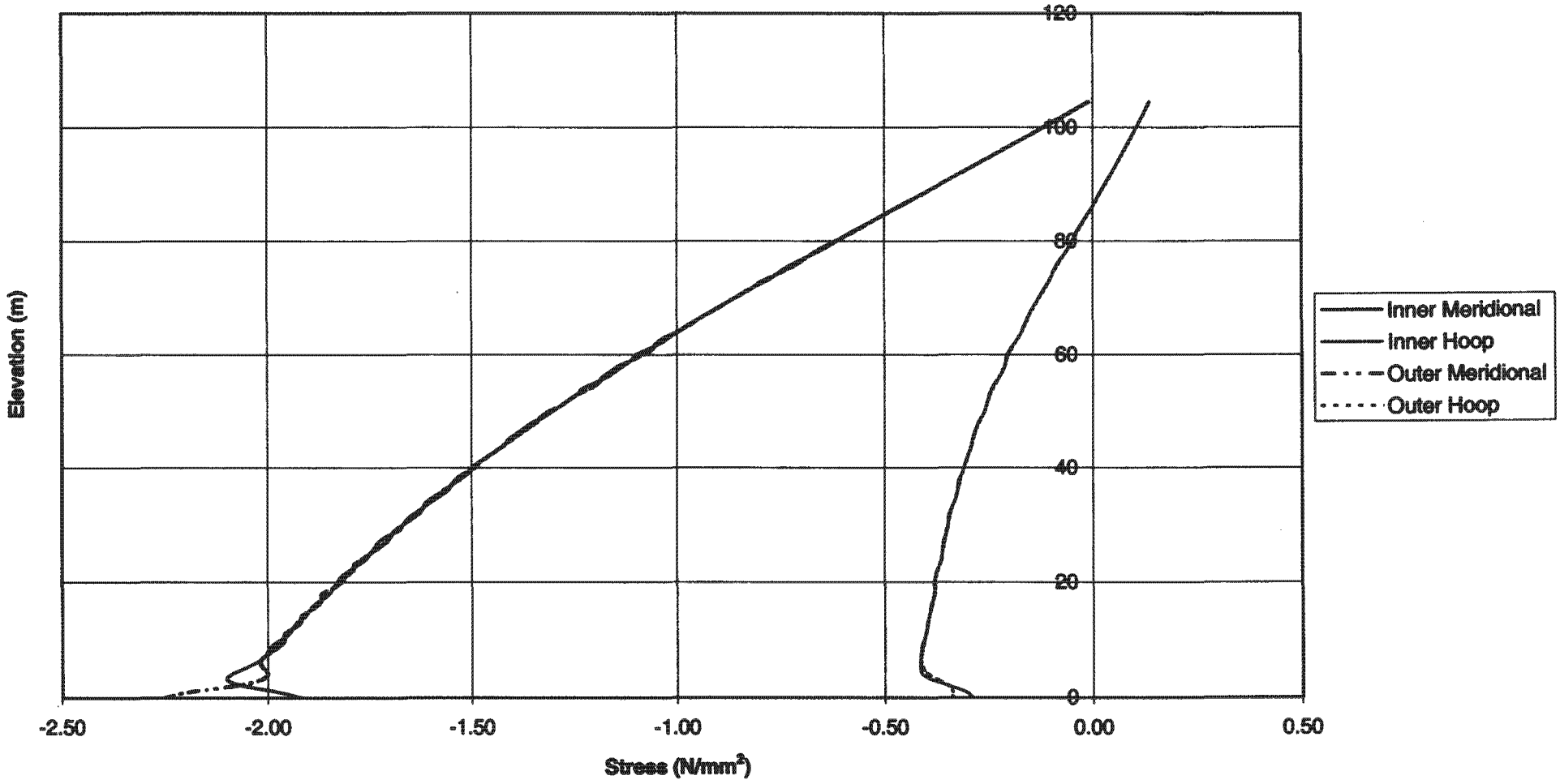

Fig. 6.10 Self- Weight Loading Consideration, b/a=2.5, $\phi_0=100^0$

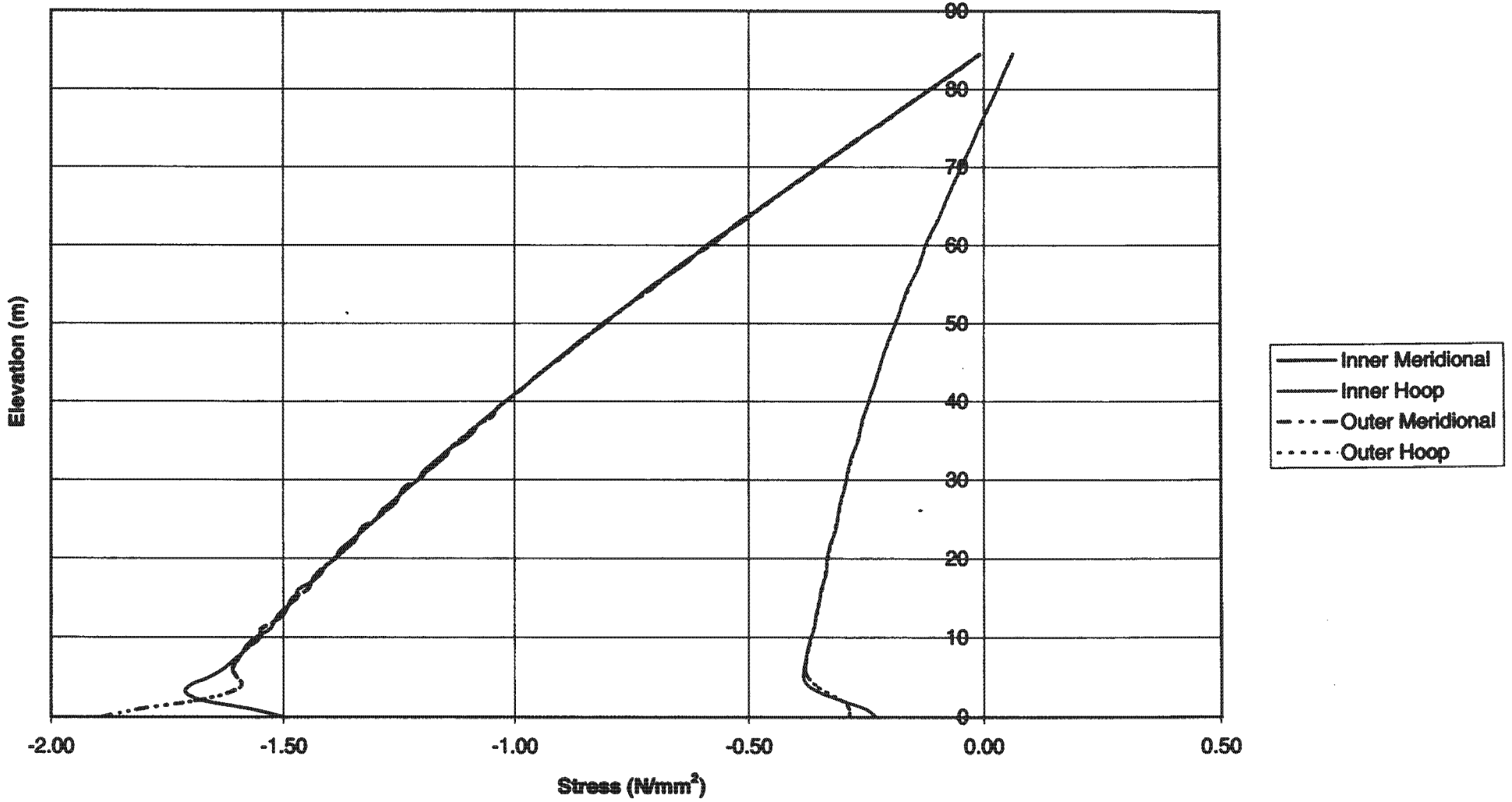

Fig. 6.11 Self-Weight Loading Consideration, b/a=2.5, $\phi_0=95^0$

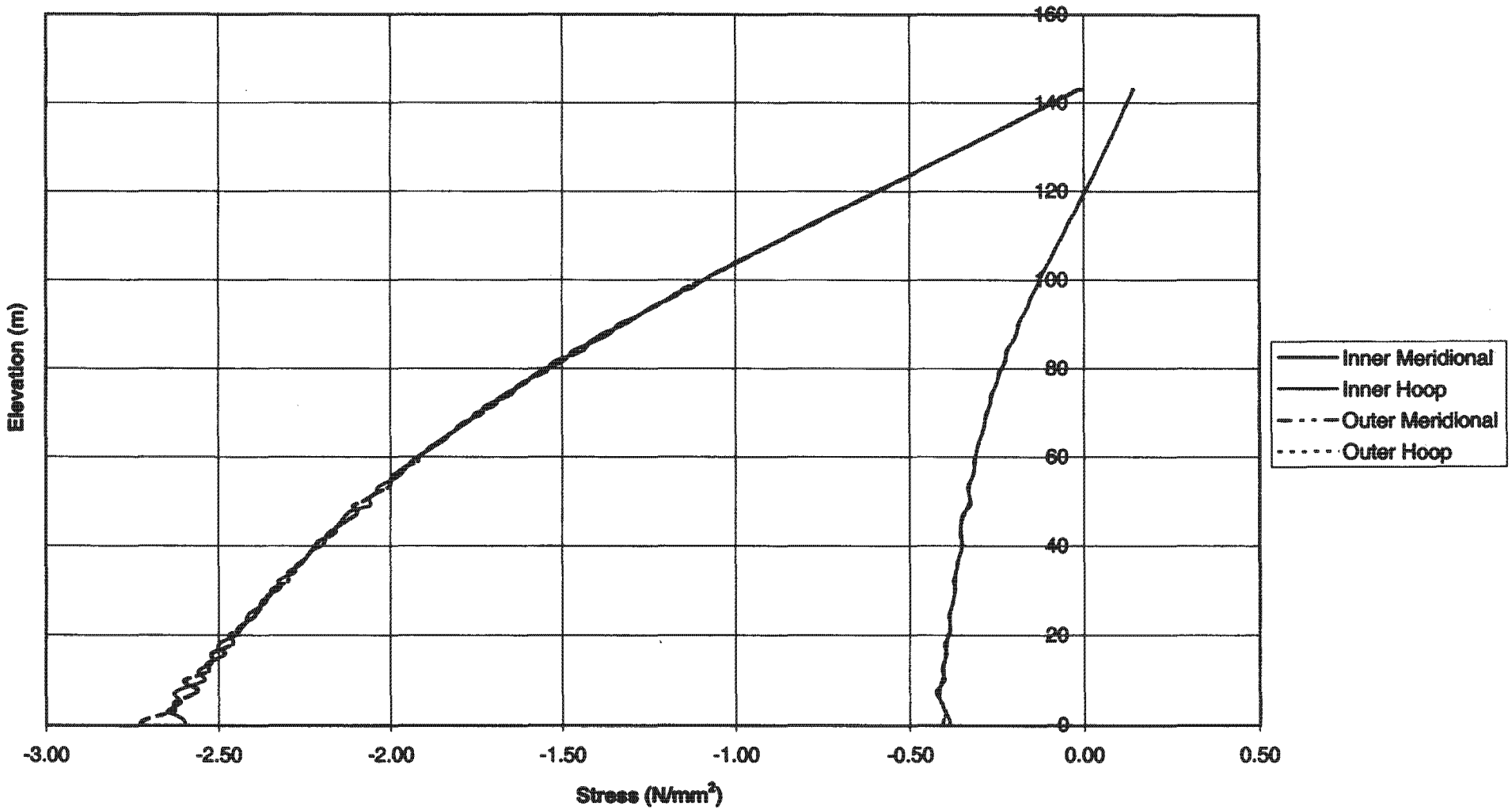

Fig. 6.12 Self-Weight Loading Consideration, b/a=2.8, $\phi_0=100^0$

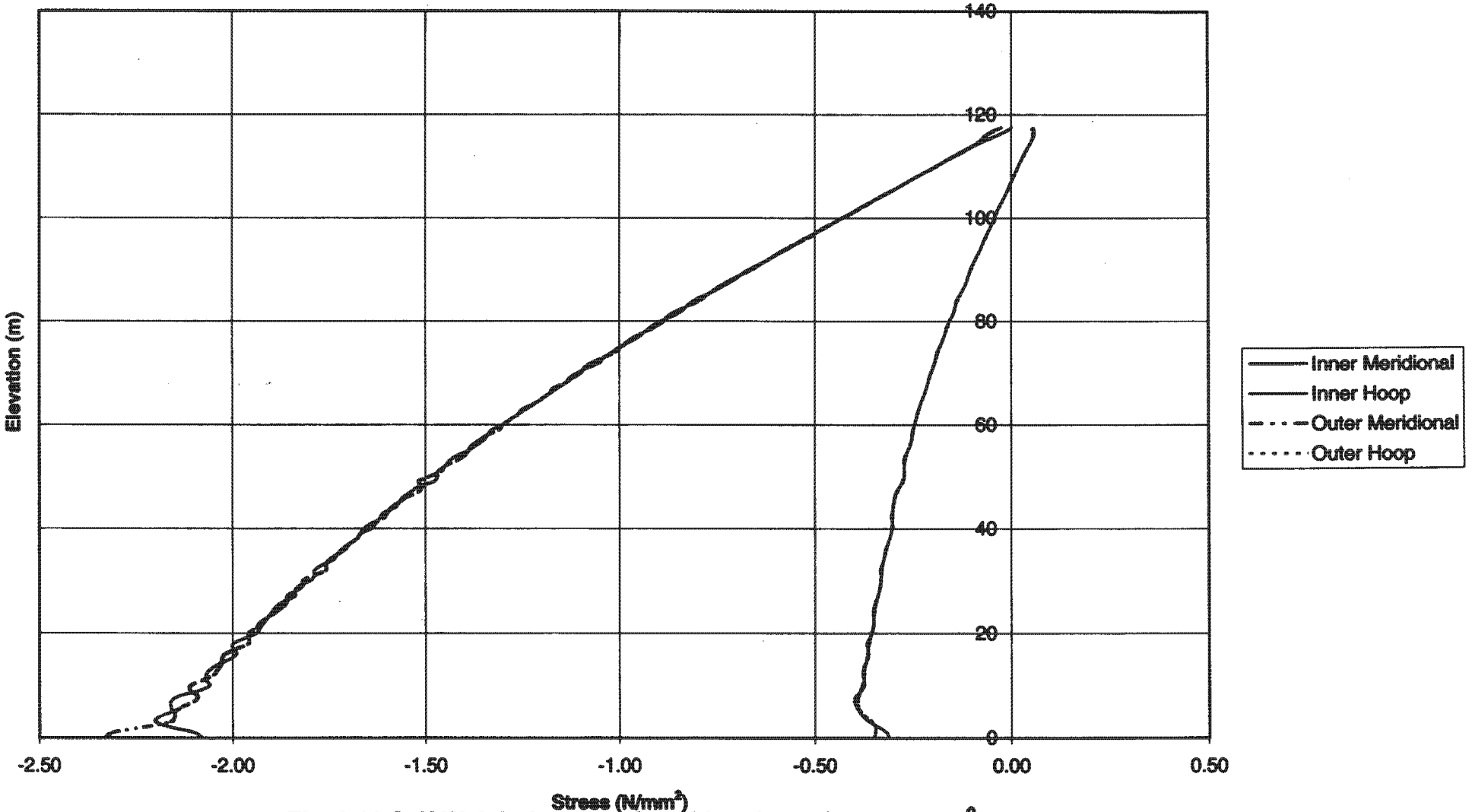

Fig. 6.13 Self-Weight Loading Consideration, b/a=2.8, $\phi_0=95^0$

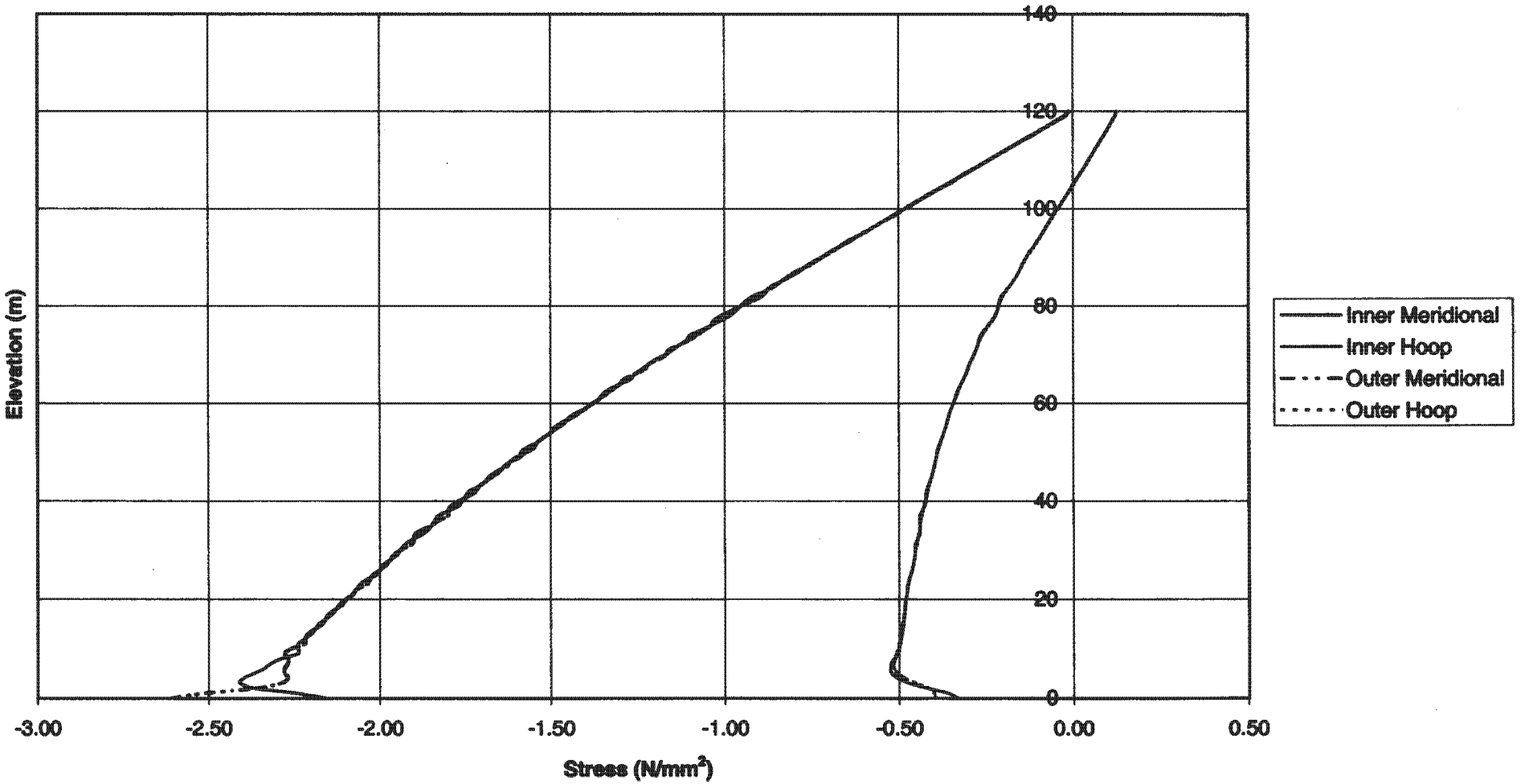

Fig. 6.14 Effect On Offset Parameter, A=10m

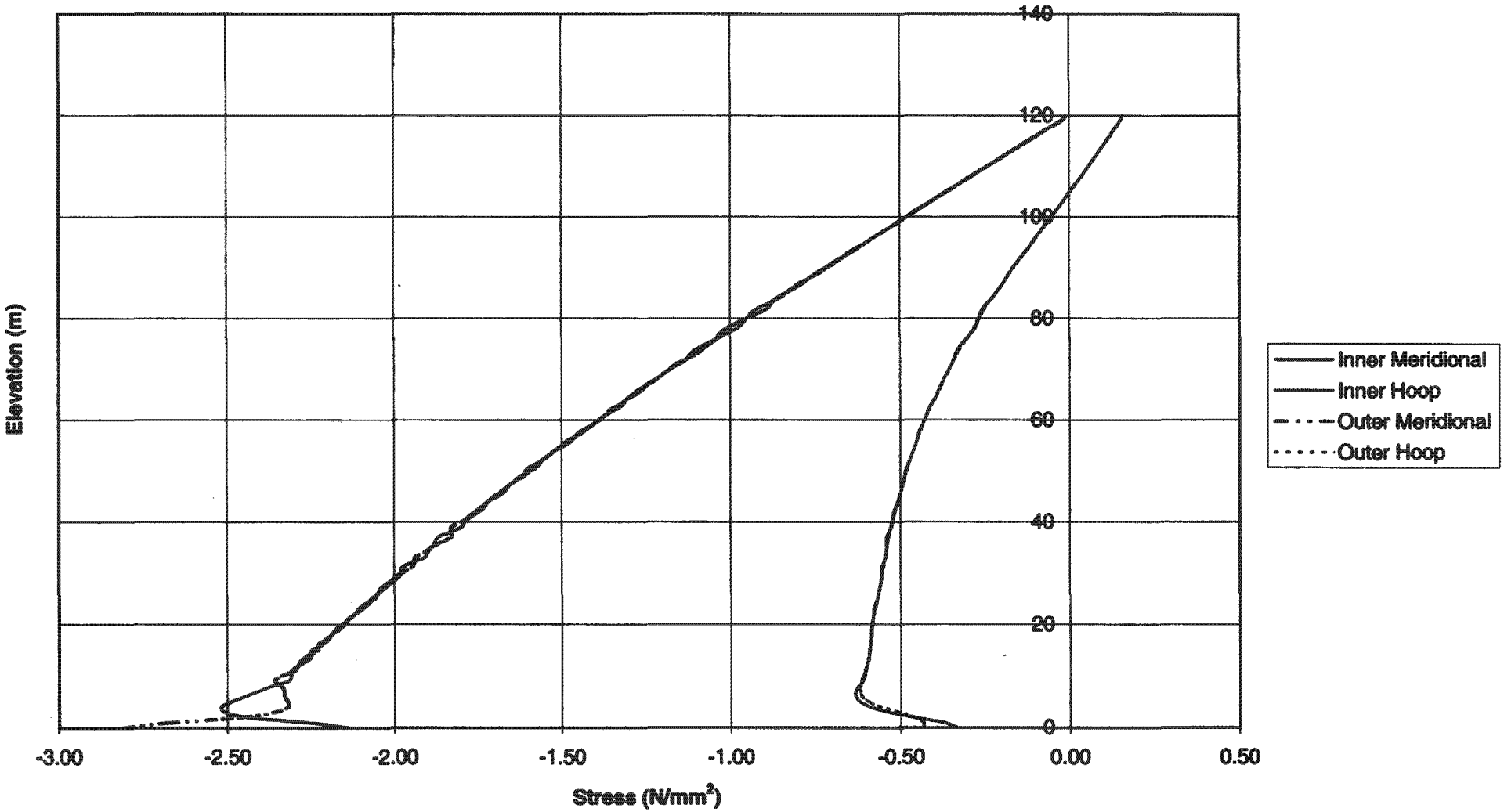

Fig. 6.15 Effect On Offset Parameter, A=20m

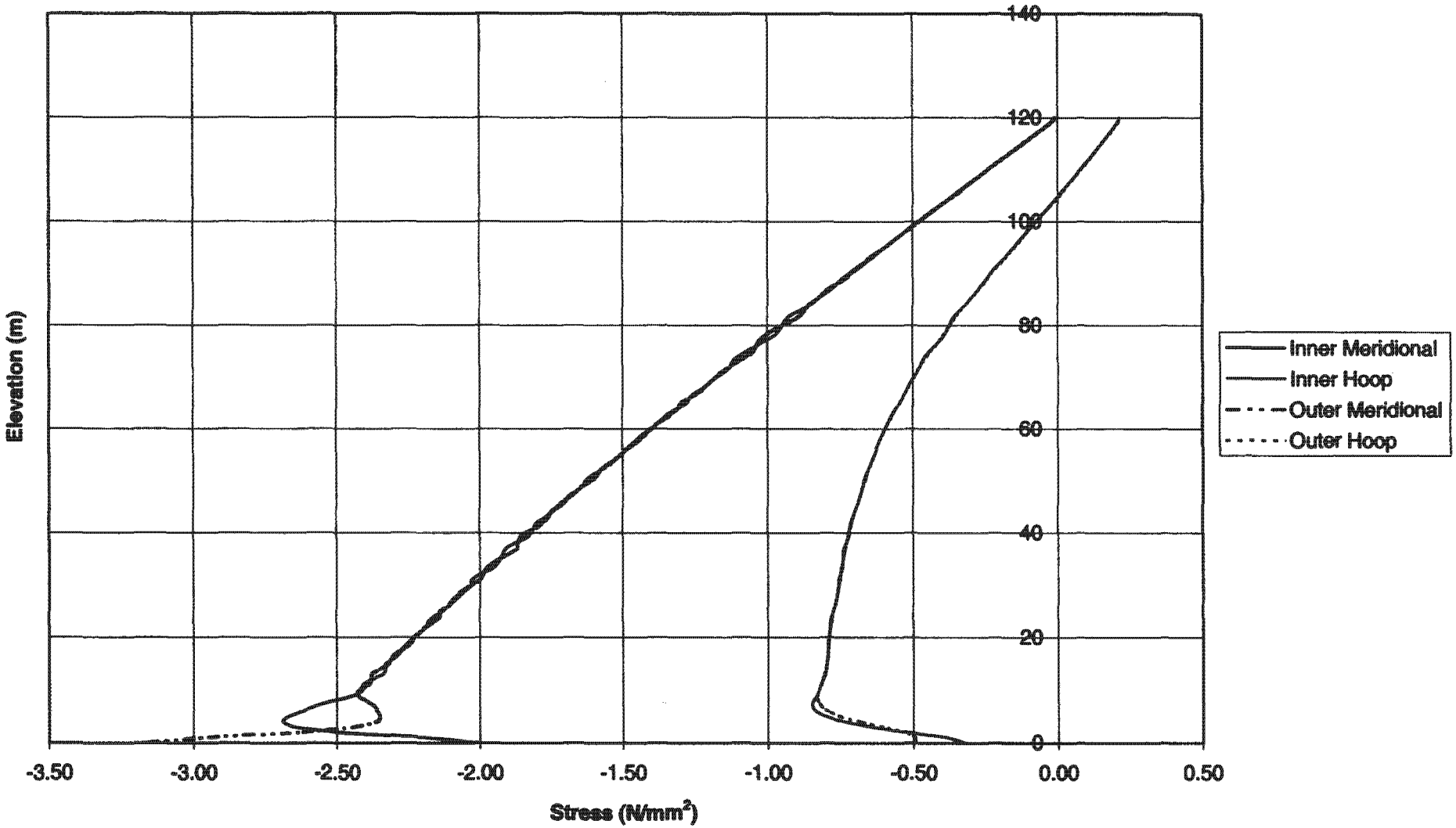

Fig. 6.16 Effect On Offset Parameter, A=40m

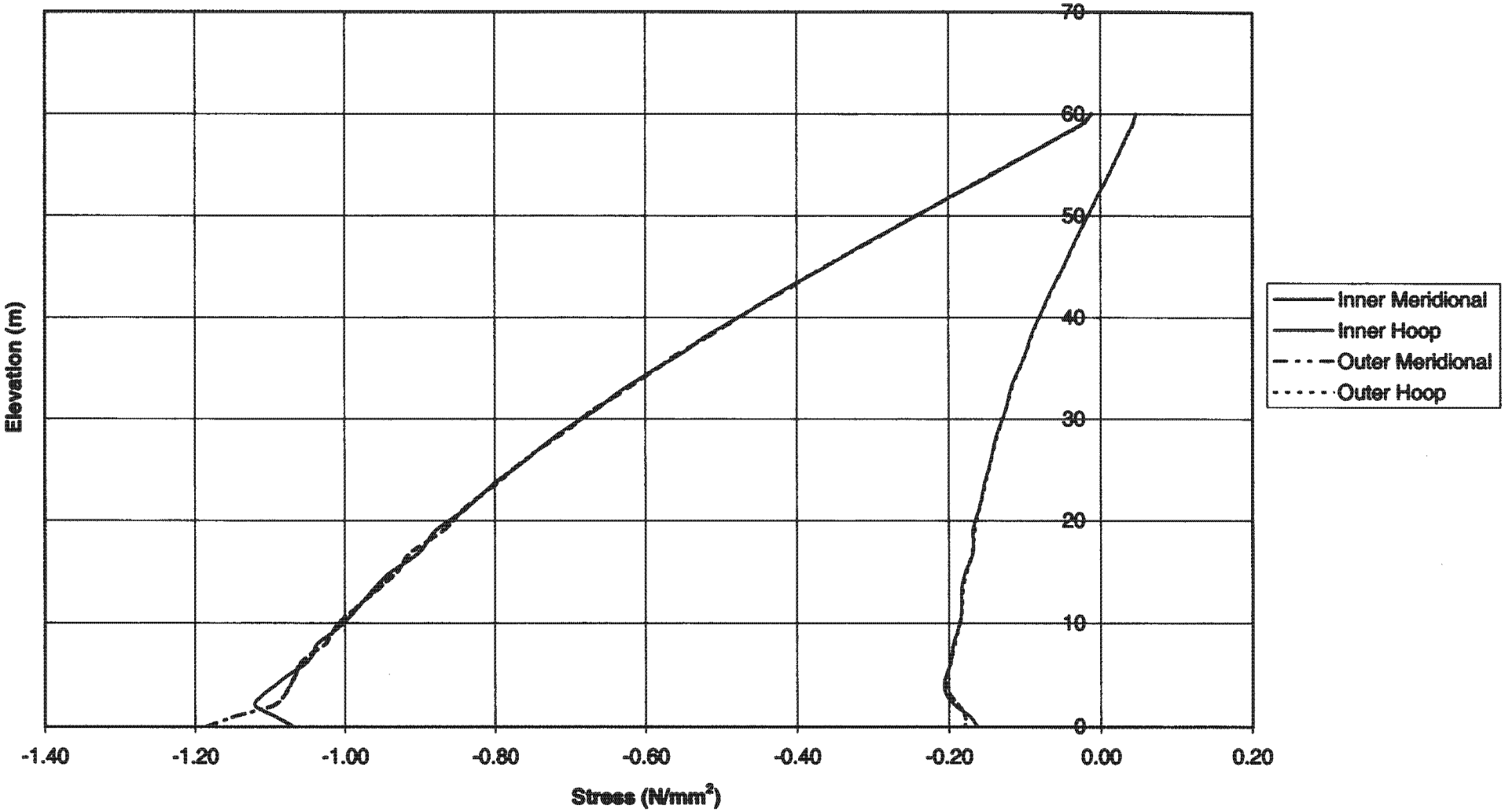

Fig. 6.17 Effect On Scale I.e. Scale Factor=0.5

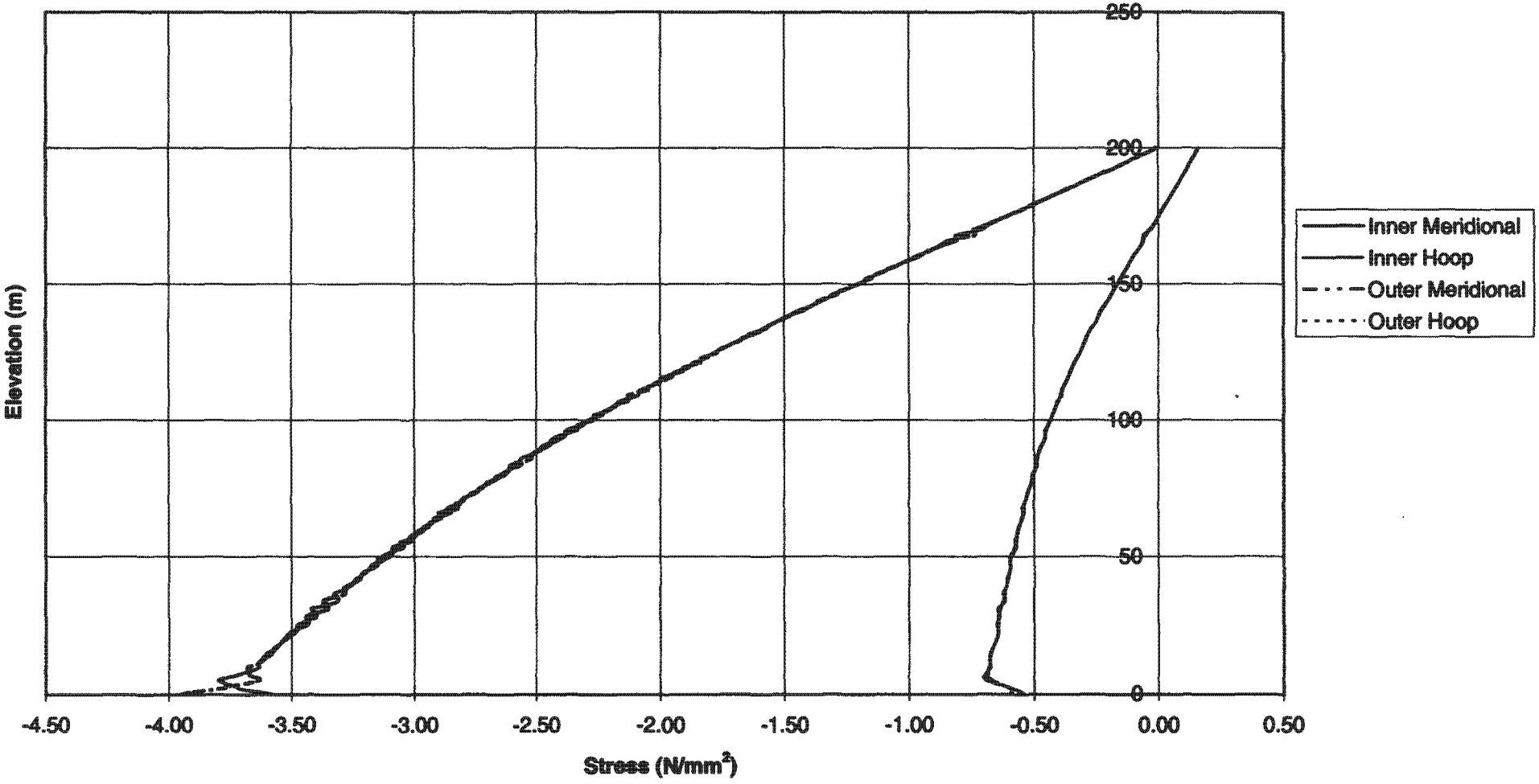

Fig. 6.18 Effect On Scale, i.e. Scale Factor=1.667

CHAPTER SEVEN

DISCUSSION OF RESULTS

7.1 INTRODUCTION

Consider a hyperbolic cooling tower with a zero offset parameter. Self-weight is always associated with meridional stress (σ_ϕ), which is continually compressive throughout the entire shell. The hoop stress (σ_θ) is compressive over almost the entire tower but changes to tensile stress a short distance above the throat of the tower. These tensile stresses are small in magnitude when compared to the stresses at the base of the tower. The tensile stress over this region can be 'arrested' by introducing a ring beam of considerable size at the top edge or by thickening the section approaching the top edge.

Each set of plots comprises the total stress values for the inner and outer surfaces of the shell.

7.2 EFFECT OF HYPERBOLIC AXIS RATIO ON STRESS

7.2.1 Hyperbolic Axis Ratio *b/a*=2.2

Figure 6.3 (see previous Chapter, page 72) illustrated the FEM (Finite-element) results for inner and outer-surface meridional and hoop stresses over the height of a cooling tower. As expected, it can be seen that the meridional stress increases rapidly from a minimum of 0.012N/mm^2 (compression) at the top (ϕ_0=100.65^0) to a net maximum of 2.49N/mm^2 (compression) at the bottom (ϕ_b=69.87^0). The magnitude of the compressive meridional stress at the bottom is a result of the bending effect around this vicinity. The effect of the bending disturbance becomes insignificant beyond an angular distance of ϕ=71.70^0.

Figure 6.3 also shows the hoop stress, which is compressive over the main part of the structure and changes to tension at an angular distance of ϕ=95.75^0 (i.e. 15m above the throat), reaching a maximum of 0.143N/mm^2 (tension) at the top. As a result of the

bending action at the base, a large hoop stress (0.571N/mm^2) is observed at an angular distance of 70.32^0 (i.e. 6m from the base).

7.2.2 Hyperbolic Axis Ratio *b/a*=2.5

Figure 6.4 (see previous Chapter, page 73) shows a plot for the meridional and hoop stresses for *b/a*=2.5. However, an increase above this amount shows a reduction in hoop stress towards the soffit of the structure. It will be noticed that at an angular distance of ϕ=73.39^0 (6m from the bottom), the stress at the inner surface attains a maximum compressive hoop stress value of 0.469N/mm^2 when compared to 0.569N/mm^2 (compression) for a *b/a*=2.2. Beyond 7m from the base, the bending disturbance becomes insignificant.

The meridional stress also follows a similar trend from the top to an angular distance of ϕ=74.21^0 (15m from the base of the cooling tower). Below this elevation, a significant increase in the meridional stress is observed. However, it can be seen that the net meridional stress reaches a maximum of 2.41N/mm^2 (compression) at the soffit (ϕ_b=72.92^0) of the structure.

7.2.3 Hyperbolic Axis Ratio *b/a*=2.8

Figure 6.5 (see previous Chapter, page 74) clearly shows a significant reduction in the magnitude of the net compressive meridional stress from 2.49N/mm^2 (b/a=2.2) to 2.37N/mm^2 at the base of the structure (ϕ=75.37^0). It is interesting to note that the influence of the bending disturbance becomes insignificant at an angular distance of ϕ=75.83^0 (6m above the base), while for other cases (i.e. *b/a*=2.2, 2.5), the bending disturbance become insignificant at 9m from the base of the tower. Beyond the bending region (i.e. ϕ=75.83^0) the profile follows a similar trend as in previous studies.

The hoop stresses also follow similar profiles as in earlier cases, except at the bottom of the tower (ϕ_b=75.37^0) where a significant reduction (i.e. a 75% reduction when compared to b/a=2.2) in hoop stress is observed (0.328N/mm^2).

It can be observed that *b/a* below the standard size (*b/a*=2.694) shows an increase in both the meridional and hoop stresses at the base of the tower. However, considering the upper limit above the standard size cooling tower, a reduction in the meridional and hoop stresses is observed which imply that the higher *b/a*, the lower is the meridional and hoop stresses at the bottom.

7.3 EFFECT OF TOP OPENING ANGLE ON STRESS

7.3.1 *b/a*=2.694, Top Opening Angle $\phi_0=100^0$

Figure 6.6 (see previous Chapter, page 75) plots the inner and outer meridional and hoop stresses at an angle of opening of 100^0. The meridional and hoop stress profiles are similar to those of the standard case cooling tower (b/a=2.694) except in a particular part of the tower, where a slight deviation occurs. Consider the lower portion of the shell towards the base, where the net meridional stress reaches a maximum of 2.610N/mm^2 (compression). The effect of the bending disturbance becomes insignificant at an angular distance of $\phi=75.64^0$ (8m above the base). However, 28m above the throat of the tower is the start point at which the meridional stress exhibits some significant bending effect, which is reduced to normal at an angular distance of $\phi=98.39^0$ (35m above the throat). Near the top (i.e. 3m below the top), a slight bending effect is observed. This action over this particular portion of the tower could be reduced by introducing ring beams around the top edge of the tower.

The hoop stress profile exhibits a similar trend to the standard plot (b/a=2.694) as it changes from compression to tension just some distance above the throat.

7.3.2 *b/a*=2.694, Top Opening Angle $\phi_0=95^0$

Figure 6.7 (see previous Chapter, page 76) depicts the meridional and hoop stress plots with $\phi_0=95^0$. The meridional stress profile from the top to the bottom is similar to the first case ($\phi_0=100^0$). It can be seen that there is a 15% reduction in the maximum net meridional compressive stress at the base from 2.61N/mm^2 ($\phi=100^0$) to 2.21N/mm^2. Similarly, it is observed that at an angular distance of $\phi=75.45^0$, there is a 7% reduction in the hoop stress.

When these cases are compared to the standard size opening angle (ϕ_0=97.36^0), it is observed that ϕ_0 towards the lower range exhibit an average 7% reduction in both the hoop and meridional stresses over the region of bending disturbances.

7.3.3 *b/a*=2.2, Top Opening Angle ϕ_0=100^0

Figure 6.8 (see previous Chapter, page 77) illustrates the inner and outer surface meridional and hoop stresses. As expected, the meridional and hoop stress profiles still follow the same trend as in the standard case. At the base, the net maximum meridional stress observed is 1.95N/mm^2 (compression). However, moving away from the base, the meridional stress is reduced to a minimum and the effect due to bending becomes insignificant at an angular distance of ϕ=76.29^0 (6m above the base).

It is interesting to note that at ϕ=76.07^0 (6m above base), the hoop stress reaches a maximum of 0.434N/mm^2 (compression) which is at the region were the bending meridional stress is at its minimum. At the base, the net hoop stress reduces to a minimum of 0.292N/mm^2 (compression). At an angular distance of ϕ=95.39^0 (14m above the throat), the hoop stress changes to tension and reaches a maximum of 0.133N/mm^2 (tension).

7.3.4 b/a=2.2, Top Opening Angle ϕ_0=95^0

Figure 6.9 (see previous Chapter, page 78) considers what happens when ϕ_0=95^0. At the base, the net maximum meridional stress is 1.64N/mm^2 (compression) which is clearly smaller than ϕ_0=100^0 at the same location. 8m above the base, the bending disturbance becomes insignificant and the stress profile remains the same as expected.

At an angular distance of ϕ=76.07^0 (6m above the base), the hoop stress reaches a maximum of 0.39N/mm^2 (compression) and a minimum of 0.143N/mm^2 (compression) at the base.

It can be seen that reducing ϕ_0 from 100^0 to 95^0 also reduces the meridional and hoop stresses at the region where the bending action is pre-eminent.

7.3.5 b/a=2.5, Top Opening Angle $\phi_0=100^0$

Figure 6.10 (see previous Chapter, page 79) shows the meridional and hoop stress for a b/a=2.5 and $\phi_0=100^0$. With regards to the meridional stress at the base, it is clear that due to bending action in this region the net meridional stress reaches a maximum compressive value of 2.25N/mm^2, which diminishes with an increase in height. At an angular distance of $\phi=75.70^0$ (6m above the base), the resulting bending action becomes insignificant.

The hoop stress reaches a maximum of 0.146N/mm^2 (compression) at a distance 6m above the soffit of the structure, and continues in compression with an increase in height to about 18m above the throat of the tower. However, at an angular distance of $\phi=95.61^0$ (19m from the throat), the hoop stress changes to tension and increases with height, attaining a maximum hoop stress of 0.137N/mm^2 (tension) at the top. When compared to the standard-size cooling tower, it can be seen that there is an average reduction of 15% in meridional stresses and a 23% for hoop stresses. Also the standard-size tower indicates that at a location 7–8m from the base, the meridional bending stress becomes insignificant.

7.3.6 b/a=2.5, Top Opening Angle $\phi_0=95^0$

Fig. 6.11 (see previous Chapter, page 80) illustrates the stress variation when $\phi_0=95^0$. Considering the location at the base, the net maximum meridional stress observed is 1.89N/mm^2 (compression). At an angular distance of 75.97^0 (8m above the base of tower), the bending effect is reduced appreciably. Above this point, the meridional stress continues to reduce with an increase in height to a minimum of 0.004N/mm^2 (compression) at the top edge.

The hoop stress attains a maximum compression of 0.384N/mm^2 at an angular distance of $\phi=75.57^0$ (5m above the base), and follows similar characteristics as shown in previous cases studied, by changing from compression to tension just a short distance above the

throat.(i.e. at an angular distance of 92.73^0 which is 9m above the throat). This tensile stress increases to a maximum of $0.061N/mm^2$ at the top edge.

7.3.7 b/a=2.8, Top Opening Angle $\phi_0=100^0$

As can be seen in Figure 6.12 (see previous Chapter, page 81), the region at which the bending disturbance is significant is a mere 4m from above the base of the tower. Meanwhile, the net meridional stress reaches a maximum of $2.73N/mm^2$ (compression) at the base and reduces with an increase in height. When compared to the standard case, it implies a 13% increase in the meridional stress.

The hoop stress, on the other hand, increases gradually from a minimum of $0.004N/mm^2$ (compression), 24m above the throat of the cooling tower to a maximum of $0.426N/mm^2$ (compression), 7m above the base ($\phi=75.44^0$) indicating a 2% increase in the hoop stress when compared to the standard case.

7.3.8 b/a=2.8, Top Opening Angle $\phi_0=95^0$

Figure 6.13 (see previous Chapter, page 82) summarises the inner and the outer surface meridional and hoop stresses for $\phi_0=95^0$. The plot profile is similar to the earlier cases discussed above. As can be expected, a reduction in the stresses is observed. For example, the net meridional stress reaches a maximum of $2.33N/mm^2$ at the base. It can also be seen that a slight bending action occurs in a region very close to the top edge. The magnitude of this stress is however insignificant when compared to the stress at the base.

As for the hoop stress, it attains a maximum compression of $0.40N/mm^2$ at about 7m above the base of the tower ($\phi=75.44^0$). When compared to the standard case, a reduction of 4% is observed.

For all the cases studied, it is observed that there is a reduction in the meridional and hoop stresses when ϕ_0 (the opening at the top of the cooling tower) is reduced from 100–95^0.

7.4 EFFECT OF OFFSET PARAMETER (*A*)

7.4.1 Offset Parameter A=10m

Figure 6.14 (see previous Chapter, page 83) presents a plot which shows the effect of the meridional and hoop stresses when the offset parameter *A* is varied beyond zero (i.e. *A*=0, standard case). The meridional profiles follow the same trend as in the previous cases (i.e. increasing rapidly from top to bottom), while the hoop stress is tensile toward the top and compressive over the major part of the tower.

With regards to the meridional stress–, the net compressive meridional stress at the base is 2.610N/mm^2 which, when compared to the standard case, is 10% higher in magnitude. The effect of the bending disturbances reduces with an increase in the height and reaches a minimum value – 12m above the base of the tower (ϕ=75.55^0). Beyond this region towards the top, the inner and outer surface meridional stress becomes more or less the same.

7.4.2 Offset Parameter A=20m

The increase in the offset parameter by 20m will obviously increase both the hoop and meridional stresses. Figure 6.15 (see page 84) shows the meridional and hoop stresses when the offset parameter *A*=20m. The plot shows an increase in hoop stress due to bending disturbance towards the base. At this stage, some buckling mode starts developing towards the base of the cooling tower. Appendix A3 shows the contour stress plots for this scenario. At an angular distance of ϕ=75.11^0, the hoop stress reaches a maximum of 0.633N/mm^2 (compression), which indicates a 40% increase in stress at this point when compared to the standard case (*A*=0). The magnitude reduces to a minimum of 0.334N/mm^2 at the base.

As a result of the offset parameter being increased to 20m, the net meridional stress increases to a maximum of 2.81N/mm^2 (compression). It is interesting to note that the position where the bending disturbances becomes insignificant, is at an angular distance of ϕ=75.45^0 (12m from the base), which happens to be the same as in the case of A=10m. Beyond this point towards the top, the meridional stress is compressive.

7.4.3 Offset Parameter A=40m

Figure 6.16 (see page 85) shows the meridional and hoop stress variation for A=40m. As a result of an increase to 40m, the structure is not capable of carrying its self-weight and thus a buckling mode is developed at this region towards the base. The hoop stress reaches a maximum of 0.849N/mm^2 (compression) at an angular distance of ϕ=75.11^0. This indicates a 50% increase in hoop stress when compared to the standard/benchmark cooling tower.

Figure 6.16 shows a maximum net meridional stress of 3.16N/mm^2 (compression) at the base. This is large in comparison to the other cases studied. It is believed at this stage that the self-weight, which is always related to the meridional stress, is not able to support the structure. As a result, the vulnerability of the entire structure is increased.

After a close look at the effect, which the offset parameter *A* has over the hoop and meridional stresses, it can be concluded that an increase in the offset parameter will also increase these stresses. Offset parameters greater than 10m should be avoided in the design consideration. An offset parameter of zero (*A*=0) should preferably be used during the preliminary design stage.

7.5 EFFECT OF SCALE ON STRESSES

7.5.1 Scale Factor=0.5

Figure 6.17 (see page 86) illustrates what happens when the standard-size cooling tower is scaled down by half its size (reduced to 60m in height). The maximum net meridional stress at the base is 1.184N/mm^2 (compression) which highlights a 50% reduction from the standard case. The hoop stress also reaches a peak magnitude of 0.206N/mm^2, 4m above the soffit (ϕ=75.19^0), also indicating a 50% reduction in stresses.

7.5.2 Scale Factor=1.66

Figure 6.18 (see page 87) shows what happens when the cooling tower is increased to 200m in height, namely 1.667 times the original size. The net meridional stress is

3.95N/mm^2, which represents a 45% increase. Similarly, a maximum hoop stress of 0.707N/mm^2 is recorded, which represents 40% increase in stress.

In conclusion, it appears from the above that an increase or decrease in the geometric dimensions of the structure will also increase or decrease the corresponding stresses. It is clearly shown from the above mentioned results that an increase in stress does not necessarily increase by the same scale factor.

7.6 CONCLUDING REMARKS

Having investigated the effect of the various parameters (b/a, ϕ_0, A, scale factor) on the distribution of stresses, the next chapter will represent and highlight general/overall conclusion with regards to the parameters that have the greatest influence on design stress, and lastly various recommendations as to how this problems can be overcome.

CHAPTER EIGHT

SUMMARY OF RESULTS, CONCLUSIONS AND RECOMMENDATIONS

8.1 SUMMARY OF RESULTS

8.1.1 Hyperbolic Axis Ratio (b/a)

After a close look at the effect of the hyperbolic axis ratio (b/a) on the meridional and hoop stresses, it is clear that b/a=2.8 shows the least value in the magnitude of the stress variations when compared to b/a=2.2 and 2.5. A maximum meridional stress of 2.37N/mm^2 (compression), a maximum hoop stress of 0.392N/mm^2 (compression) at the base and a tensile hoop stress of 0.088N/mm^2 at the top edge of the cooling tower are recorded.

8.1.2 Top-Opening Angle (ϕ_0)

The effect of the top-edge angle ϕ_0 on the stress variations shows that an increase in ϕ_0 from 95-100^0 will result in an increase in both the meridional and the hoop stresses for all the cases investigated (i.e. b/a= 2.2, 2.5, 2.694, 2.8). These increases recorded lie between 14-24% for meridional stress and between 6–10% for hoop stress.

8.1.3 Offset Parameter (*A*)

It is observed that with an increase of the offset parameter *A* from 0 to 40m, the meridional and hoop stresses also increases; at the tower base, however, a critical bending disturbance will also occur. It is worthwhile to note that at *A*=10, 20 and 40m, the maximum meridional stress increases by 8, 15 and 24% respectively when compared to the standard benchmark cooling tower with *A*=0. The hoop stresses also show increases by 20, 33 and 50%, highlighting that the offset parameter must be kept at a minimum distance to achieve a reduction in the stress variations at the base of the tower.

8.1.4 Scale Factor

The effect of scale on stress levels in the shell structure indicates that, a reduction in the actual geometric scale of the structure will result in a reduction in the meridional and hoop stresses by the same scale-factor. But increasing the geometric scale of the structure will not necessarily increase the corresponding stresses by the same scale factor.

8.2 CONLUSIONS AND RECOMMENDATIONS

A parametric study on the use of the numerical analysis to determine the static effect of b/a, ϕ_0, A, and scale factor on the meridional and hoop stresses of a hyperbolic cooling tower with uniform thickness is presented herein. The numeric analysis was checked by comparing the results obtained with closed-form analytical membrane solution and this method was shown to be accurate.

Due to the fact that only the static stresses are considered in the present analysis, the meridional stress is of more significance. The meridional compression stress increases steeply from the top to the bottom, reaching its maximum stress at the base of the structure, which results in the loss in bending resistance. In order to control the increasing meridional compression, (which may give rise to buckling problems in the shell) and the hoop tension (which may give rise to cracking in the concrete shell) as one moves downwards, a number of measures are recommended. First, the high stress at the base could be reduced by gradually increasing the thickness of the shell as one approaches the base. By so doing, the stresses are reduced appreciably. Above the lower region towards the throat, the shell section must be kept at its minimum constant thickness. The reason for this is that the stress level in this region is generally small. Above the throat in a narrow region adjacent the top edge, the shell thickness may either be gradually increased to reduce the tensile stress and/or a ring beam of modest proportion may be provided around the top edge if only the effect of self-weight is of main concern. Secondly, the provision of double layers of steel reinforcement to prevent wide-spread cracks in the concrete and the introduction of concrete stiffening rings at a reasonable distance along the entire height of the cooling tower could also help to reduce the stresses.

Based on the observations of the study, and as a measure for controlling increasing meridional and hoop stresses, it can be concluded that for preliminary design purposes, a hyperbolic axis ratio of b/a=2.2, a top opening angle $\phi_0=95^0$ and a zero offset parameter (A=0) should be adopted.

Further research on numeric analysis should consider the combination of self-weight and wind loading, incorporating the actual column support for gradually varying wall thickness, which is also necessary.

REFERENCES

1. **Medwadosski S.** Concepyual Design of Shells in ACI Publication, Concrete Thin Shells, SP- 28 ACI, Detroit Michigan, 1971.
2. **Harry Kraus.** Thin Elastic Shells, John Wiley and Sons, New York, 1967.
3. **Novozhilov V.V.** Thin Shell Theory, Wolters-Noordhoff Publishing, Groningen, The Netherlands, 1970.
4. **Zingoni A.** Shell Structures in Civil and Mechanical Engineering, Thomas Telford Publishing, London, 1997.
5. **Timoshenko S.P.** History of Strength of Materials, McGraw-Hill, New York, 1953. (Also published by Denver Publications, New York, 1983).
6. **Mckelvey K.K and Maxey Brooke.** The Industrial Cooling Tower (with special reference to the design, construction, operation and maintenance of water cooling towers), Elsevier Publishing Company, New York, 1959.
7. **Rish R.F and T.F Steel.** Design and Selection of Hyperbolic Cooling Towers, Journal of the Power Division. Proc. ASCE, Oct 1959, PO 5.
8. **Jean- Francois Julian, Waeil Aflak, Yuan L'huby.** Cause of Deformed Shapes in Cooling Towers, Journal Structural Engineering Vol. 120 No 5- 6 1994.
9. **Harte R, Kratzig W.B.** Lifetime-Oriented Analysis and Design of Large-Scale Cooling Towers. Structural Engineering, Mechanics and Computation, Vol. 1, 2001 Elsevier Science Ltd.
10. **Martin, D. W., Scriven, W. E.** The Calculation of Membrane Stresses in Hyperbolic Cooling Towers, Proceedings, Institution of Civil Engineers, Vol. 19, 1961, pg. 503-13.
11. **Jurgen Straub.** Innovation as to Design and Construction of Natural Draught Cooling Towers from the Point of View of a Construction Company; Proceedings of the 4th international symposium on natural draught cooling towers/ Kaiserslautern/ Germany; Natural draught Cooling Towers, pg 3-14, A.A. Balkema Publishers,1996.
12. **Ihsan Mungan.** Wind Buckling Approach for Reinforced Cooling Towers, Civil Engineering Practice, Structures, pg. 627, Technomi Publishing Company, Inc., 1987.
13. **Flugge, W.** Stresses in Shells, Springer Verlag, Berlin, 1962.
14. **Martin, D. W. Muddock, J. S. and Scriven, W. E.** Membrane Displacements in Hyperbolic Cooling Towers Due to Wind and Dead Loading, Proceeding, Institution of Civil Engineers, Vol. 28, 1964, p327–338.
15. **Billington, D. P.** Thin Shell Concrete Structures, McGraw-Hill Book Co. Inc., New York, 1965.
16. **Gould, P. L. and Lee, S. L.** Hyperbolic Cooling Towers Under Seismic Design Load, Journal of the Structural Division, ASCE, Vol. 93, No. ST3, Proc. Paper 5268, June 1967, p. 87-109.
17. **Gould, P. L. and Lee, S. L.** Bending of Hyperbolic Cooling Tower, Journal of the Structural Division, ASCE, Vol. 93, No. ST5, Oct. 1967.
18. **Gould, P. L.** Minimum Weight Design of Hyperbolic Cooling Towers, Journal of the Structural Division, ASCE, Vol. 93, No. ST2, Feb. 1969.
19. Central Electricity Generating Board: Report of the Committee of Inquiry into the Collapse of Cooling Towers at Ferribridges, Monday, 1 November 1965, London, August 1966.

20. Central Electricity Generating Board: Report on the collapse of cooling tower B2 at Fiddlers Ferry Power Station on 13 January 1984, London, 1985.
21. **Adam Al-Dabbagh & Ajaya k. Gupta.** Meridional Imperfection in Cooling Tower Design: Journal of the Structural Division, ASCE, Vol. 105, June 1979.
22. **Ihsan Mungan.** Buckling Stresses of Stiffened Hyperboloidal Shells, Journal of the Structural Division, ASCE, Vol. 105, Aug. 1979.
23. **Abu-Shitta, S.H and Hashish M.G.** Dynamic Wind Stresses in Hyperbolic Cooling Towers, Journal of Structural Division, ASCE, Vol. 99, No ST 9, Sept, 1973.
24. **Davenport A.G.** The Application of Statistical Concept to the Wind Loading of Structures, Proceedings of Institute of Civil Engineer; Vol. 19, Aug. 1961.
25. **Davenport A.G.** Gust Loading Factors, Journal of Structural Division, ASCE, Vol.93, No. ST3, June, 1967
26. **Isymov, N, Abu-Shitta, S.H & Davenport, A.G.** Approaches to the Design of Hyperbolic Cooling Towers Against the Dynamic Action of Wind and Earthquake, International Association of Shell Structures, Bulletin No 48, March 1972.
27. **Paul Rogers & Eliwin Cohen.** Hyperbolic Cooling Towers Development and Practice, Journal of Power Division, ASCE, Vol.45, PO1, January, 1970.
28. **Hashi,M.G & Abu-Shitta S.H.** Responses of Hyperbolic Cooling Tower to Turbulent Wind, Journal of Structural Division, ASCE, Vol. 100, No ST 5, May, 1974.
29. **Ray, L. Steinmetz, David, P. Billington & John, F. Abel.** Hyperbolic Cooling Tower Dynamic Response to Wind. Journal of Structural Division, ASCE, No ST. 1, Jan, 1978.
30. **John Armitt.** Wind Loading in Cooling Towers, Journal of Structural Division, ASCE, Vol. 106, ST3, March, 1980.
31. **Hans-Jurgen Niemann.** Wind Effect on Cooling Towers Shells. Journal of Structural Division, Vol. 106, No ST. 3, March 1980.
32. **R.A Pope, K.P Grubb, J.D Blackhell.** Structural Deficiencies of Natural Draught Cooling Towers at UK Power Stations. Part 2: Surveying and Structural Appraisal, Proceedings of Institute of Civil Engineers, Structures and Buildings, 1994, Vol. 104, Feb 11-23.
33. **T. Hara, S. Kato and P.L. Gould.** Influence of Reinforcing Arrangement into the Ultimate Strength of R/C cooling Tower Shell, Proceedings of the 4th International symposium on Natural Draught Cooling Towers,
34. **Calladine, C.R.** Theory of Shell Structures, Cambridge University Press, Cambridge, 1983.
35. **Pavlovic, M.N.** A Simple Model for Thin shell Theory–Part 2. Discritized surface, Bending Theory and Membrane Theory, Int. Journal of Mechanical Engineering education vol. 13, No 3, Feb. 1984, Ellis Horwood Limited, Chichester, England.
36. **Zingoni** A. Bending-Disturbance Considerations in the Axisymmetric Response of Non-Shallow Spherical Shell Structures. PhD Thesis, University of London, 1991.
37. **Zingoni A. and Pavlovic M.N.** Some observations on the exactness of the membrane hypothesis in the bending analysis of symmetrically-loaded shells of revolution. Int. Journal of Mechanical Engineering Education, 19(4), 1991, 305-311.
38. **Ugural A.C.** Stresses in Plates and Shells, McGraw-Hill Book Company, 1981.
39. **Gould P.L.** Static Analysis of Shells, Lexington Books, 1977.

40. **Almannai A. Basar, Y and Mungun I.** Basic Aspects of Buckling of Cooling Tower Shells. Journal of the Structural Division, ASCE, Vol. 107, No. ST3, 1981.
41. **Zingoni, A.** Self-Weight Stresses in Hyperbolic Cooling Towers of General Shape. International Journal of Space Structures, Vol.14, No.4, 1999, 281-294.
42. **Gradshteyn, I.S. and Ryzhik, I.M.** Table of Integrals, Series and Products. Academic Press, New York, 1980.
43. **Burnett, D.S.** Finite Element Analysis from Concepts to Applications, Addison-Wesley Publishing Company, Amsterdam, 1987.
44. **Cook, R.D, Malkus, D.S, & Plesha, M.E.** Concepts & Applications of Finite Element Analysis, 3rd Edition, Wiley & Sons, 1989.
45. **Gould, P.L.** Finite Element Analysis of Shells of Revolution, Pitman Publishing Pty. Ltd, 1985.
46. **Baguley, D & Hose, D.R.** How to Model & Interpret Results, Part 1: An Illustration of Idealisation & Modelling Strategies, BENCHmark,July, 2000, Pgs 4-7.
47. **ABAQUS Standard** User's Manual (version 6.2). New York: Habbitt, Karlsson & Sorensen Inc., 2001.

APPENDIX A1

TABLES FOR NUMERIC ANALYSIS OF STRESSES

TABLE 6.3 NUMERIC ANALYSIS OF STRESSES
Uniform Thickness, b/a=2.694

Y (m)	ϕ	Stresses at Inner Surface		Stresses at Outer Surface	
		σ_ϕ (N/mm^2)	σ_θ (N/mm^2)	σ_ϕ (N/mm^2)	σ_θ (N/mm^2)
0	74.561	-2.130	-0.323	-2.380	-0.360
1	74.634	-2.180	-0.339	-2.320	-0.359
2	74.709	-2.250	-0.371	-2.240	-0.368
3	74.786	-2.260	-0.397	-2.200	-0.386
4	74.864	-2.250	-0.412	-2.190	-0.402
5	74.944	-2.220	-0.418	-2.180	-0.411
6	75.025	-2.200	-0.417	-2.180	-0.413
7	75.107	-2.190	-0.414	-2.170	-0.410
8	75.191	-2.170	-0.407	-2.160	-0.405
9	75.277	-2.140	-0.397	-2.170	-0.402
10	75.365	-2.130	-0.396	-2.150	-0.398
11	75.454	-2.140	-0.398	-2.120	-0.394
12	75.545	-2.120	-0.395	-2.110	-0.393
13	75.638	-2.090	-0.390	-2.110	-0.392
14	75.733	-2.090	-0.389	-2.090	-0.389
15	75.829	-2.080	-0.388	-2.070	-0.386
16	75.928	-2.060	-0.385	-2.070	-0.385
17	76.028	-2.050	-0.382	-2.050	-0.383
18	76.130	-2.040	-0.382	-2.030	-0.381
19	76.234	-2.030	-0.381	-2.020	-0.379
20	76.341	-2.010	-0.378	-2.010	-0.378
21	76.449	-1.990	-0.376	-2.000	-0.376
22	76.560	-1.980	-0.374	-1.980	-0.374
23	76.672	-1.980	-0.373	-1.960	-0.371
24	76.787	-1.960	-0.370	-1.950	-0.368
25	76.904	-1.940	-0.364	-1.940	-0.365
26	77.023	-1.930	-0.361	-1.930	-0.361
27	77.145	-1.910	-0.358	-1.910	-0.358
28	77.269	-1.900	-0.355	-1.900	-0.356
29	77.395	-1.880	-0.353	-1.890	-0.354
30	77.524	-1.870	-0.353	-1.870	-0.353
31	77.655	-1.870	-0.354	-1.840	-0.350
32	77.788	-1.840	-0.348	-1.840	-0.347
33	77.924	-1.820	-0.342	-1.830	-0.344
34	78.063	-1.800	-0.339	-1.820	-0.341
35	78.204	-1.790	-0.340	-1.800	-0.340
36	78.348	-1.790	-0.342	-1.770	-0.339
37	78.494	-1.780	-0.341	-1.750	-0.337
38	78.643	-1.750	-0.334	-1.750	-0.334
39	78.795	-1.720	-0.327	-1.740	-0.330
40	78.950	-1.710	-0.325	-1.720	-0.326
41	79.107	-1.710	-0.326	-1.700	-0.324
42	79.267	-1.690	-0.324	-1.680	-0.322
43	79.430	-1.670	-0.320	-1.670	-0.319
44	79.596	-1.650	-0.316	-1.650	-0.315
45	79.764	-1.630	-0.311	-1.640	-0.311
46	79.935	-1.620	-0.308	-1.620	-0.308
47	80.110	-1.610	-0.306	-1.600	-0.305
48	80.287	-1.590	-0.303	-1.590	-0.302
49	80.467	-1.560	-0.300	-1.570	-0.301

48	80.287	-1.590	-0.303	-1.590	-0.302
49	80.467	-1.560	-0.300	-1.570	-0.301
50	80.650	-1.560	-0.299	-1.550	-0.297
51	80.836	-1.540	-0.296	-1.530	-0.294
52	81.025	-1.510	-0.291	-1.520	-0.291
53	81.216	-1.500	-0.287	-1.500	-0.286
54	81.411	-1.480	-0.282	-1.480	-0.282
55	81.609	-1.460	-0.278	-1.460	-0.279
56	81.809	-1.440	-0.275	-1.450	-0.276
57	82.012	-1.430	-0.273	-1.420	-0.272
58	82.219	-1.410	-0.270	-1.400	-0.269
59	82.428	-1.390	-0.265	-1.390	-0.265
60	82.640	-1.370	-0.261	-1.370	-0.261
61	82.854	-1.350	-0.257	-1.350	-0.257
62	83.072	-1.340	-0.254	-1.330	-0.253
63	83.292	-1.320	-0.249	-1.310	-0.248
64	83.515	-1.290	-0.243	-1.290	-0.243
65	83.740	-1.270	-0.236	-1.280	-0.238
66	83.968	-1.250	-0.233	-1.250	-0.233
67	84.199	-1.240	-0.230	-1.230	-0.229
68	84.432	-1.210	-0.225	-1.210	-0.225
69	84.667	-1.190	-0.221	-1.190	-0.220
70	84.905	-1.170	-0.215	-1.170	-0.215
71	85.144	-1.140	-0.209	-1.160	-0.211
72	85.387	-1.130	-0.206	-1.130	-0.207
73	85.631	-1.110	-0.204	-1.100	-0.203
74	85.877	-1.090	-0.200	-1.080	-0.198
75	86.125	-1.070	-0.194	-1.060	-0.192
76	86.375	-1.050	-0.184	-1.040	-0.183
77	86.626	-1.020	-0.174	-1.030	-0.175
78	86.880	-0.988	-0.165	-1.010	-0.168
79	87.134	-0.970	-0.162	-0.983	-0.164
80	87.390	-0.956	-0.162	-0.952	-0.161
81	87.648	-0.940	-0.161	-0.923	-0.158
82	87.906	-0.920	-0.156	-0.899	-0.153
83	88.165	-0.887	-0.146	-0.886	-0.146
84	88.426	-0.859	-0.137	-0.869	-0.138
85	88.687	-0.841	-0.130	-0.840	-0.130
86	88.949	-0.816	-0.123	-0.819	-0.124
87	89.211	-0.790	-0.117	-0.799	-0.118
88	89.474	-0.773	-0.113	-0.769	-0.112
89	89.737	-0.751	-0.108	-0.744	-0.107
90	90.000	-0.725	-0.101	-0.724	-0.101
91	90.263	-0.703	-0.095	-0.698	-0.094
92	90.526	-0.679	-0.087	-0.676	-0.087
93	90.789	-0.649	-0.079	-0.657	-0.080
94	91.051	-0.628	-0.072	-0.631	-0.073
95	91.313	-0.608	-0.067	-0.604	-0.066
96	91.574	-0.582	-0.060	-0.581	-0.060
97	91.835	-0.557	-0.054	-0.558	-0.054
98	92.094	-0.534	-0.047	-0.533	-0.047
99	92.352	-0.512	-0.041	-0.507	-0.040
100	92.610	-0.486	-0.033	-0.484	-0.033
101	92.866	-0.459	-0.026	-0.463	-0.026
102	93.120	-0.436	-0.019	-0.437	-0.019
103	93.374	-0.411	-0.012	-0.414	-0.013

106	94.123	-0.341	0.006	-0.338	0.007
107	94.369	-0.313	0.014	-0.317	0.014
108	94.613	-0.289	0.021	-0.291	0.021
109	94.856	-0.266	0.027	-0.266	0.027
110	95.095	-0.242	0.034	-0.242	0.034
111	95.333	-0.218	0.040	-0.217	0.040
112	95.568	-0.193	0.047	-0.193	0.047
113	95.801	-0.169	0.053	-0.169	0.053
114	96.032	-0.144	0.060	-0.145	0.060
115	96.260	-0.120	0.066	-0.121	0.066
116	96.485	-0.096	0.073	-0.096	0.073
117	96.708	-0.072	0.079	-0.072	0.079
118	96.928	-0.049	0.085	-0.047	0.085
119	97.146	-0.024	0.092	-0.024	0.092
120	97.360	-0.012	0.095	-0.012	0.095

TABLE 6.4 NUMERIC ANALYSIS OF STRESSES
Uniform Thickness, b/a=2.2

Y (m)	ϕ	Stresses at Inner Surface		Stresses at Outer Surface	
		σ_ϕ (N/mm^2)	σ_θ (N/mm^2)	σ_ϕ (N/mm^2)	σ_θ (N/mm^2)
0	69.870	-1.890	-0.297	-2.490	-0.386
1	69.942	-2.010	-0.342	-2.350	-0.389
2	70.017	-2.190	-0.430	-2.150	-0.420
3	70.093	-2.250	-0.503	-2.070	-0.474
4	70.171	-2.230	-0.548	-2.070	-0.520
5	70.251	-2.190	-0.567	-2.080	-0.549
6	70.332	-2.150	-0.571	-2.100	-0.562
7	70.416	-2.130	-0.569	-2.100	-0.564
8	70.501	-2.110	-0.563	-2.090	-0.561
9	70.589	-2.090	-0.556	-2.090	-0.555
10	70.678	-2.080	-0.549	-2.070	-0.547
11	70.770	-2.060	-0.539	-2.070	-0.541
12	70.864	-2.040	-0.532	-2.060	-0.535
13	70.960	-2.030	-0.528	-2.050	-0.531
14	71.058	-2.020	-0.528	-2.030	-0.529
15	71.159	-2.030	-0.532	-2.000	-0.527
16	71.262	-2.020	-0.529	-1.990	-0.524
17	71.367	-1.990	-0.522	-1.990	-0.521
18	71.476	-1.970	-0.515	-1.990	-0.517
19	71.586	-1.960	-0.511	-1.970	-0.513
20	71.700	-1.950	-0.511	-1.950	-0.510
21	71.816	-1.950	-0.511	-1.930	-0.508
22	71.935	-1.930	-0.508	-1.930	-0.507
23	72.057	-1.910	-0.505	-1.920	-0.505
24	72.182	-1.910	-0.503	-1.890	-0.500
25	72.310	-1.890	-0.497	-1.890	-0.497
26	72.441	-1.870	-0.492	-1.880	-0.494
27	72.575	-1.870	-0.490	-1.860	-0.489
28	72.713	-1.860	-0.488	-1.840	-0.485
29	72.854	-1.840	-0.482	-1.830	-0.481
30	72.998	-1.820	-0.477	-1.830	-0.478
31	73.146	-1.800	-0.473	-1.820	-0.476
32	73.298	-1.800	-0.475	-1.790	-0.474
33	73.453	-1.790	-0.476	-1.770	-0.472
34	73.612	-1.770	-0.473	-1.760	-0.471
35	73.775	-1.760	-0.468	-1.750	-0.466
36	73.942	-1.740	-0.461	-1.740	-0.461
37	74.113	-1.720	-0.454	-1.740	-0.456
38	74.288	-1.710	-0.451	-1.720	-0.452
39	74.468	-1.700	-0.451	-1.700	-0.450
40	74.651	-1.690	-0.450	-1.680	-0.449
41	74.839	-1.670	-0.448	-1.670	-0.447
42	75.032	-1.660	-0.447	-1.650	-0.444
43	75.229	-1.650	-0.442	-1.630	-0.439
44	75.431	-1.620	-0.433	-1.630	-0.433
45	75.637	-1.590	-0.425	-1.620	-0.429
46	75.849	-1.580	-0.424	-1.600	-0.426
47	76.065	-1.590	-0.428	-1.570	-0.425
48	76.286	-1.580	-0.428	-1.550	-0.423

49	76.512	-1.550	-0.421	-1.540	-0.420
50	76.743	-1.520	-0.414	-1.540	-0.416
51	76.980	-1.520	-0.410	-1.510	-0.410
52	77.221	-1.500	-0.406	-1.490	-0.404
53	77.468	-1.470	-0.399	-1.490	-0.401
54	77.721	-1.460	-0.395	-1.470	-0.396
55	77.978	-1.450	-0.393	-1.440	-0.391
56	78.241	-1.430	-0.389	-1.430	-0.389
57	78.510	-1.410	-0.385	-1.420	-0.386
58	78.783	-1.400	-0.383	-1.390	-0.381
59	79.063	-1.380	-0.378	-1.370	-0.376
60	79.348	-1.360	-0.371	-1.370	-0.372
61	79.638	-1.340	-0.366	-1.340	-0.367
62	79.934	-1.330	-0.363	-1.320	-0.362
63	80.235	-1.310	-0.358	-1.300	-0.357
64	80.541	-1.290	-0.352	-1.290	-0.351
65	80.853	-1.270	-0.346	-1.260	-0.344
66	81.170	-1.250	-0.338	-1.250	-0.337
67	81.493	-1.220	-0.329	-1.240	-0.331
68	81.820	-1.210	-0.325	-1.220	-0.326
69	82.153	-1.190	-0.322	-1.190	-0.321
70	82.490	-1.180	-0.319	-1.160	-0.316
71	82.833	-1.160	-0.312	-1.150	-0.310
72	83.180	-1.130	-0.303	-1.130	-0.303
73	83.531	-1.110	-0.295	-1.110	-0.295
74	83.887	-1.090	-0.288	-1.090	-0.287
75	84.248	-1.070	-0.280	-1.070	-0.280
76	84.612	-1.050	-0.272	-1.050	-0.273
77	84.980	-1.030	-0.267	-1.020	-0.265
78	85.351	-1.010	-0.259	-1.000	-0.259
79	85.726	-0.985	-0.251	-0.984	-0.251
80	86.105	-0.968	-0.243	-0.957	-0.242
81	86.486	-0.938	-0.233	-0.943	-0.234
82	86.869	-0.915	-0.224	-0.922	-0.225
83	87.255	-0.899	-0.217	-0.892	-0.216
84	87.643	-0.874	-0.208	-0.872	-0.208
85	88.033	-0.851	-0.199	-0.850	-0.199
86	88.425	-0.830	-0.190	-0.825	-0.189
87	88.818	-0.803	-0.180	-0.806	-0.180
88	89.211	-0.780	-0.171	-0.783	-0.171
89	89.605	-0.760	-0.163	-0.756	-0.162
90	90.000	-0.738	-0.153	-0.732	-0.153
91	90.395	-0.713	-0.143	-0.709	-0.142
92	90.789	-0.686	-0.132	-0.689	-0.132
93	91.182	-0.662	-0.122	-0.665	-0.122
94	91.575	-0.641	-0.112	-0.638	-0.112
95	91.967	-0.616	-0.102	-0.615	-0.102
96	92.357	-0.592	-0.092	-0.591	-0.092
97	92.745	-0.569	-0.082	-0.565	-0.081
98	93.131	-0.541	-0.070	-0.544	-0.071
99	93.514	-0.516	-0.060	-0.520	-0.061
100	93.895	-0.496	-0.051	-0.491	-0.050
101	94.274	-0.469	-0.041	-0.469	-0.041
102	94.649	-0.444	-0.030	-0.444	-0.030
103	95.020	-0.421	-0.020	-0.418	-0.020
104	95.388	-0.394	-0.009	-0.396	-0.009

105	95.752	-0.369	0.001	-0.371	0.001
106	96.113	-0.346	0.011	-0.345	0.012
107	96.469	-0.321	0.021	-0.321	0.021
108	96.820	-0.295	0.031	-0.297	0.031
109	97.167	-0.272	0.041	-0.271	0.041
110	97.510	-0.247	0.051	-0.246	0.052
111	97.847	-0.221	0.061	-0.222	0.061
112	98.180	-0.196	0.071	-0.198	0.071
113	98.507	-0.172	0.081	-0.172	0.081
114	98.830	-0.147	0.090	-0.147	0.091
115	99.147	-0.122	0.100	-0.123	0.100
116	99.459	-0.098	0.109	-0.098	0.109
117	99.765	-0.074	0.119	-0.073	0.119
118	100.066	-0.050	0.128	-0.048	0.128
119	100.362	-0.025	0.137	-0.024	0.138
120	100.652	-0.013	0.142	-0.012	0.143

TABLE 6.5 NUMERIC ANALYSIS OF STRESSES
Uniform Thickness, b/a=2.5

Y (m)	ϕ	Stresses at Inner Surface		Stresses at Outer Surface	
		σ_ϕ (N/mm^2)	σ_θ (N/mm^2)	σ_ϕ (N/mm^2)	σ_θ (N/mm^2)
0	72.918	-2.050	-0.314	-2.410	-0.368
1	72.992	-2.120	-0.339	-2.330	-0.368
2	73.068	-2.220	-0.390	-2.200	-0.384
3	73.145	-2.250	-0.432	-2.150	-0.415
4	73.224	-2.230	-0.456	-2.140	-0.441
5	73.304	-2.200	-0.466	-2.150	-0.457
6	73.386	-2.180	-0.469	-2.150	-0.464
7	73.470	-2.160	-0.468	-2.140	-0.463
8	73.555	-2.150	-0.463	-2.130	-0.460
9	73.643	-2.130	-0.455	-2.120	-0.454
10	73.732	-2.110	-0.447	-2.120	-0.448
11	73.823	-2.090	-0.440	-2.120	-0.444
12	73.916	-2.080	-0.439	-2.100	-0.441
13	74.011	-2.080	-0.441	-2.080	-0.440
14	74.108	-2.080	-0.443	-2.050	-0.439
15	74.207	-2.070	-0.441	-2.030	-0.435
16	74.308	-2.040	-0.432	-2.040	-0.432
17	74.411	-2.020	-0.424	-2.040	-0.427
18	74.517	-2.010	-0.421	-2.020	-0.421
19	74.624	-2.000	-0.418	-2.000	-0.419
20	74.734	-1.980	-0.417	-1.990	-0.418
21	74.847	-1.970	-0.418	-1.980	-0.419
22	74.961	-1.970	-0.421	-1.950	-0.419
23	75.078	-1.960	-0.422	-1.930	-0.418
24	75.198	-1.940	-0.417	-1.930	-0.416
25	75.320	-1.920	-0.412	-1.920	-0.411
26	75.445	-1.910	-0.406	-1.900	-0.405
27	75.572	-1.890	-0.399	-1.900	-0.401
28	75.702	-1.870	-0.395	-1.890	-0.398
29	75.835	-1.860	-0.396	-1.870	-0.396
30	75.970	-1.850	-0.396	-1.850	-0.395
31	76.109	-1.850	-0.397	-1.830	-0.394
32	76.250	-1.830	-0.393	-1.820	-0.392
33	76.394	-1.800	-0.388	-1.810	-0.390
34	76.541	-1.790	-0.386	-1.790	-0.386
35	76.692	-1.780	-0.384	-1.770	-0.382
36	76.845	-1.760	-0.380	-1.770	-0.380
37	77.001	-1.750	-0.377	-1.750	-0.377
38	77.161	-1.740	-0.376	-1.730	-0.373
39	77.324	-1.720	-0.370	-1.720	-0.370
40	77.490	-1.690	-0.365	-1.710	-0.368
41	77.659	-1.690	-0.365	-1.690	-0.365
42	77.832	-1.680	-0.365	-1.670	-0.363
43	78.008	-1.660	-0.362	-1.650	-0.361
44	78.188	-1.650	-0.358	-1.640	-0.356
45	78.371	-1.620	-0.352	-1.630	-0.352
46	78.558	-1.600	-0.347	-1.620	-0.348
47	78.748	-1.590	-0.345	-1.590	-0.345
48	78.941	-1.580	-0.343	-1.580	-0.343
49	79.139	-1.570	-0.342	-1.550	-0.339

50	79.340	-1.550	-0.337	-1.540	-0.336
51	79.544	-1.520	-0.332	-1.530	-0.333
52	79.752	-1.510	-0.329	-1.510	-0.330
53	79.964	-1.500	-0.328	-1.490	-0.326
54	80.180	-1.480	-0.325	-1.470	-0.323
55	80.399	-1.460	-0.319	-1.450	-0.319
56	80.622	-1.440	-0.313	-1.440	-0.313
57	80.849	-1.420	-0.307	-1.430	-0.308
58	81.079	-1.400	-0.304	-1.410	-0.305
59	81.313	-1.390	-0.302	-1.380	-0.301
60	81.550	-1.370	-0.300	-1.360	-0.297
61	81.791	-1.350	-0.293	-1.350	-0.293
62	82.036	-1.330	-0.287	-1.330	-0.288
63	82.284	-1.310	-0.283	-1.310	-0.283
64	82.536	-1.290	-0.278	-1.290	-0.278
65	82.791	-1.270	-0.273	-1.270	-0.273
66	83.049	-1.250	-0.268	-1.250	-0.269
67	83.311	-1.230	-0.265	-1.230	-0.264
68	83.576	-1.210	-0.261	-1.210	-0.260
69	83.844	-1.190	-0.256	-1.190	-0.255
70	84.116	-1.170	-0.250	-1.170	-0.248
71	84.390	-1.150	-0.242	-1.150	-0.242
72	84.667	-1.130	-0.235	-1.130	-0.236
73	84.947	-1.110	-0.231	-1.110	-0.231
74	85.229	-1.090	-0.226	-1.090	-0.226
75	85.515	-1.070	-0.221	-1.060	-0.221
76	85.802	-1.050	-0.216	-1.040	-0.215
77	86.092	-1.030	-0.209	-1.020	-0.207
78	86.384	-0.998	-0.199	-1.000	-0.200
79	86.678	-0.974	-0.191	-0.984	-0.192
80	86.974	-0.952	-0.185	-0.961	-0.186
81	87.271	-0.936	-0.182	-0.933	-0.181
82	87.571	-0.919	-0.178	-0.905	-0.176
83	87.871	-0.896	-0.171	-0.883	-0.169
84	88.173	-0.866	-0.161	-0.867	-0.161
85	88.476	-0.838	-0.151	-0.849	-0.153
86	88.780	-0.819	-0.144	-0.822	-0.145
87	89.084	-0.800	-0.138	-0.795	-0.138
88	89.389	-0.775	-0.131	-0.774	-0.131
89	89.694	-0.751	-0.124	-0.751	-0.124
90	90.000	-0.730	-0.117	-0.725	-0.116
91	90.306	-0.704	-0.109	-0.704	-0.109
92	90.611	-0.680	-0.101	-0.680	-0.101
93	90.916	-0.659	-0.094	-0.654	-0.093
94	91.220	-0.632	-0.085	-0.634	-0.085
95	91.524	-0.605	-0.077	-0.612	-0.078
96	91.827	-0.584	-0.070	-0.585	-0.070
97	92.129	-0.564	-0.064	-0.557	-0.063
98	92.429	-0.540	-0.057	-0.532	-0.056
99	92.729	-0.513	-0.047	-0.511	-0.047
100	93.026	-0.485	-0.038	-0.490	-0.038
101	93.322	-0.461	-0.029	-0.466	-0.030
102	93.616	-0.438	-0.022	-0.440	-0.022
103	93.908	-0.416	-0.016	-0.413	-0.015
104	94.198	-0.392	-0.008	-0.388	-0.008
105	94.485	-0.366	0.000	-0.365	0.000

106	94.771	-0.341	0.008	-0.341	0.008
107	95.053	-0.316	0.016	-0.317	0.016
108	95.333	-0.291	0.025	-0.293	0.024
109	95.610	-0.267	0.032	-0.268	0.032
110	95.884	-0.244	0.039	-0.242	0.040
111	96.156	-0.219	0.047	-0.218	0.047
112	96.424	-0.194	0.054	-0.194	0.055
113	96.689	-0.170	0.062	-0.170	0.062
114	96.951	-0.145	0.070	-0.146	0.070
115	97.209	-0.121	0.077	-0.122	0.077
116	97.464	-0.097	0.084	-0.097	0.084
117	97.716	-0.073	0.092	-0.072	0.092
118	97.964	-0.049	0.099	-0.048	0.099
119	98.209	-0.024	0.106	-0.024	0.107
120	98.450	-0.012	0.110	-0.012	0.110

TABLE 6.6 NUMERIC ANALYSIS OF STRESSES
Uniform Thickness, b/a=2.8

Y (m)	ϕ	Stresses at Inner Surface		Stresses at Outer Surface	
		σ_ϕ (N/mm^2)	σ_θ (N/mm^2)	σ_ϕ (N/mm^2)	σ_θ (N/mm^2)
0	75.367	-2.180	-0.328	-2.370	-0.357
1	75.440	-2.220	-0.340	-2.320	-0.353
2	75.515	-2.270	-0.359	-2.240	-0.354
3	75.591	-2.250	-0.369	-2.230	-0.365
4	75.668	-2.230	-0.376	-2.230	-0.376
5	75.747	-2.230	-0.386	-2.210	-0.382
6	75.827	-2.230	-0.392	-2.190	-0.385
7	75.909	-2.210	-0.390	-2.180	-0.386
8	75.992	-2.190	-0.385	-2.170	-0.382
9	76.077	-2.160	-0.377	-2.180	-0.379
10	76.163	-2.140	-0.373	-2.170	-0.377
11	76.251	-2.150	-0.376	-2.140	-0.374
12	76.341	-2.150	-0.378	-2.110	-0.372
13	76.432	-2.120	-0.372	-2.110	-0.370
14	76.525	-2.090	-0.365	-2.110	-0.367
15	76.620	-2.080	-0.362	-2.100	-0.363
16	76.717	-2.070	-0.361	-2.080	-0.361
17	76.815	-2.060	-0.361	-2.060	-0.361
18	76.915	-2.060	-0.363	-2.040	-0.360
19	77.017	-2.040	-0.362	-2.030	-0.359
20	77.121	-2.030	-0.357	-2.020	-0.356
21	77.227	-2.000	-0.351	-2.020	-0.353
22	77.335	-1.990	-0.349	-2.000	-0.349
23	77.445	-1.980	-0.347	-1.980	-0.346
24	77.557	-1.960	-0.343	-1.980	-0.346
25	77.671	-1.950	-0.344	-1.950	-0.344
26	77.787	-1.950	-0.347	-1.920	-0.342
27	77.905	-1.930	-0.343	-1.920	-0.341
28	78.026	-1.900	-0.338	-1.920	-0.339
29	78.148	-1.890	-0.336	-1.890	-0.336
30	78.273	-1.890	-0.334	-1.870	-0.332
31	78.400	-1.860	-0.329	-1.860	-0.329
32	78.529	-1.850	-0.324	-1.850	-0.325
33	78.661	-1.830	-0.321	-1.830	-0.320
34	78.794	-1.810	-0.317	-1.830	-0.319
35	78.931	-1.800	-0.316	-1.810	-0.318
36	79.069	-1.800	-0.320	-1.780	-0.317
37	79.210	-1.780	-0.320	-1.770	-0.318
38	79.354	-1.750	-0.317	-1.760	-0.317
39	79.499	-1.740	-0.316	-1.740	-0.315
40	79.648	-1.730	-0.314	-1.720	-0.312
41	79.799	-1.720	-0.310	-1.700	-0.307
42	79.952	-1.700	-0.302	-1.690	-0.300
43	80.108	-1.660	-0.290	-1.690	-0.296
44	80.266	-1.650	-0.288	-1.670	-0.291
45	80.427	-1.640	-0.289	-1.640	-0.289
46	80.591	-1.620	-0.290	-1.630	-0.290
47	80.757	-1.620	-0.292	-1.600	-0.289
48	80.925	-1.600	-0.289	-1.580	-0.286

49	81.097	-1.570	-0.282	-1.570	-0.282
50	81.271	-1.550	-0.275	-1.560	-0.277
51	81.447	-1.530	-0.272	-1.540	-0.274
52	81.626	-1.520	-0.272	-1.520	-0.271
53	81.808	-1.510	-0.271	-1.490	-0.268
54	81.992	-1.480	-0.267	-1.480	-0.266
55	82.179	-1.460	-0.263	-1.470	-0.263
56	82.368	-1.450	-0.260	-1.440	-0.259
57	82.560	-1.430	-0.257	-1.430	-0.256
58	82.754	-1.410	-0.252	-1.410	-0.251
59	82.951	-1.390	-0.246	-1.390	-0.246
60	83.150	-1.370	-0.241	-1.370	-0.241
61	83.352	-1.350	-0.237	-1.360	-0.237
62	83.556	-1.330	-0.234	-1.330	-0.234
63	83.763	-1.320	-0.232	-1.310	-0.230
64	83.972	-1.300	-0.228	-1.290	-0.226
65	84.183	-1.270	-0.221	-1.280	-0.222
66	84.396	-1.250	-0.216	-1.260	-0.218
67	84.612	-1.240	-0.215	-1.230	-0.214
68	84.830	-1.220	-0.212	-1.200	-0.210
69	85.049	-1.190	-0.206	-1.190	-0.205
70	85.271	-1.170	-0.199	-1.170	-0.200
71	85.495	-1.140	-0.194	-1.150	-0.195
72	85.720	-1.130	-0.192	-1.130	-0.191
73	85.948	-1.110	-0.189	-1.100	-0.186
74	86.177	-1.090	-0.182	-1.080	-0.181
75	86.408	-1.060	-0.173	-1.070	-0.175
76	86.640	-1.030	-0.168	-1.050	-0.171
77	86.874	-1.020	-0.167	-1.020	-0.166
78	87.109	-1.010	-0.165	-0.987	-0.162
79	87.345	-0.980	-0.157	-0.971	-0.156
80	87.582	-0.950	-0.148	-0.956	-0.149
81	87.821	-0.925	-0.141	-0.936	-0.142
82	88.061	-0.904	-0.136	-0.912	-0.137
83	88.301	-0.887	-0.133	-0.883	-0.133
84	88.542	-0.869	-0.130	-0.856	-0.128
85	88.784	-0.842	-0.124	-0.837	-0.123
86	89.027	-0.817	-0.117	-0.816	-0.116
87	89.270	-0.792	-0.109	-0.794	-0.110
88	89.513	-0.766	-0.103	-0.773	-0.104
89	89.756	-0.747	-0.098	-0.746	-0.098
90	90.000	-0.727	-0.093	-0.719	-0.092
91	90.244	-0.700	-0.086	-0.698	-0.086
92	90.487	-0.673	-0.079	-0.679	-0.080
93	90.730	-0.651	-0.073	-0.653	-0.074
94	90.973	-0.628	-0.068	-0.628	-0.068
95	91.216	-0.606	-0.063	-0.603	-0.063
96	91.458	-0.584	-0.057	-0.576	-0.056
97	91.699	-0.557	-0.050	-0.555	-0.050
98	91.939	-0.530	-0.042	-0.535	-0.043
99	92.179	-0.506	-0.036	-0.510	-0.036
100	92.418	-0.485	-0.030	-0.483	-0.030
101	92.655	-0.461	-0.025	-0.458	-0.024
102	92.891	-0.435	-0.018	-0.435	-0.018
103	93.126	-0.412	-0.012	-0.410	-0.012
104	93.360	-0.386	-0.005	-0.388	-0.006

105	93.592	-0.361	0.001	-0.365	0.000
106	93.823	-0.340	0.006	-0.337	0.006
107	94.052	-0.316	0.012	-0.312	0.013
108	94.280	-0.290	0.019	-0.290	0.019
109	94.505	-0.264	0.025	-0.267	0.025
110	94.729	-0.240	0.032	-0.242	0.031
111	94.951	-0.217	0.037	-0.217	0.037
112	95.170	-0.193	0.043	-0.192	0.043
113	95.388	-0.169	0.049	-0.168	0.049
114	95.604	-0.143	0.055	-0.145	0.055
115	95.817	-0.119	0.061	-0.121	0.061
116	96.028	-0.096	0.067	-0.096	0.067
117	96.237	-0.072	0.073	-0.072	0.073
118	96.444	-0.048	0.079	-0.048	0.079
119	96.648	-0.024	0.085	-0.024	0.085
120	96.850	-0.012	0.088	-0.012	0.088

TABLE 6.7 NUMERIC ANALYSIS OF STRESSES
Uniform Thickness, b/a=2.694, $\phi_0=100^0$

Y (m)	ϕ	Stresses at Inner Surface		Stresses at Outer Surface	
		σ_ϕ (N/mm^2)	σ_θ (N/mm^2)	σ_ϕ (N/mm^2)	σ_θ (N/mm^2)
0	75.000	-2.300	-0.344	-2.610	-0.391
1	75.025	-2.340	-0.353	-2.560	-0.385
2	75.107	-2.420	-0.373	-2.470	-0.379
3	75.191	-2.450	-0.391	-2.420	-0.386
4	75.277	-2.430	-0.402	-2.420	-0.399
5	75.365	-2.420	-0.413	-2.400	-0.408
6	75.454	-2.430	-0.420	-2.370	-0.411
7	75.545	-2.400	-0.417	-2.380	-0.413
8	75.638	-2.370	-0.411	-2.380	-0.413
9	75.733	-2.360	-0.409	-2.370	-0.409
10	75.829	-2.360	-0.408	-2.350	-0.406
11	75.928	-2.340	-0.404	-2.350	-0.405
12	76.028	-2.320	-0.402	-2.340	-0.403
13	76.130	-2.320	-0.402	-2.320	-0.401
14	76.234	-2.310	-0.402	-2.300	-0.400
15	76.341	-2.300	-0.400	-2.290	-0.399
16	76.449	-2.280	-0.397	-2.280	-0.398
17	76.560	-2.270	-0.396	-2.270	-0.396
18	76.672	-2.270	-0.396	-2.250	-0.394
19	76.787	-2.250	-0.393	-2.240	-0.391
20	76.904	-2.230	-0.387	-2.240	-0.389
21	77.023	-2.220	-0.385	-2.220	-0.384
22	77.145	-2.210	-0.382	-2.210	-0.382
23	77.269	-2.190	-0.379	-2.200	-0.380
24	77.395	-2.180	-0.378	-2.190	-0.379
25	77.524	-2.170	-0.379	-2.170	-0.378
26	77.655	-2.170	-0.381	-2.140	-0.375
27	77.788	-2.150	-0.375	-2.140	-0.373
28	77.924	-2.120	-0.368	-2.140	-0.371
29	78.063	-2.110	-0.366	-2.130	-0.368
30	78.204	-2.100	-0.368	-2.110	-0.368
31	78.348	-2.100	-0.371	-2.080	-0.368
32	78.494	-2.090	-0.371	-2.060	-0.366
33	78.643	-2.070	-0.364	-2.060	-0.363
34	78.795	-2.040	-0.356	-2.060	-0.360
35	78.950	-2.030	-0.355	-2.040	-0.357
36	79.107	-2.030	-0.357	-2.020	-0.355
37	79.267	-2.010	-0.356	-2.000	-0.354
38	79.430	-2.000	-0.353	-1.990	-0.351
39	79.596	-1.980	-0.348	-1.980	-0.348
40	79.764	-1.960	-0.344	-1.970	-0.344
41	79.935	-1.940	-0.341	-1.950	-0.342
42	80.110	-1.930	-0.340	-1.930	-0.339
43	80.287	-1.920	-0.337	-1.920	-0.337
44	80.467	-1.890	-0.335	-1.910	-0.336
45	80.650	-1.890	-0.335	-1.880	-0.333

46	80.836	-1.870	-0.333	-1.860	-0.331
47	81.025	-1.850	-0.328	-1.860	-0.329
48	81.216	-1.840	-0.326	-1.840	-0.325
49	81.411	-1.820	-0.323	-1.820	-0.322
50	81.609	-1.810	-0.319	-1.800	-0.317
51	81.809	-1.780	-0.311	-1.790	-0.312
52	82.012	-1.760	-0.306	-1.780	-0.310
53	82.219	-1.750	-0.307	-1.750	-0.307
54	82.428	-1.740	-0.308	-1.720	-0.305
55	82.640	-1.720	-0.305	-1.710	-0.304
56	82.854	-1.700	-0.301	-1.700	-0.301
57	83.072	-1.680	-0.298	-1.680	-0.296
58	83.292	-1.670	-0.293	-1.660	-0.291
59	83.515	-1.640	-0.286	-1.640	-0.286
60	83.740	-1.620	-0.279	-1.630	-0.281
61	83.968	-1.600	-0.277	-1.610	-0.277
62	84.199	-1.590	-0.275	-1.580	-0.274
63	84.432	-1.570	-0.271	-1.570	-0.271
64	84.667	-1.550	-0.268	-1.540	-0.267
65	84.905	-1.530	-0.263	-1.520	-0.262
66	85.144	-1.510	-0.257	-1.510	-0.257
67	85.387	-1.480	-0.251	-1.490	-0.252
68	85.631	-1.460	-0.246	-1.470	-0.248
69	85.877	-1.450	-0.246	-1.440	-0.244
70	86.125	-1.440	-0.242	-1.410	-0.239
71	86.375	-1.400	-0.233	-1.410	-0.233
72	86.626	-1.380	-0.225	-1.390	-0.226
73	86.880	-1.360	-0.219	-1.360	-0.219
74	87.134	-1.340	-0.214	-1.350	-0.215
75	87.390	-1.320	-0.211	-1.320	-0.211
76	87.648	-1.300	-0.208	-1.290	-0.206
77	87.906	-1.280	-0.201	-1.270	-0.201
78	88.165	-1.250	-0.194	-1.250	-0.195
79	88.426	-1.230	-0.188	-1.230	-0.188
80	88.687	-1.210	-0.182	-1.200	-0.181
81	88.949	-1.180	-0.174	-1.190	-0.174
82	89.211	-1.150	-0.167	-1.170	-0.169
83	89.474	-1.140	-0.164	-1.140	-0.163
84	89.737	-1.120	-0.159	-1.110	-0.158
85	90.000	-1.090	-0.153	-1.090	-0.152
86	90.263	-1.070	-0.146	-1.060	-0.145
87	90.526	-1.050	-0.138	-1.040	-0.137
88	90.789	-1.010	-0.128	-1.030	-0.130
89	91.051	-0.994	-0.122	-0.998	-0.123
90	91.313	-0.975	-0.117	-0.969	-0.116
91	91.574	-0.948	-0.110	-0.947	-0.110
92	91.835	-0.923	-0.104	-0.924	-0.104
93	92.094	-0.900	-0.098	-0.898	-0.097
94	92.352	-0.879	-0.091	-0.870	-0.090
95	92.610	-0.851	-0.083	-0.848	-0.083
96	92.866	-0.822	-0.074	-0.828	-0.075

97	93.120	-0.799	-0.067	-0.801	-0.067
98	93.374	-0.772	-0.060	-0.778	-0.061
99	93.625	-0.750	-0.055	-0.751	-0.055
100	93.875	-0.731	-0.050	-0.719	-0.048
101	94.123	-0.703	-0.042	-0.697	-0.041
102	94.369	-0.671	-0.033	-0.678	-0.034
103	94.613	-0.648	-0.026	-0.652	-0.026
104	94.856	-0.624	-0.019	-0.625	-0.019
105	95.095	-0.600	-0.013	-0.598	-0.012
106	95.333	-0.575	-0.006	-0.573	-0.006
107	95.568	-0.548	0.001	-0.549	0.001
108	95.801	-0.525	0.008	-0.522	0.009
109	96.032	-0.499	0.016	-0.498	0.016
110	96.260	-0.472	0.024	-0.474	0.024
111	96.485	-0.449	0.031	-0.446	0.031
112	96.708	-0.423	0.039	-0.422	0.039
113	96.928	-0.391	0.047	-0.403	0.046
114	97.146	-0.354	0.054	-0.390	0.048
115	97.360	-0.350	0.050	-0.344	0.051
116	97.572	-0.355	0.048	-0.288	0.058
117	97.781	-0.303	0.063	-0.291	0.065
118	97.988	-0.253	0.079	-0.290	0.074
119	98.191	-0.238	0.087	-0.255	0.085
120	98.391	-0.221	0.091	-0.222	0.091
121	98.589	-0.198	0.096	-0.195	0.096
122	98.784	-0.174	0.101	-0.169	0.102
123	98.975	-0.149	0.107	-0.145	0.108
124	99.164	-0.124	0.114	-0.121	0.115
125	99.350	-0.097	0.122	-0.098	0.122
126	99.533	-0.067	0.130	-0.079	0.128
127	99.713	-0.034	0.135	-0.063	0.131
128	99.890	-0.008	0.135	-0.040	0.130
128.929	100.000	0.001	0.133	-0.025	0.129

TABLE 6.8 NUMERIC ANALYSIS OF STRESSES
Uniform Thickness, b/a=2.694, $\phi_0=95^0$

Y (m)	ϕ	Stresses at Inner Surface		Stresses at Outer Surface	
		σ_ϕ (N/mm^2)	σ_θ (N/mm^2)	σ_ϕ (N/mm^2)	σ_θ (N/mm^2)
0	75.000	-1.810	-0.271	-2.210	-0.331
1	75.025	-1.860	-0.284	-2.150	-0.326
2	75.107	-1.960	-0.317	-2.020	-0.325
3	75.191	-2.000	-0.349	-1.950	-0.340
4	75.277	-1.990	-0.370	-1.940	-0.362
5	75.365	-1.980	-0.384	-1.930	-0.376
6	75.454	-1.970	-0.392	-1.910	-0.382
7	75.545	-1.940	-0.388	-1.910	-0.384
8	75.638	-1.900	-0.381	-1.920	-0.383
9	75.733	-1.890	-0.378	-1.900	-0.378
10	75.829	-1.890	-0.375	-1.880	-0.374
11	75.928	-1.860	-0.371	-1.870	-0.371
12	76.028	-1.850	-0.368	-1.860	-0.369
13	76.130	-1.840	-0.367	-1.840	-0.366
14	76.234	-1.830	-0.366	-1.820	-0.364
15	76.341	-1.810	-0.363	-1.810	-0.362
16	76.449	-1.790	-0.360	-1.800	-0.360
17	76.560	-1.780	-0.358	-1.780	-0.358
18	76.672	-1.770	-0.357	-1.760	-0.355
19	76.787	-1.750	-0.353	-1.750	-0.352
20	76.904	-1.730	-0.348	-1.740	-0.349
21	77.023	-1.720	-0.345	-1.720	-0.344
22	77.145	-1.700	-0.341	-1.700	-0.341
23	77.269	-1.690	-0.338	-1.690	-0.339
24	77.395	-1.670	-0.336	-1.680	-0.337
25	77.524	-1.660	-0.335	-1.660	-0.335
26	77.655	-1.650	-0.335	-1.630	-0.331
27	77.788	-1.630	-0.330	-1.620	-0.329
28	77.924	-1.600	-0.323	-1.620	-0.325
29	78.063	-1.590	-0.321	-1.600	-0.322
30	78.204	-1.580	-0.320	-1.580	-0.321
31	78.348	-1.570	-0.322	-1.550	-0.319
32	78.494	-1.560	-0.320	-1.530	-0.316
33	78.643	-1.530	-0.313	-1.530	-0.313
34	78.795	-1.500	-0.306	-1.520	-0.309
35	78.950	-1.490	-0.304	-1.500	-0.305
36	79.107	-1.480	-0.304	-1.470	-0.302
37	79.267	-1.470	-0.302	-1.450	-0.300
38	79.430	-1.450	-0.298	-1.440	-0.297
39	79.596	-1.430	-0.293	-1.430	-0.292
40	79.764	-1.410	-0.288	-1.410	-0.288
41	79.935	-1.390	-0.284	-1.390	-0.285
42	80.110	-1.370	-0.282	-1.370	-0.281
43	80.287	-1.350	-0.278	-1.350	-0.278
44	80.467	-1.330	-0.275	-1.340	-0.276
45	80.650	-1.320	-0.273	-1.310	-0.272
46	80.836	-1.300	-0.270	-1.290	-0.269
47	81.025	-1.280	-0.265	-1.280	-0.266

48	81.216	-1.260	-0.261	-1.260	-0.261
49	81.411	-1.250	-0.258	-1.240	-0.257
50	81.609	-1.230	-0.253	-1.220	-0.251
51	81.809	-1.200	-0.246	-1.210	-0.247
52	82.012	-1.180	-0.240	-1.190	-0.243
53	82.219	-1.170	-0.239	-1.160	-0.239
54	82.428	-1.150	-0.238	-1.140	-0.236
55	82.640	-1.130	-0.233	-1.120	-0.233
56	82.854	-1.110	-0.229	-1.110	-0.229
57	83.072	-1.090	-0.224	-1.080	-0.223
58	83.292	-1.070	-0.219	-1.060	-0.218
59	83.515	-1.040	-0.213	-1.040	-0.212
60	83.740	-1.020	-0.206	-1.030	-0.207
61	83.968	-1.000	-0.202	-1.000	-0.202
62	84.199	-0.986	-0.199	-0.979	-0.198
63	84.432	-0.962	-0.194	-0.961	-0.194
64	84.667	-0.943	-0.189	-0.938	-0.189
65	84.905	-0.921	-0.184	-0.917	-0.183
66	85.144	-0.898	-0.178	-0.897	-0.178
67	85.387	-0.874	-0.172	-0.878	-0.172
68	85.631	-0.850	-0.166	-0.858	-0.167
69	85.877	-0.836	-0.163	-0.829	-0.162
70	86.125	-0.817	-0.159	-0.803	-0.157
71	86.375	-0.788	-0.151	-0.788	-0.151
72	86.626	-0.763	-0.143	-0.768	-0.144
73	86.880	-0.742	-0.137	-0.744	-0.137
74	87.134	-0.718	-0.131	-0.723	-0.132
75	87.390	-0.699	-0.127	-0.697	-0.127
76	87.648	-0.679	-0.122	-0.671	-0.121
77	87.906	-0.653	-0.116	-0.652	-0.116
78	88.165	-0.629	-0.109	-0.630	-0.109
79	88.426	-0.607	-0.103	-0.607	-0.103
80	88.687	-0.585	-0.096	-0.582	-0.096
81	88.949	-0.559	-0.089	-0.561	-0.089
82	89.211	-0.534	-0.082	-0.540	-0.083
83	89.474	-0.515	-0.077	-0.512	-0.077
84	89.737	-0.492	-0.072	-0.488	-0.071
85	90.000	-0.467	-0.065	-0.466	-0.065
86	90.263	-0.445	-0.059	-0.441	-0.058
87	90.526	-0.420	-0.052	-0.418	-0.051
88	90.789	-0.393	-0.044	-0.398	-0.045
89	91.051	-0.371	-0.037	-0.373	-0.038
90	91.313	-0.349	-0.032	-0.347	-0.031
91	91.574	-0.325	-0.025	-0.324	-0.025
92	91.835	-0.300	-0.019	-0.301	-0.019
93	92.094	-0.277	-0.012	-0.277	-0.012
94	92.352	-0.254	-0.006	-0.252	-0.005
95	92.610	-0.229	0.001	-0.229	0.001
96	92.866	-0.204	0.008	-0.206	0.008
97	93.120	-0.181	0.015	-0.182	0.015
98	93.374	-0.157	0.022	-0.158	0.021
99	93.625	-0.133	0.028	-0.134	0.028
100	93.875	-0.110	0.034	-0.109	0.034
101	94.123	-0.086	0.040	-0.085	0.040
102	94.369	-0.062	0.047	-0.062	0.047
103	94.613	-0.038	0.054	-0.038	0.054
104	94.856	-0.017	0.060	-0.017	0.060
104.902	95.000	-0.007	0.062	-0.007	0.063

TABLE 6.9 NUMERIC ANALYSIS OF STRESSES

Uniform Thickness, b/a=2.2, $\phi_0=100^0$

Y (m)	ϕ	Stresses at Inner Surface		Stresses at Outer Surface	
		σ_ϕ (N/mm^2)	σ_θ (N/mm^2)	σ_ϕ (N/mm^2)	σ_θ (N/mm^2)
0	75.000	-1.260	-0.189	-1.950	-0.292
1	75.032	-1.350	-0.212	-1.850	-0.287
2	75.229	-1.520	-0.276	-1.660	-0.294
3	75.431	-1.620	-0.347	-1.530	-0.331
4	75.637	-1.620	-0.396	-1.500	-0.377
5	75.849	-1.590	-0.424	-1.500	-0.408
6	76.065	-1.560	-0.434	-1.490	-0.423
7	76.286	-1.540	-0.431	-1.490	-0.424
8	76.512	-1.500	-0.420	-1.490	-0.419
9	76.743	-1.470	-0.408	-1.490	-0.412
10	76.980	-1.460	-0.403	-1.460	-0.403
11	77.221	-1.450	-0.398	-1.440	-0.396
12	77.468	-1.420	-0.390	-1.440	-0.392
13	77.721	-1.410	-0.387	-1.420	-0.388
14	77.978	-1.400	-0.385	-1.390	-0.383
15	78.241	-1.380	-0.381	-1.380	-0.381
16	78.510	-1.360	-0.377	-1.360	-0.377
17	78.783	-1.350	-0.375	-1.340	-0.372
18	79.063	-1.330	-0.369	-1.320	-0.368
19	79.348	-1.300	-0.362	-1.310	-0.363
20	79.638	-1.290	-0.357	-1.290	-0.357
21	79.934	-1.270	-0.353	-1.270	-0.352
22	80.235	-1.250	-0.347	-1.250	-0.346
23	80.541	-1.230	-0.340	-1.230	-0.341
24	80.853	-1.210	-0.335	-1.220	-0.335
25	81.170	-1.200	-0.330	-1.190	-0.329
26	81.493	-1.180	-0.325	-1.170	-0.323
27	81.820	-1.150	-0.317	-1.160	-0.317
28	82.153	-1.130	-0.311	-1.140	-0.312
29	82.490	-1.120	-0.306	-1.110	-0.305
30	82.833	-1.100	-0.300	-1.090	-0.299
31	83.180	-1.070	-0.291	-1.080	-0.292
32	83.531	-1.060	-0.285	-1.050	-0.284
33	83.887	-1.040	-0.277	-1.030	-0.276
34	84.248	-1.010	-0.269	-1.010	-0.269
35	84.612	-0.989	-0.261	-0.994	-0.262
36	84.980	-0.974	-0.255	-0.966	-0.254
37	85.351	-0.950	-0.248	-0.948	-0.247
38	85.726	-0.927	-0.240	-0.926	-0.239
39	86.105	-0.910	-0.232	-0.900	-0.230
40	86.486	-0.881	-0.221	-0.885	-0.222
41	86.869	-0.857	-0.212	-0.864	-0.213
42	87.255	-0.841	-0.205	-0.835	-0.204
43	87.643	-0.817	-0.196	-0.814	-0.196
44	88.033	-0.793	-0.187	-0.792	-0.187
45	88.425	-0.772	-0.178	-0.768	-0.177
46	88.818	-0.745	-0.168	-0.748	-0.168
47	89.211	-0.722	-0.159	-0.725	-0.159
48	89.605	-0.702	-0.150	-0.698	-0.150
49	90.000	-0.679	-0.141	-0.674	-0.140

50	90.395	-0.655	-0.131	-0.651	-0.130
51	90.789	-0.628	-0.120	-0.631	-0.120
52	91.182	-0.604	-0.110	-0.607	-0.110
53	91.575	-0.583	-0.100	-0.580	-0.100
54	91.967	-0.558	-0.090	-0.557	-0.090
55	92.357	-0.534	-0.080	-0.533	-0.080
56	92.745	-0.511	-0.070	-0.507	-0.069
57	93.131	-0.483	-0.059	-0.487	-0.059
58	93.514	-0.459	-0.049	-0.462	-0.049
59	93.895	-0.438	-0.040	-0.434	-0.039
60	94.274	-0.412	-0.029	-0.411	-0.029
61	94.649	-0.387	-0.019	-0.387	-0.019
62	95.020	-0.364	-0.009	-0.361	-0.008
63	95.388	-0.337	0.002	-0.339	0.002
64	95.752	-0.312	0.012	-0.314	0.012
65	96.113	-0.289	0.022	-0.288	0.022
66	96.469	-0.264	0.032	-0.264	0.032
67	96.820	-0.239	0.042	-0.240	0.042
68	97.167	-0.215	0.052	-0.215	0.052
69	97.510	-0.191	0.062	-0.190	0.062
70	97.847	-0.165	0.072	-0.166	0.072
71	98.180	-0.140	0.081	-0.142	0.081
72	98.507	-0.117	0.091	-0.117	0.091
73	98.830	-0.092	0.100	-0.092	0.100
74	99.147	-0.068	0.110	-0.068	0.110
75	99.459	-0.044	0.119	-0.043	0.119
76	99.765	-0.021	0.128	-0.020	0.128
76.943	100.000	-0.010	0.132	-0.009	0.133

TABLE 6.10 NUMERIC ANALYSIS OF STRESSES
Uniform Thickness, b/a=2.2, $\phi_0=95^0$

Y (m)	ϕ	Stresses at Inner Surface		Stresses at Outer Surface	
		σ_ϕ (N/mm^2)	σ_θ (N/mm^2)	σ_ϕ (N/mm^2)	σ_θ (N/mm^2)
0	75.000	-0.948	-0.143	-1.640	-0.246
1	75.032	-1.030	-0.167	-1.550	-0.242
2	75.229	-1.210	-0.232	-1.350	-0.251
3	75.431	-1.310	-0.306	-1.210	-0.289
4	75.637	-1.310	-0.356	-1.180	-0.335
5	75.849	-1.280	-0.382	-1.180	-0.366
6	76.065	-1.240	-0.390	-1.170	-0.379
7	76.286	-1.210	-0.386	-1.170	-0.380
8	76.512	-1.170	-0.374	-1.170	-0.374
9	76.743	-1.140	-0.362	-1.160	-0.365
10	76.980	-1.130	-0.355	-1.140	-0.356
11	77.221	-1.120	-0.349	-1.120	-0.348
12	77.468	-1.090	-0.341	-1.110	-0.343
13	77.721	-1.080	-0.337	-1.080	-0.338
14	77.978	-1.070	-0.334	-1.060	-0.332
15	78.241	-1.040	-0.328	-1.040	-0.328
16	78.510	-1.020	-0.323	-1.030	-0.324
17	78.783	-1.010	-0.319	-0.999	-0.318
18	79.063	-0.988	-0.313	-0.981	-0.312
19	79.348	-0.962	-0.305	-0.968	-0.306
20	79.638	-0.944	-0.299	-0.946	-0.300
21	79.934	-0.928	-0.294	-0.922	-0.293
22	80.235	-0.907	-0.287	-0.903	-0.287
23	80.541	-0.884	-0.280	-0.885	-0.280
24	80.853	-0.863	-0.273	-0.866	-0.274
25	81.170	-0.845	-0.267	-0.842	-0.267
26	81.493	-0.826	-0.261	-0.819	-0.260
27	81.820	-0.800	-0.253	-0.803	-0.253
28	82.153	-0.778	-0.245	-0.783	-0.246
29	82.490	-0.763	-0.239	-0.756	-0.238
30	82.833	-0.741	-0.232	-0.735	-0.231
31	83.180	-0.715	-0.223	-0.717	-0.224
32	83.531	-0.695	-0.216	-0.694	-0.215
33	83.887	-0.675	-0.208	-0.670	-0.207
34	84.248	-0.650	-0.199	-0.652	-0.199
35	84.612	-0.627	-0.191	-0.630	-0.191
36	84.980	-0.609	-0.183	-0.604	-0.183
37	85.351	-0.585	-0.175	-0.583	-0.175
38	85.726	-0.562	-0.166	-0.561	-0.166
39	86.105	-0.542	-0.158	-0.536	-0.157
40	86.486	-0.515	-0.148	-0.517	-0.148
41	86.869	-0.491	-0.138	-0.495	-0.139
42	87.255	-0.472	-0.130	-0.468	-0.129
43	87.643	-0.448	-0.121	-0.446	-0.121
44	88.033	-0.424	-0.111	-0.424	-0.111
45	88.425	-0.402	-0.102	-0.400	-0.102
46	88.818	-0.377	-0.092	-0.378	-0.092
47	89.211	-0.353	-0.083	-0.355	-0.083
48	89.605	-0.332	-0.074	-0.330	-0.073
49	90.000	-0.308	-0.064	-0.306	-0.064

50	90.395	-0.284	-0.054	-0.283	-0.054
51	90.789	-0.259	-0.044	-0.260	-0.044
52	91.182	-0.236	-0.034	-0.237	-0.034
53	91.575	-0.213	-0.024	-0.212	-0.024
54	91.967	-0.189	-0.014	-0.189	-0.014
55	92.357	-0.165	-0.005	-0.165	-0.005
56	92.745	-0.142	0.005	-0.141	0.005
57	93.131	-0.117	0.015	-0.118	0.015
58	93.514	-0.093	0.025	-0.094	0.025
59	93.895	-0.071	0.034	-0.069	0.035
60	94.274	-0.047	0.044	-0.045	0.045
61	94.649	-0.023	0.054	-0.022	0.055
61.11	95.000	-0.012	0.060	-0.011	0.060

TABLE 6.11 NUMERIC ANALYSIS OF STRESSES
Uniform Thickness, b/a=2.5, $\phi_0=100^0$

Y (m)	ϕ	Stresses at Inner Surface		Stresses at Outer Surface	
		σ_ϕ (N/mm^2)	σ_θ (N/mm^2)	σ_ϕ (N/mm^2)	σ_θ (N/mm^2)
0	75.000	-1.920	-0.290	-2.250	-0.340
1	75.078	-1.980	-0.308	-2.190	-0.339
2	75.198	-2.060	-0.347	-2.080	-0.349
3	75.320	-2.100	-0.386	-2.020	-0.373
4	75.445	-2.090	-0.410	-2.000	-0.395
5	75.572	-2.060	-0.416	-2.010	-0.409
6	75.702	-2.030	-0.416	-2.020	-0.414
7	75.835	-2.010	-0.415	-2.010	-0.413
8	75.970	-2.000	-0.413	-1.990	-0.412
9	76.109	-1.990	-0.412	-1.970	-0.409
10	76.250	-1.970	-0.407	-1.960	-0.406
11	76.394	-1.950	-0.402	-1.960	-0.404
12	76.541	-1.940	-0.400	-1.940	-0.400
13	76.692	-1.930	-0.399	-1.920	-0.397
14	76.845	-1.910	-0.395	-1.920	-0.395
15	77.001	-1.900	-0.392	-1.900	-0.392
16	77.161	-1.890	-0.391	-1.880	-0.388
17	77.324	-1.870	-0.386	-1.870	-0.386
18	77.490	-1.850	-0.381	-1.870	-0.384
19	77.659	-1.840	-0.382	-1.840	-0.381
20	77.832	-1.830	-0.382	-1.820	-0.380
21	78.008	-1.820	-0.379	-1.810	-0.378
22	78.188	-1.800	-0.376	-1.790	-0.374
23	78.371	-1.780	-0.369	-1.790	-0.370
24	78.558	-1.760	-0.364	-1.770	-0.366
25	78.748	-1.750	-0.363	-1.750	-0.363
26	78.941	-1.740	-0.362	-1.730	-0.361
27	79.139	-1.730	-0.361	-1.710	-0.358
28	79.340	-1.710	-0.356	-1.700	-0.355
29	79.544	-1.680	-0.351	-1.690	-0.353
30	79.752	-1.670	-0.349	-1.670	-0.350
31	79.964	-1.660	-0.349	-1.650	-0.347
32	80.180	-1.640	-0.346	-1.630	-0.344
33	80.399	-1.620	-0.340	-1.620	-0.340
34	80.622	-1.600	-0.334	-1.610	-0.334
35	80.849	-1.580	-0.329	-1.590	-0.330
36	81.079	-1.560	-0.325	-1.570	-0.327
37	81.313	-1.550	-0.325	-1.550	-0.323
38	81.550	-1.540	-0.322	-1.530	-0.320
39	81.791	-1.520	-0.316	-1.510	-0.316
40	82.036	-1.490	-0.311	-1.500	-0.311
41	82.284	-1.480	-0.307	-1.480	-0.306
42	82.536	-1.460	-0.302	-1.460	-0.302
43	82.791	-1.440	-0.297	-1.440	-0.297
44	83.049	-1.420	-0.293	-1.420	-0.293
45	83.311	-1.410	-0.290	-1.400	-0.289
46	83.576	-1.390	-0.286	-1.380	-0.285
47	83.844	-1.370	-0.281	-1.360	-0.280
48	84.116	-1.350	-0.276	-1.340	-0.274

49	84.390	-1.320	-0.268	-1.330	-0.268
50	84.667	-1.300	-0.261	-1.310	-0.262
51	84.947	-1.280	-0.257	-1.280	-0.257
52	85.229	-1.260	-0.253	-1.260	-0.253
53	85.515	-1.240	-0.249	-1.240	-0.248
54	85.802	-1.230	-0.244	-1.210	-0.242
55	86.092	-1.200	-0.236	-1.190	-0.235
56	86.384	-1.170	-0.226	-1.180	-0.227
57	86.678	-1.150	-0.218	-1.160	-0.220
58	86.974	-1.130	-0.212	-1.140	-0.214
59	87.271	-1.110	-0.210	-1.110	-0.209
60	87.571	-1.100	-0.207	-1.080	-0.204
61	87.871	-1.070	-0.199	-1.060	-0.197
62	88.173	-1.040	-0.189	-1.050	-0.189
63	88.476	-1.020	-0.179	-1.030	-0.181
64	88.780	-0.997	-0.172	-1.000	-0.173
65	89.084	-0.979	-0.167	-0.973	-0.166
66	89.389	-0.953	-0.160	-0.952	-0.160
67	89.694	-0.930	-0.153	-0.930	-0.153
68	90.000	-0.909	-0.146	-0.903	-0.145
69	90.306	-0.882	-0.138	-0.882	-0.138
70	90.611	-0.859	-0.130	-0.859	-0.130
71	90.916	-0.838	-0.122	-0.832	-0.121
72	91.220	-0.810	-0.113	-0.812	-0.113
73	91.524	-0.782	-0.104	-0.792	-0.106
74	91.827	-0.762	-0.099	-0.763	-0.099
75	92.129	-0.743	-0.093	-0.733	-0.092
76	92.429	-0.719	-0.086	-0.708	-0.084
77	92.729	-0.691	-0.076	-0.688	-0.075
78	93.026	-0.661	-0.065	-0.668	-0.066
79	93.322	-0.637	-0.056	-0.644	-0.057
80	93.616	-0.614	-0.049	-0.617	-0.050
81	93.908	-0.593	-0.043	-0.589	-0.042
82	94.198	-0.569	-0.036	-0.563	-0.035
83	94.485	-0.542	-0.027	-0.541	-0.027
84	94.771	-0.516	-0.019	-0.516	-0.019
85	95.053	-0.491	-0.010	-0.492	-0.010
86	95.333	-0.465	-0.001	-0.468	-0.002
87	95.610	-0.440	0.006	-0.443	0.006
88	95.884	-0.418	0.013	-0.415	0.014
89	96.156	-0.392	0.021	-0.391	0.021
90	96.424	-0.367	0.029	-0.366	0.029
91	96.689	-0.342	0.037	-0.341	0.037
92	96.951	-0.316	0.045	-0.317	0.045
93	97.209	-0.291	0.053	-0.292	0.053
94	97.464	-0.267	0.061	-0.267	0.061
95	97.716	-0.242	0.068	-0.242	0.068
96	97.964	-0.216	0.076	-0.218	0.076
97	98.209	-0.192	0.083	-0.193	0.083
98	98.450	-0.168	0.090	-0.167	0.090
99	98.687	-0.143	0.098	-0.143	0.098
100	98.921	-0.118	0.105	-0.119	0.105
101	99.151	-0.093	0.112	-0.094	0.112
102	99.378	-0.069	0.119	-0.069	0.119
103	99.601	-0.045	0.126	-0.044	0.126
104	99.820	-0.022	0.133	-0.021	0.133
104.499	100.000	-0.010	0.136	-0.010	0.137

TABLE 6.12 NUMERIC ANALYSIS OF STRESSES
Uniform Thickness, b/a=2.5, $\phi_0=95^0$

Y (m)	ϕ	Stresses at Inner Surface		Stresses at Outer Surface	
		σ_ϕ (N/mm^2)	σ_θ (N/mm^2)	σ_ϕ (N/mm^2)	σ_θ (N/mm^2)
0	75.000	-1.500	-0.230	-1.890	-0.287
1	75.078	-1.570	-0.252	-1.810	-0.287
2	75.198	-1.670	-0.301	-1.690	-0.302
3	75.320	-1.710	-0.347	-1.620	-0.332
4	75.445	-1.700	-0.375	-1.590	-0.358
5	75.572	-1.660	-0.384	-1.600	-0.374
6	75.702	-1.630	-0.383	-1.610	-0.380
7	75.835	-1.610	-0.380	-1.600	-0.378
8	75.970	-1.590	-0.376	-1.590	-0.376
9	76.109	-1.580	-0.373	-1.570	-0.371
10	76.250	-1.560	-0.368	-1.550	-0.367
11	76.394	-1.530	-0.362	-1.550	-0.363
12	76.541	-1.520	-0.359	-1.520	-0.359
13	76.692	-1.510	-0.357	-1.500	-0.355
14	76.845	-1.490	-0.352	-1.490	-0.353
15	77.001	-1.470	-0.349	-1.480	-0.349
16	77.161	-1.470	-0.347	-1.450	-0.345
17	77.324	-1.440	-0.341	-1.440	-0.341
18	77.490	-1.420	-0.336	-1.430	-0.338
19	77.659	-1.410	-0.335	-1.410	-0.335
20	77.832	-1.390	-0.334	-1.390	-0.332
21	78.008	-1.380	-0.330	-1.370	-0.329
22	78.188	-1.360	-0.326	-1.350	-0.324
23	78.371	-1.340	-0.319	-1.340	-0.320
24	78.558	-1.320	-0.314	-1.330	-0.316
25	78.748	-1.300	-0.311	-1.300	-0.312
26	78.941	-1.290	-0.309	-1.280	-0.308
27	79.139	-1.270	-0.306	-1.260	-0.305
28	79.340	-1.250	-0.302	-1.250	-0.301
29	79.544	-1.230	-0.296	-1.240	-0.297
30	79.752	-1.210	-0.293	-1.210	-0.293
31	79.964	-1.200	-0.290	-1.190	-0.289
32	80.180	-1.180	-0.286	-1.170	-0.285
33	80.399	-1.160	-0.281	-1.150	-0.280
34	80.622	-1.140	-0.274	-1.140	-0.274
35	80.849	-1.110	-0.268	-1.120	-0.269
36	81.079	-1.090	-0.264	-1.100	-0.265
37	81.313	-1.080	-0.261	-1.080	-0.260
38	81.550	-1.060	-0.257	-1.050	-0.256
39	81.791	-1.040	-0.251	-1.040	-0.251
40	82.036	-1.020	-0.245	-1.020	-0.245
41	82.284	-0.999	-0.240	-0.997	-0.240
42	82.536	-0.978	-0.234	-0.977	-0.234
43	82.791	-0.956	-0.229	-0.958	-0.229
44	83.049	-0.935	-0.224	-0.937	-0.224
45	83.311	-0.917	-0.219	-0.913	-0.219
46	83.576	-0.896	-0.214	-0.892	-0.214
47	83.844	-0.875	-0.208	-0.871	-0.208
48	84.116	-0.855	-0.202	-0.849	-0.201
49	84.390	-0.829	-0.195	-0.832	-0.195

50	84.667	-0.806	-0.188	-0.811	-0.189
51	84.947	-0.787	-0.182	-0.787	-0.182
52	85.229	-0.766	-0.177	-0.764	-0.177
53	85.515	-0.744	-0.171	-0.742	-0.171
54	85.802	-0.725	-0.166	-0.717	-0.164
55	86.092	-0.702	-0.158	-0.696	-0.157
56	86.384	-0.675	-0.149	-0.678	-0.150
57	86.678	-0.650	-0.141	-0.657	-0.142
58	86.974	-0.628	-0.135	-0.634	-0.136
59	87.271	-0.610	-0.130	-0.607	-0.130
60	87.571	-0.590	-0.125	-0.581	-0.124
61	87.871	-0.567	-0.118	-0.559	-0.116
62	88.173	-0.539	-0.109	-0.540	-0.109
63	88.476	-0.513	-0.100	-0.520	-0.101
64	88.780	-0.492	-0.093	-0.494	-0.093
65	89.084	-0.472	-0.086	-0.468	-0.086
66	89.389	-0.447	-0.079	-0.446	-0.079
67	89.694	-0.423	-0.072	-0.423	-0.072
68	90.000	-0.401	-0.064	-0.398	-0.064
69	90.306	-0.376	-0.057	-0.376	-0.057
70	90.611	-0.352	-0.049	-0.352	-0.049
71	90.916	-0.330	-0.041	-0.328	-0.041
72	91.220	-0.305	-0.033	-0.305	-0.033
73	91.524	-0.279	-0.025	-0.283	-0.026
74	91.827	-0.257	-0.018	-0.258	-0.018
75	92.129	-0.235	-0.011	-0.232	-0.011
76	92.429	-0.211	-0.004	-0.208	-0.003
77	92.729	-0.186	0.004	-0.186	0.004
78	93.026	-0.161	0.013	-0.163	0.012
79	93.322	-0.137	0.020	-0.139	0.020
80	93.616	-0.114	0.028	-0.115	0.028
81	93.908	-0.091	0.035	-0.090	0.035
82	94.198	-0.068	0.042	-0.066	0.043
83	94.485	-0.043	0.050	-0.043	0.050
84	94.771	-0.021	0.058	-0.020	0.058
84.477	95.000	-0.010	0.061	-0.010	0.061

TABLE 6.13 NUMERIC ANALYSIS OF STRESSES

Uniform Thickness, b/a=2.8, $\phi_0=100^0$

Y (m)	ϕ	Stresses at Inner Surface		Stresses at Outer Surface	
		σ_ϕ (N/mm^2)	σ_θ (N/mm^2)	σ_ϕ (N/mm^2)	σ_θ (N/mm^2)
0	75.000	-2.600	-0.388	-2.730	-0.407
1	75.021	-2.600	-0.387	-2.720	-0.405
2	75.088	-2.620	-0.392	-2.680	-0.400
3	75.156	-2.650	-0.401	-2.630	-0.398
4	75.225	-2.630	-0.406	-2.630	-0.404
5	75.295	-2.610	-0.409	-2.630	-0.412
6	75.367	-2.620	-0.418	-2.600	-0.416
7	75.440	-2.630	-0.426	-2.570	-0.416
8	75.515	-2.610	-0.422	-2.560	-0.414
9	75.591	-2.570	-0.409	-2.590	-0.412
10	75.668	-2.540	-0.400	-2.600	-0.408
11	75.747	-2.550	-0.403	-2.560	-0.404
12	75.827	-2.560	-0.408	-2.530	-0.404
13	75.909	-2.540	-0.407	-2.530	-0.404
14	75.992	-2.530	-0.404	-2.520	-0.401
15	76.077	-2.500	-0.397	-2.520	-0.399
16	76.163	-2.480	-0.394	-2.520	-0.399
17	76.251	-2.500	-0.399	-2.490	-0.396
18	76.341	-2.500	-0.402	-2.460	-0.395
19	76.432	-2.480	-0.396	-2.460	-0.393
20	76.525	-2.450	-0.388	-2.470	-0.391
21	76.620	-2.440	-0.385	-2.450	-0.387
22	76.717	-2.430	-0.385	-2.440	-0.386
23	76.815	-2.420	-0.386	-2.420	-0.386
24	76.915	-2.420	-0.389	-2.400	-0.386
25	77.017	-2.410	-0.388	-2.390	-0.385
26	77.121	-2.390	-0.383	-2.380	-0.382
27	77.227	-2.370	-0.377	-2.380	-0.380
28	77.335	-2.360	-0.376	-2.370	-0.376
29	77.445	-2.360	-0.374	-2.350	-0.373
30	77.557	-2.330	-0.370	-2.350	-0.374
31	77.671	-2.320	-0.372	-2.330	-0.373
32	77.787	-2.330	-0.377	-2.300	-0.371
33	77.905	-2.310	-0.373	-2.300	-0.371
34	78.026	-2.280	-0.368	-2.300	-0.370
35	78.148	-2.280	-0.367	-2.280	-0.366
36	78.273	-2.270	-0.366	-2.260	-0.363
37	78.400	-2.250	-0.361	-2.250	-0.360
38	78.529	-2.240	-0.356	-2.240	-0.357
39	78.661	-2.230	-0.353	-2.230	-0.352
40	78.794	-2.200	-0.349	-2.220	-0.352
41	78.931	-2.190	-0.350	-2.210	-0.352
42	79.069	-2.190	-0.355	-2.180	-0.352
43	79.210	-2.180	-0.356	-2.160	-0.353
44	79.354	-2.160	-0.354	-2.160	-0.354
45	79.499	-2.150	-0.354	-2.140	-0.353
46	79.648	-2.140	-0.353	-2.120	-0.350
47	79.799	-2.130	-0.349	-2.100	-0.345
48	79.952	-2.110	-0.340	-2.100	-0.338
49	80.108	-2.060	-0.327	-2.110	-0.334
50	80.266	-2.060	-0.325	-2.080	-0.329

51	80.427	-2.060	-0.329	-2.060	-0.328
52	80.591	-2.040	-0.331	-2.040	-0.331
53	80.757	-2.040	-0.335	-2.010	-0.330
54	80.925	-2.020	-0.332	-2.000	-0.328
55	81.097	-1.990	-0.324	-2.000	-0.324
56	81.271	-1.970	-0.317	-1.990	-0.320
57	81.447	-1.960	-0.315	-1.970	-0.317
58	81.626	-1.950	-0.316	-1.950	-0.315
59	81.808	-1.940	-0.317	-1.920	-0.313
60	81.992	-1.920	-0.313	-1.920	-0.312
61	82.179	-1.900	-0.309	-1.900	-0.310
62	82.368	-1.890	-0.308	-1.880	-0.307
63	82.560	-1.870	-0.305	-1.860	-0.303
64	82.754	-1.850	-0.300	-1.840	-0.299
65	82.951	-1.830	-0.295	-1.830	-0.295
66	83.150	-1.810	-0.289	-1.810	-0.290
67	83.352	-1.790	-0.285	-1.800	-0.287
68	83.556	-1.770	-0.284	-1.780	-0.284
69	83.763	-1.760	-0.283	-1.750	-0.281
70	83.972	-1.750	-0.280	-1.730	-0.277
71	84.183	-1.710	-0.272	-1.730	-0.274
72	84.396	-1.690	-0.268	-1.710	-0.271
73	84.612	-1.690	-0.269	-1.680	-0.267
74	84.830	-1.670	-0.267	-1.650	-0.264
75	85.049	-1.650	-0.261	-1.640	-0.259
76	85.271	-1.620	-0.253	-1.630	-0.255
77	85.495	-1.600	-0.248	-1.610	-0.250
78	85.720	-1.590	-0.247	-1.580	-0.246
79	85.948	-1.570	-0.246	-1.550	-0.242
80	86.177	-1.550	-0.239	-1.540	-0.237
81	86.408	-1.510	-0.228	-1.530	-0.232
82	86.640	-1.490	-0.224	-1.510	-0.227
83	86.874	-1.480	-0.225	-1.470	-0.224
84	87.109	-1.470	-0.224	-1.440	-0.220
85	87.345	-1.440	-0.216	-1.430	-0.214
86	87.582	-1.410	-0.205	-1.420	-0.207
87	87.821	-1.380	-0.197	-1.400	-0.200
88	88.061	-1.360	-0.193	-1.380	-0.195
89	88.301	-1.350	-0.192	-1.350	-0.191
90	88.542	-1.340	-0.190	-1.320	-0.187
91	88.784	-1.310	-0.184	-1.300	-0.183
92	89.027	-1.280	-0.176	-1.280	-0.176
93	89.270	-1.260	-0.168	-1.260	-0.169
94	89.513	-1.230	-0.161	-1.240	-0.163
95	89.756	-1.210	-0.157	-1.210	-0.157
96	90.000	-1.190	-0.153	-1.180	-0.151
97	90.244	-1.170	-0.145	-1.160	-0.145
98	90.487	-1.130	-0.137	-1.150	-0.139
99	90.730	-1.110	-0.132	-1.120	-0.133
100	90.973	-1.090	-0.128	-1.090	-0.127
101	91.216	-1.070	-0.123	-1.070	-0.122
102	91.458	-1.050	-0.118	-1.040	-0.116
103	91.699	-1.020	-0.109	-1.020	-0.109
104	91.939	-0.990	-0.100	-1.000	-0.101
105	92.179	-0.966	-0.093	-0.974	-0.094
106	92.418	-0.947	-0.088	-0.944	-0.088

107	92.655	-0.924	-0.083	-0.918	-0.082
108	92.891	-0.896	-0.076	-0.896	-0.076
109	93.126	-0.873	-0.069	-0.869	-0.069
110	93.360	-0.844	-0.062	-0.848	-0.062
111	93.592	-0.817	-0.055	-0.825	-0.056
112	93.823	-0.799	-0.051	-0.792	-0.050
113	94.052	-0.776	-0.045	-0.765	-0.044
114	94.280	-0.746	-0.037	-0.745	-0.037
115	94.505	-0.716	-0.029	-0.724	-0.030
116	94.729	-0.691	-0.022	-0.698	-0.023
117	94.951	-0.671	-0.017	-0.668	-0.017
118	95.170	-0.647	-0.012	-0.641	-0.011
119	95.388	-0.621	-0.004	-0.617	-0.004
120	95.604	-0.590	0.004	-0.597	0.003
121	95.817	-0.565	0.010	-0.571	0.009
122	96.028	-0.545	0.015	-0.540	0.016
123	96.237	-0.519	0.022	-0.515	0.022
124	96.444	-0.491	0.029	-0.492	0.029
125	96.648	-0.465	0.036	-0.467	0.035
126	96.850	-0.440	0.042	-0.442	0.041
127	97.049	-0.415	0.047	-0.416	0.047
128	97.246	-0.390	0.053	-0.390	0.053
129	97.440	-0.365	0.059	-0.364	0.059
130	97.632	-0.340	0.065	-0.339	0.065
131	97.821	-0.314	0.071	-0.315	0.071
132	98.008	-0.289	0.077	-0.290	0.077
133	98.192	-0.265	0.083	-0.263	0.083
134	98.374	-0.239	0.089	-0.239	0.089
135	98.553	-0.213	0.096	-0.215	0.095
136	98.729	-0.188	0.101	-0.190	0.101
137	98.903	-0.164	0.107	-0.165	0.107
138	99.075	-0.140	0.112	-0.139	0.112
139	99.243	-0.115	0.117	-0.114	0.118
140	99.409	-0.090	0.123	-0.091	0.123
141	99.573	-0.065	0.129	-0.066	0.129
142	99.734	-0.041	0.134	-0.041	0.134
143	99.892	-0.019	0.140	-0.019	0.140
143.011	100.000	-0.008	0.142	-0.008	0.142

TABLE 6.14 NUMERIC ANALYSIS OF STRESSES

Uniform Thickness, b/a=2.8, $\phi_0=95^0$

Y (m)	ϕ	Stresses at Inner Surface		Stresses at Outer Surface	
		σ_ϕ (N/mm^2)	σ_θ (N/mm^2)	σ_ϕ (N/mm^2)	σ_θ (N/mm^2)
0	75.000	-2.080	-0.312	-2.330	-0.349
1	75.021	-2.100	-0.317	-2.310	-0.347
2	75.088	-2.160	-0.336	-2.230	-0.346
3	75.156	-2.200	-0.361	-2.160	-0.355
4	75.225	-2.190	-0.377	-2.150	-0.370
5	75.295	-2.160	-0.386	-2.150	-0.383
6	75.367	-2.160	-0.395	-2.130	-0.390
7	75.440	-2.160	-0.400	-2.100	-0.391
8	75.515	-2.140	-0.396	-2.090	-0.389
9	75.591	-2.090	-0.382	-2.110	-0.385
10	75.668	-2.060	-0.374	-2.110	-0.381
11	75.747	-2.070	-0.375	-2.080	-0.376
12	75.827	-2.070	-0.378	-2.050	-0.375
13	75.909	-2.060	-0.377	-2.040	-0.374
14	75.992	-2.040	-0.374	-2.030	-0.371
15	76.077	-2.010	-0.367	-2.030	-0.369
16	76.163	-1.990	-0.363	-2.020	-0.367
17	76.251	-2.000	-0.366	-1.990	-0.365
18	76.341	-2.000	-0.368	-1.960	-0.362
19	76.432	-1.970	-0.362	-1.960	-0.360
20	76.525	-1.940	-0.355	-1.960	-0.357
21	76.620	-1.930	-0.352	-1.940	-0.353
22	76.717	-1.920	-0.350	-1.930	-0.351
23	76.815	-1.910	-0.351	-1.910	-0.351
24	76.915	-1.900	-0.352	-1.890	-0.349
25	77.017	-1.890	-0.350	-1.870	-0.347
26	77.121	-1.870	-0.346	-1.860	-0.344
27	77.227	-1.840	-0.340	-1.860	-0.341
28	77.335	-1.840	-0.337	-1.840	-0.337
29	77.445	-1.830	-0.335	-1.820	-0.334
30	77.557	-1.800	-0.331	-1.820	-0.334
31	77.671	-1.790	-0.332	-1.790	-0.332
32	77.787	-1.790	-0.334	-1.760	-0.330
33	77.905	-1.770	-0.330	-1.760	-0.328
34	78.026	-1.740	-0.325	-1.750	-0.326
35	78.148	-1.730	-0.323	-1.730	-0.322
36	78.273	-1.720	-0.321	-1.710	-0.318
37	78.400	-1.700	-0.316	-1.700	-0.315
38	78.529	-1.680	-0.311	-1.680	-0.311
39	78.661	-1.670	-0.307	-1.670	-0.307
40	78.794	-1.640	-0.303	-1.660	-0.305
41	78.931	-1.630	-0.302	-1.640	-0.304
42	79.069	-1.620	-0.305	-1.610	-0.303
43	79.210	-1.610	-0.304	-1.600	-0.302
44	79.354	-1.580	-0.301	-1.590	-0.302
45	79.499	-1.570	-0.300	-1.570	-0.299
46	79.648	-1.560	-0.298	-1.550	-0.296
47	79.799	-1.540	-0.294	-1.520	-0.290
48	79.952	-1.520	-0.285	-1.510	-0.284

49	80.108	-1.480	-0.275	-1.520	-0.279
50	80.266	-1.470	-0.272	-1.490	-0.274
51	80.427	-1.470	-0.273	-1.460	-0.272
52	80.591	-1.450	-0.273	-1.450	-0.273
53	80.757	-1.440	-0.274	-1.420	-0.271
54	80.925	-1.420	-0.271	-1.400	-0.268
55	81.097	-1.390	-0.263	-1.390	-0.264
56	81.271	-1.370	-0.257	-1.380	-0.259
57	81.447	-1.350	-0.253	-1.360	-0.255
58	81.626	-1.340	-0.253	-1.340	-0.252
59	81.808	-1.330	-0.251	-1.310	-0.249
60	81.992	-1.300	-0.247	-1.300	-0.247
61	82.179	-1.280	-0.243	-1.280	-0.243
62	82.368	-1.260	-0.240	-1.260	-0.239
63	82.560	-1.250	-0.236	-1.240	-0.235
64	82.754	-1.220	-0.231	-1.220	-0.231
65	82.951	-1.200	-0.226	-1.200	-0.226
66	83.150	-1.180	-0.220	-1.180	-0.221
67	83.352	-1.160	-0.216	-1.170	-0.216
68	83.556	-1.140	-0.212	-1.140	-0.213
69	83.763	-1.130	-0.210	-1.120	-0.209
70	83.972	-1.110	-0.206	-1.100	-0.204
71	84.183	-1.080	-0.199	-1.090	-0.200
72	84.396	-1.050	-0.194	-1.070	-0.196
73	84.612	-1.040	-0.192	-1.040	-0.191
74	84.830	-1.020	-0.189	-1.010	-0.187
75	85.049	-1.000	-0.183	-0.995	-0.182
76	85.271	-0.973	-0.176	-0.980	-0.177
77	85.495	-0.950	-0.171	-0.960	-0.172
78	85.720	-0.935	-0.168	-0.932	-0.167
79	85.948	-0.918	-0.164	-0.905	-0.162
80	86.177	-0.894	-0.158	-0.886	-0.157
81	86.408	-0.862	-0.150	-0.874	-0.151
82	86.640	-0.839	-0.144	-0.852	-0.146
83	86.874	-0.826	-0.142	-0.821	-0.142
84	87.109	-0.809	-0.139	-0.793	-0.137
85	87.345	-0.782	-0.132	-0.775	-0.131
86	87.582	-0.753	-0.124	-0.758	-0.125
87	87.821	-0.729	-0.117	-0.738	-0.118
88	88.061	-0.707	-0.112	-0.714	-0.113
89	88.301	-0.689	-0.108	-0.686	-0.108
90	88.542	-0.669	-0.104	-0.660	-0.103
91	88.784	-0.643	-0.098	-0.639	-0.098
92	89.027	-0.618	-0.091	-0.618	-0.091
93	89.270	-0.594	-0.084	-0.596	-0.085
94	89.513	-0.569	-0.078	-0.574	-0.079
95	89.756	-0.548	-0.073	-0.548	-0.073
96	90.000	-0.528	-0.068	-0.521	-0.067
97	90.244	-0.502	-0.061	-0.500	-0.061
98	90.487	-0.475	-0.054	-0.479	-0.055
99	90.730	-0.453	-0.048	-0.454	-0.049
100	90.973	-0.430	-0.043	-0.430	-0.043
101	91.216	-0.407	-0.038	-0.405	-0.037
102	91.458	-0.385	-0.032	-0.380	-0.031
103	91.699	-0.359	-0.025	-0.358	-0.025
104	91.939	-0.333	-0.018	-0.336	-0.018

105	92.179	-0.309	-0.011	-0.312	-0.012
106	92.418	-0.287	-0.006	-0.286	-0.006
107	92.655	-0.263	0.000	-0.262	0.000
108	92.891	-0.239	0.006	-0.239	0.006
109	93.126	-0.215	0.012	-0.214	0.012
110	93.360	-0.191	0.018	-0.191	0.018
111	93.592	-0.167	0.025	-0.167	0.024
112	93.823	-0.145	0.030	-0.141	0.031
113	94.052	-0.121	0.037	-0.117	0.038
114	94.280	-0.095	0.045	-0.095	0.045
115	94.505	-0.066	0.053	-0.077	0.051
116	94.729	-0.033	0.059	-0.062	0.055
117	94.951	-0.007	0.058	-0.040	0.054
117.546	95.000	0.001	0.056	-0.025	0.052

TABLE 6.15 EFFECT ON OFFSET PARAMETER *A*=10m ON STRESSES (Numerical analysis) Uniform Thickness, b/a=2.694

Y (m)	ϕ	Stresses at Inner Surface		Stresses at Outer Surface	
		σ_ϕ (N/mm^2)	σ_θ (N/mm^2)	σ_ϕ (N/mm^2)	σ_θ (N/mm^2)
0	74.561	-2.160	-0.333	-2.610	-0.399
1	74.634	-2.250	-0.362	-2.510	-0.400
2	74.709	-2.370	-0.422	-2.360	-0.418
3	74.786	-2.410	-0.473	-2.290	-0.454
4	74.864	-2.400	-0.506	-2.270	-0.486
5	74.944	-2.370	-0.522	-2.280	-0.507
6	75.025	-2.340	-0.526	-2.280	-0.516
7	75.107	-2.320	-0.524	-2.270	-0.516
8	75.191	-2.290	-0.515	-2.270	-0.513
9	75.277	-2.240	-0.503	-2.280	-0.509
10	75.365	-2.240	-0.500	-2.260	-0.503
11	75.454	-2.240	-0.501	-2.220	-0.498
12	75.545	-2.220	-0.497	-2.220	-0.496
13	75.638	-2.200	-0.492	-2.210	-0.494
14	75.733	-2.190	-0.491	-2.190	-0.491
15	75.829	-2.180	-0.491	-2.170	-0.488
16	75.928	-2.160	-0.487	-2.160	-0.488
17	76.028	-2.140	-0.485	-2.150	-0.486
18	76.130	-2.130	-0.485	-2.130	-0.484
19	76.234	-2.120	-0.484	-2.110	-0.483
20	76.341	-2.100	-0.482	-2.100	-0.481
21	76.449	-2.080	-0.479	-2.080	-0.479
22	76.560	-2.070	-0.478	-2.070	-0.477
23	76.672	-2.060	-0.476	-2.040	-0.474
24	76.787	-2.040	-0.473	-2.030	-0.471
25	76.904	-2.010	-0.467	-2.020	-0.468
26	77.023	-2.000	-0.463	-2.000	-0.463
27	77.145	-1.980	-0.460	-1.990	-0.460
28	77.269	-1.970	-0.457	-1.970	-0.458
29	77.395	-1.950	-0.455	-1.960	-0.456
30	77.524	-1.940	-0.455	-1.940	-0.454
31	77.655	-1.930	-0.455	-1.910	-0.450
32	77.788	-1.910	-0.449	-1.900	-0.448
33	77.924	-1.880	-0.442	-1.900	-0.445
34	78.063	-1.860	-0.440	-1.880	-0.442
35	78.204	-1.850	-0.440	-1.850	-0.441
36	78.348	-1.840	-0.442	-1.830	-0.439
37	78.494	-1.830	-0.441	-1.800	-0.436
38	78.643	-1.800	-0.434	-1.800	-0.433
39	78.795	-1.770	-0.426	-1.790	-0.430
40	78.950	-1.760	-0.424	-1.770	-0.425
41	79.107	-1.750	-0.424	-1.740	-0.422
42	79.267	-1.740	-0.422	-1.720	-0.419
43	79.430	-1.710	-0.417	-1.710	-0.416
44	79.596	-1.690	-0.412	-1.690	-0.412
45	79.764	-1.670	-0.407	-1.680	-0.407
46	79.935	-1.650	-0.403	-1.660	-0.404
47	80.110	-1.640	-0.400	-1.630	-0.399
48	80.287	-1.620	-0.397	-1.620	-0.396

49	80.467	-1.590	-0.393	-1.600	-0.394
50	80.650	-1.590	-0.392	-1.570	-0.390
51	80.836	-1.570	-0.388	-1.550	-0.386
52	81.025	-1.540	-0.382	-1.540	-0.382
53	81.216	-1.520	-0.377	-1.520	-0.377
54	81.411	-1.500	-0.372	-1.500	-0.372
55	81.609	-1.480	-0.367	-1.490	-0.368
56	81.809	-1.460	-0.363	-1.470	-0.363
57	82.012	-1.450	-0.360	-1.440	-0.359
58	82.219	-1.430	-0.356	-1.420	-0.355
59	82.428	-1.400	-0.350	-1.400	-0.350
60	82.640	-1.380	-0.345	-1.380	-0.345
61	82.854	-1.360	-0.340	-1.360	-0.340
62	83.072	-1.350	-0.335	-1.340	-0.334
63	83.292	-1.330	-0.329	-1.320	-0.328
64	83.515	-1.300	-0.322	-1.300	-0.322
65	83.740	-1.270	-0.314	-1.290	-0.316
66	83.968	-1.260	-0.309	-1.260	-0.309
67	84.199	-1.240	-0.304	-1.230	-0.303
68	84.432	-1.220	-0.298	-1.220	-0.298
69	84.667	-1.200	-0.292	-1.190	-0.291
70	84.905	-1.170	-0.285	-1.170	-0.285
71	85.144	-1.150	-0.278	-1.160	-0.280
72	85.387	-1.130	-0.274	-1.130	-0.274
73	85.631	-1.110	-0.271	-1.100	-0.269
74	85.877	-1.100	-0.265	-1.080	-0.262
75	86.125	-1.070	-0.256	-1.060	-0.254
76	86.375	-1.040	-0.244	-1.040	-0.244
77	86.626	-1.010	-0.232	-1.030	-0.234
78	86.880	-0.984	-0.222	-1.010	-0.226
79	87.134	-0.967	-0.217	-0.982	-0.219
80	87.390	-0.954	-0.215	-0.950	-0.214
81	87.648	-0.940	-0.212	-0.919	-0.209
82	87.906	-0.919	-0.206	-0.893	-0.202
83	88.165	-0.885	-0.194	-0.881	-0.194
84	88.426	-0.855	-0.183	-0.865	-0.184
85	88.687	-0.837	-0.173	-0.838	-0.174
86	88.949	-0.811	-0.164	-0.817	-0.165
87	89.211	-0.786	-0.156	-0.796	-0.157
88	89.474	-0.769	-0.150	-0.765	-0.149
89	89.737	-0.748	-0.143	-0.740	-0.141
90	90.000	-0.722	-0.134	-0.719	-0.134
91	90.263	-0.700	-0.125	-0.694	-0.124
92	90.526	-0.675	-0.115	-0.672	-0.115
93	90.789	-0.645	-0.105	-0.654	-0.106
94	91.051	-0.624	-0.096	-0.628	-0.097
95	91.313	-0.604	-0.088	-0.600	-0.088
96	91.574	-0.578	-0.080	-0.578	-0.079
97	91.835	-0.554	-0.071	-0.554	-0.071
98	92.094	-0.531	-0.062	-0.529	-0.062
99	92.352	-0.509	-0.054	-0.503	-0.053
100	92.610	-0.483	-0.044	-0.482	-0.044
101	92.866	-0.456	-0.034	-0.460	-0.034
102	93.120	-0.433	-0.025	-0.435	-0.025
103	93.374	-0.408	-0.016	-0.412	-0.017
104	93.625	-0.385	-0.008	-0.386	-0.008

105	93.875	-0.365	0.000	-0.358	0.001
106	94.123	-0.339	0.009	-0.336	0.010
107	94.369	-0.312	0.019	-0.315	0.018
108	94.613	-0.288	0.028	-0.290	0.027
109	94.856	-0.265	0.036	-0.265	0.036
110	95.095	-0.241	0.045	-0.241	0.045
111	95.333	-0.217	0.053	-0.216	0.053
112	95.568	-0.192	0.062	-0.193	0.062
113	95.801	-0.168	0.070	-0.168	0.071
114	96.032	-0.144	0.079	-0.145	0.079
115	96.260	-0.119	0.087	-0.121	0.087
116	96.485	-0.096	0.096	-0.096	0.096
117	96.708	-0.072	0.104	-0.072	0.104
118	96.928	-0.049	0.112	-0.047	0.112
119	97.146	-0.024	0.120	-0.024	0.120
120	97.360	-0.012	0.125	-0.012	0.125

TABLE 6.16 EFFECT ON OFFSET PARAMETER *A* =20m ON STRESSES (Numerical analysis) Uniform Thickness, b/a=2.694

Y (m)	ϕ	Stresses at Inner Surface		Stresses at Outer Surface	
		σ_ϕ (N/mm^2)	σ_θ (N/mm^2)	σ_ϕ (N/mm^2)	σ_θ (N/mm^2)
0	74.561	-2.140	-0.334	-2.810	-0.433
1	74.634	-2.260	-0.376	-2.670	-0.435
2	74.709	-2.440	-0.462	-2.460	-0.461
3	74.786	-2.510	-0.538	-2.360	-0.511
4	74.864	-2.520	-0.591	-2.320	-0.560
5	74.944	-2.490	-0.621	-2.320	-0.595
6	75.025	-2.450	-0.633	-2.330	-0.615
7	75.107	-2.410	-0.633	-2.330	-0.621
8	75.191	-2.370	-0.624	-2.340	-0.620
9	75.277	-2.320	-0.612	-2.360	-0.617
10	75.365	-2.310	-0.606	-2.340	-0.610
11	75.454	-2.310	-0.606	-2.300	-0.603
12	75.545	-2.290	-0.600	-2.290	-0.600
13	75.638	-2.260	-0.595	-2.280	-0.598
14	75.733	-2.250	-0.594	-2.260	-0.594
15	75.829	-2.250	-0.593	-2.230	-0.591
16	75.928	-2.220	-0.590	-2.230	-0.591
17	76.028	-2.200	-0.588	-2.210	-0.589
18	76.130	-2.190	-0.588	-2.190	-0.587
19	76.234	-2.180	-0.587	-2.170	-0.586
20	76.341	-2.160	-0.585	-2.150	-0.584
21	76.449	-2.140	-0.583	-2.140	-0.583
22	76.560	-2.120	-0.581	-2.120	-0.580
23	76.672	-2.110	-0.580	-2.100	-0.577
24	76.787	-2.090	-0.575	-2.080	-0.573
25	76.904	-2.060	-0.569	-2.070	-0.570
26	77.023	-2.050	-0.566	-2.050	-0.566
27	77.145	-2.030	-0.562	-2.040	-0.562
28	77.269	-2.010	-0.559	-2.020	-0.559
29	77.395	-1.990	-0.556	-2.000	-0.557
30	77.524	-1.980	-0.556	-1.980	-0.555
31	77.655	-1.980	-0.556	-1.950	-0.551
32	77.788	-1.950	-0.550	-1.940	-0.549
33	77.924	-1.910	-0.543	-1.940	-0.547
34	78.063	-1.900	-0.541	-1.910	-0.543
35	78.204	-1.890	-0.541	-1.890	-0.541
36	78.348	-1.880	-0.542	-1.860	-0.539
37	78.494	-1.870	-0.541	-1.830	-0.536
38	78.643	-1.830	-0.533	-1.830	-0.533
39	78.795	-1.800	-0.526	-1.830	-0.529
40	78.950	-1.790	-0.523	-1.800	-0.524
41	79.107	-1.780	-0.522	-1.770	-0.520
42	79.267	-1.760	-0.519	-1.750	-0.517
43	79.430	-1.740	-0.514	-1.730	-0.513
44	79.596	-1.720	-0.508	-1.720	-0.508
45	79.764	-1.690	-0.503	-1.700	-0.503
46	79.935	-1.670	-0.498	-1.680	-0.499

47	80.110	-1.660	-0.495	-1.660	-0.494
48	80.287	-1.640	-0.491	-1.640	-0.491
49	80.467	-1.610	-0.486	-1.620	-0.488
50	80.650	-1.610	-0.485	-1.590	-0.482
51	80.836	-1.590	-0.480	-1.570	-0.478
52	81.025	-1.560	-0.473	-1.560	-0.473
53	81.216	-1.540	-0.467	-1.540	-0.467
54	81.411	-1.520	-0.461	-1.520	-0.462
55	81.609	-1.490	-0.456	-1.500	-0.456
56	81.809	-1.470	-0.451	-1.480	-0.451
57	82.012	-1.460	-0.447	-1.450	-0.446
58	82.219	-1.440	-0.442	-1.430	-0.440
59	82.428	-1.410	-0.435	-1.410	-0.435
60	82.640	-1.390	-0.428	-1.390	-0.429
61	82.854	-1.370	-0.422	-1.370	-0.422
62	83.072	-1.360	-0.417	-1.340	-0.415
63	83.292	-1.330	-0.409	-1.320	-0.408
64	83.515	-1.310	-0.400	-1.310	-0.400
65	83.740	-1.280	-0.391	-1.290	-0.393
66	83.968	-1.260	-0.385	-1.270	-0.385
67	84.199	-1.250	-0.379	-1.240	-0.378
68	84.432	-1.220	-0.371	-1.220	-0.371
69	84.667	-1.200	-0.364	-1.200	-0.363
70	84.905	-1.180	-0.356	-1.180	-0.356
71	85.144	-1.150	-0.348	-1.160	-0.349
72	85.387	-1.130	-0.342	-1.130	-0.342
73	85.631	-1.120	-0.337	-1.100	-0.334
74	85.877	-1.100	-0.329	-1.080	-0.326
75	86.125	-1.070	-0.318	-1.060	-0.315
76	86.375	-1.040	-0.305	-1.040	-0.304
77	86.626	-1.010	-0.290	-1.030	-0.293
78	86.880	-0.981	-0.278	-1.010	-0.283
79	87.134	-0.964	-0.271	-0.983	-0.274
80	87.390	-0.953	-0.267	-0.948	-0.267
81	87.648	-0.939	-0.263	-0.916	-0.259
82	87.906	-0.919	-0.255	-0.890	-0.250
83	88.165	-0.885	-0.242	-0.878	-0.241
84	88.426	-0.854	-0.228	-0.863	-0.229
85	88.687	-0.834	-0.217	-0.836	-0.217
86	88.949	-0.808	-0.205	-0.815	-0.206
87	89.211	-0.783	-0.194	-0.794	-0.196
88	89.474	-0.767	-0.186	-0.763	-0.186
89	89.737	-0.746	-0.177	-0.737	-0.176
90	90.000	-0.720	-0.167	-0.716	-0.166
91	90.263	-0.698	-0.156	-0.691	-0.155
92	90.526	-0.673	-0.144	-0.669	-0.143
93	90.789	-0.643	-0.131	-0.651	-0.132
94	91.051	-0.621	-0.120	-0.626	-0.121
95	91.313	-0.601	-0.110	-0.598	-0.109
96	91.574	-0.576	-0.099	-0.576	-0.099
97	91.835	-0.552	-0.088	-0.552	-0.088
98	92.094	-0.529	-0.077	-0.527	-0.077
99	92.352	-0.507	-0.066	-0.501	-0.065
100	92.610	-0.481	-0.054	-0.480	-0.054
101	92.866	-0.454	-0.042	-0.459	-0.043
102	93.120	-0.431	-0.031	-0.434	-0.031

103	93.374	-0.407	-0.020	-0.410	-0.020
104	93.625	-0.384	-0.010	-0.385	-0.010
105	93.875	-0.364	0.000	-0.357	0.001
106	94.123	-0.338	0.012	-0.335	0.012
107	94.369	-0.311	0.024	-0.314	0.023
108	94.613	-0.287	0.035	-0.290	0.034
109	94.856	-0.264	0.045	-0.265	0.045
110	95.095	-0.240	0.056	-0.240	0.056
111	95.333	-0.216	0.066	-0.216	0.067
112	95.568	-0.192	0.077	-0.193	0.077
113	95.801	-0.168	0.088	-0.168	0.088
114	96.032	-0.143	0.098	-0.144	0.098
115	96.260	-0.119	0.109	-0.121	0.108
116	96.485	-0.096	0.119	-0.096	0.119
117	96.708	-0.072	0.128	-0.072	0.129
118	96.928	-0.049	0.139	-0.047	0.139
119	97.146	-0.025	0.149	-0.023	0.149
120	97.360	-0.012	0.154	-0.012	0.154

TABLE 6.17 EFFECT ON OFFSET PARAMETER *A* =40m ON STRESSES (Numerical analysis) Uniform Thickness, b/a=2.694

Y (m)	ϕ	Stresses at inner Surface		Stresses at Outer Surface	
		σ_ϕ (N/mm^2)	σ_θ (N/mm^2)	σ_ϕ (N/mm^2)	σ_θ (N/mm^2)
0	74.561	-2.010	-0.321	-3.160	-0.493
1	74.634	-2.200	-0.386	-2.950	-0.495
2	74.709	-2.500	-0.518	-2.620	-0.530
3	74.786	-2.650	-0.642	-2.440	-0.606
4	74.864	-2.690	-0.738	-2.360	-0.685
5	74.944	-2.670	-0.801	-2.350	-0.750
6	75.025	-2.620	-0.835	-2.360	-0.795
7	75.107	-2.570	-0.849	-2.370	-0.819
8	75.191	-2.510	-0.845	-2.400	-0.829
9	75.277	-2.440	-0.833	-2.430	-0.832
10	75.365	-2.410	-0.825	-2.420	-0.826
11	75.454	-2.410	-0.820	-2.390	-0.818
12	75.545	-2.380	-0.811	-2.380	-0.812
13	75.638	-2.340	-0.803	-2.380	-0.808
14	75.733	-2.330	-0.800	-2.350	-0.802
15	75.829	-2.330	-0.799	-2.320	-0.798
16	75.928	-2.300	-0.795	-2.310	-0.797
17	76.028	-2.280	-0.794	-2.290	-0.795
18	76.130	-2.270	-0.794	-2.260	-0.793
19	76.234	-2.250	-0.794	-2.240	-0.792
20	76.341	-2.230	-0.792	-2.230	-0.791
21	76.449	-2.210	-0.789	-2.210	-0.789
22	76.560	-2.190	-0.787	-2.190	-0.786
23	76.672	-2.180	-0.786	-2.160	-0.782
24	76.787	-2.160	-0.781	-2.140	-0.779
25	76.904	-2.130	-0.774	-2.140	-0.776
26	77.023	-2.110	-0.770	-2.110	-0.771
27	77.145	-2.090	-0.766	-2.100	-0.767
28	77.269	-2.070	-0.762	-2.080	-0.763
29	77.395	-2.050	-0.759	-2.060	-0.761
30	77.524	-2.030	-0.758	-2.030	-0.758
31	77.655	-2.030	-0.758	-2.000	-0.753
32	77.788	-2.000	-0.752	-1.990	-0.751
33	77.924	-1.960	-0.745	-1.980	-0.749
34	78.063	-1.940	-0.743	-1.960	-0.745
35	78.204	-1.930	-0.742	-1.930	-0.742
36	78.348	-1.920	-0.742	-1.900	-0.739
37	78.494	-1.910	-0.740	-1.870	-0.735
38	78.643	-1.880	-0.732	-1.870	-0.731
39	78.795	-1.840	-0.724	-1.860	-0.728
40	78.950	-1.820	-0.720	-1.840	-0.722
41	79.107	-1.810	-0.718	-1.800	-0.716
42	79.267	-1.800	-0.714	-1.780	-0.712
43	79.430	-1.770	-0.708	-1.760	-0.707
44	79.596	-1.750	-0.701	-1.750	-0.701
45	79.764	-1.720	-0.694	-1.730	-0.695
46	79.935	-1.700	-0.689	-1.710	-0.690
47	80.110	-1.690	-0.684	-1.680	-0.684

48	80.287	-1.660	-0.679	-1.660	-0.679
49	80.467	-1.640	-0.673	-1.640	-0.674
50	80.650	-1.630	-0.670	-1.610	-0.667
51	80.836	-1.610	-0.664	-1.590	-0.661
52	81.025	-1.580	-0.656	-1.580	-0.656
53	81.216	-1.560	-0.648	-1.550	-0.648
54	81.411	-1.530	-0.641	-1.530	-0.641
55	81.609	-1.510	-0.633	-1.510	-0.634
56	81.809	-1.490	-0.626	-1.490	-0.627
57	82.012	-1.470	-0.620	-1.460	-0.619
58	82.219	-1.450	-0.613	-1.440	-0.612
59	82.428	-1.430	-0.605	-1.420	-0.604
60	82.640	-1.400	-0.596	-1.400	-0.596
61	82.854	-1.380	-0.587	-1.380	-0.587
62	83.072	-1.360	-0.579	-1.350	-0.577
63	83.292	-1.340	-0.569	-1.330	-0.568
64	83.515	-1.310	-0.558	-1.310	-0.558
65	83.740	-1.280	-0.546	-1.300	-0.548
66	83.968	-1.270	-0.537	-1.270	-0.537
67	84.199	-1.250	-0.528	-1.240	-0.527
68	84.432	-1.220	-0.518	-1.220	-0.518
69	84.667	-1.200	-0.508	-1.200	-0.507
70	84.905	-1.180	-0.497	-1.180	-0.497
71	85.144	-1.150	-0.486	-1.160	-0.487
72	85.387	-1.130	-0.477	-1.130	-0.477
73	85.631	-1.120	-0.468	-1.100	-0.465
74	85.877	-1.100	-0.457	-1.070	-0.453
75	86.125	-1.070	-0.442	-1.050	-0.439
76	86.375	-1.040	-0.425	-1.040	-0.424
77	86.626	-1.010	-0.407	-1.030	-0.410
78	86.880	-0.977	-0.392	-1.010	-0.397
79	87.134	-0.961	-0.381	-0.983	-0.384
80	87.390	-0.951	-0.373	-0.947	-0.373
81	87.648	-0.939	-0.365	-0.912	-0.361
82	87.906	-0.920	-0.353	-0.885	-0.348
83	88.165	-0.885	-0.336	-0.874	-0.335
84	88.426	-0.853	-0.319	-0.859	-0.320
85	88.687	-0.832	-0.304	-0.833	-0.304
86	88.949	-0.805	-0.288	-0.813	-0.289
87	89.211	-0.780	-0.273	-0.792	-0.275
88	89.474	-0.764	-0.260	-0.760	-0.259
89	89.737	-0.744	-0.246	-0.734	-0.245
90	90.000	-0.718	-0.231	-0.712	-0.231
91	90.263	-0.696	-0.216	-0.687	-0.215
92	90.526	-0.670	-0.200	-0.666	-0.199
93	90.789	-0.640	-0.183	-0.649	-0.184
94	91.051	-0.618	-0.168	-0.623	-0.168
95	91.313	-0.598	-0.153	-0.596	-0.153
96	91.574	-0.574	-0.138	-0.573	-0.137
97	91.835	-0.550	-0.122	-0.549	-0.122
98	92.094	-0.527	-0.107	-0.525	-0.107
99	92.352	-0.505	-0.092	-0.499	-0.091
100	92.610	-0.479	-0.075	-0.478	-0.075
101	92.866	-0.452	-0.059	-0.457	-0.059
102	93.120	-0.429	-0.043	-0.433	-0.043
103	93.374	-0.405	-0.028	-0.409	-0.028

104	93.625	-0.382	-0.013	-0.384	-0.013
105	93.875	-0.362	0.001	-0.356	0.003
106	94.123	-0.337	0.017	-0.333	0.018
107	94.369	-0.309	0.033	-0.313	0.033
108	94.613	-0.286	0.048	-0.289	0.048
109	94.856	-0.263	0.063	-0.264	0.063
110	95.095	-0.239	0.078	-0.240	0.078
111	95.333	-0.215	0.093	-0.216	0.093
112	95.568	-0.191	0.107	-0.192	0.107
113	95.801	-0.167	0.122	-0.168	0.122
114	96.032	-0.143	0.136	-0.145	0.136
115	96.260	-0.118	0.151	-0.121	0.150
116	96.485	-0.096	0.165	-0.096	0.165
117	96.708	-0.072	0.178	-0.072	0.179
118	96.928	-0.049	0.192	-0.047	0.193
119	97.146	-0.025	0.206	-0.023	0.207
120	97.360	-0.012	0.213	-0.012	0.214

TABLE 6.18 EFFECT OF SCALE ON STRESSES
SCALE FACTOR=0.5 (Numerical analysis)
Uniform Thickness, b/a=2.694

Y (m)	ϕ	Stresses at Inner Surface		Stresses at Outer Surface	
		σ_ϕ (N/mm^2)	σ_θ (N/mm^2)	σ_ϕ (N/mm^2)	σ_θ (N/mm^2)
0	74.561	-1.069	-0.163	-1.184	-0.179
1	74.710	-1.094	-0.173	-1.146	-0.180
2	74.864	-1.120	-0.191	-1.096	-0.187
3	75.025	-1.111	-0.203	-1.081	-0.198
4	75.192	-1.093	-0.206	-1.073	-0.203
5	75.365	-1.075	-0.204	-1.066	-0.202
6	75.546	-1.054	-0.199	-1.061	-0.199
7	75.733	-1.043	-0.196	-1.046	-0.196
8	75.928	-1.037	-0.195	-1.026	-0.193
9	76.131	-1.019	-0.190	-1.018	-0.190
10	76.341	-1.002	-0.186	-1.008	-0.186
11	76.560	-0.989	-0.184	-0.993	-0.184
12	76.787	-0.978	-0.183	-0.977	-0.183
13	77.024	-0.966	-0.183	-0.961	-0.182
14	77.269	-0.953	-0.182	-0.945	-0.181
15	77.524	-0.939	-0.179	-0.930	-0.177
16	77.789	-0.917	-0.172	-0.923	-0.173
17	78.063	-0.900	-0.168	-0.911	-0.170
18	78.348	-0.890	-0.168	-0.890	-0.168
19	78.644	-0.880	-0.169	-0.869	-0.167
20	78.950	-0.861	-0.166	-0.856	-0.165
21	79.267	-0.842	-0.161	-0.844	-0.161
22	79.596	-0.826	-0.158	-0.827	-0.158
23	79.936	-0.811	-0.155	-0.809	-0.155
24	80.287	-0.795	-0.152	-0.791	-0.151
25	80.650	-0.775	-0.148	-0.776	-0.148
26	81.025	-0.758	-0.145	-0.759	-0.145
27	81.411	-0.741	-0.142	-0.740	-0.142
28	81.809	-0.724	-0.139	-0.720	-0.138
29	82.219	-0.706	-0.135	-0.701	-0.134
30	82.640	-0.684	-0.130	-0.685	-0.130
31	83.072	-0.664	-0.125	-0.668	-0.126
32	83.515	-0.647	-0.122	-0.645	-0.122
33	83.968	-0.629	-0.119	-0.623	-0.118
34	84.432	-0.607	-0.114	-0.604	-0.113
35	84.905	-0.586	-0.108	-0.584	-0.107
36	85.387	-0.562	-0.101	-0.566	-0.102
37	85.877	-0.542	-0.097	-0.544	-0.097
38	86.375	-0.524	-0.093	-0.519	-0.092
39	86.880	-0.501	-0.088	-0.498	-0.087
40	87.390	-0.477	-0.081	-0.477	-0.081
41	87.906	-0.454	-0.075	-0.455	-0.075
42	88.426	-0.433	-0.069	-0.431	-0.069
43	88.949	-0.410	-0.063	-0.408	-0.063
44	89.474	-0.385	-0.056	-0.386	-0.056
45	90.000	-0.362	-0.049	-0.363	-0.049
46	90.526	-0.338	-0.043	-0.339	-0.043

47	91.051	-0.316	-0.037	-0.314	-0.037
48	91.574	-0.292	-0.031	-0.290	-0.030
49	92.094	-0.267	-0.024	-0.267	-0.024
50	92.610	-0.242	-0.017	-0.243	-0.017
51	93.120	-0.219	-0.010	-0.218	-0.010
52	93.625	-0.195	-0.003	-0.193	-0.003
53	94.123	-0.169	0.004	-0.170	0.004
54	94.613	-0.144	0.011	-0.146	0.011
55	95.095	-0.121	0.017	-0.121	0.017
56	95.568	-0.097	0.023	-0.096	0.023
57	96.032	-0.072	0.030	-0.072	0.030
58	96.485	-0.049	0.036	-0.048	0.036
59	96.928	-0.024	0.043	-0.024	0.043
60	97.360	-0.012	0.046	-0.012	0.047

TABLE 6.19 EFFECT OF SCALE ON STRESSES
SCALE FACTOR=1.667 (Numerical analysis)
Uniform Thickness, b/a=2.694

Y (m)	ϕ	Stresses at Inner Surface		Stresses at Outer Surface	
		σ_ϕ (N/mm^2)	σ_θ (N/mm^2)	σ_ϕ (N/mm^2)	σ_θ (N/mm^2)
0	74.572	-3.580	-0.540	-3.950	-0.594
1	74.616	-3.640	-0.556	-3.890	-0.591
2	74.661	-3.710	-0.588	-3.790	-0.599
3	74.706	-3.730	-0.624	-3.750	-0.624
4	74.752	-3.770	-0.663	-3.690	-0.648
5	74.798	-3.800	-0.693	-3.630	-0.667
6	74.844	-3.770	-0.701	-3.640	-0.682
7	74.891	-3.720	-0.697	-3.670	-0.689
8	74.939	-3.690	-0.690	-3.670	-0.686
9	74.987	-3.650	-0.680	-3.680	-0.685
10	75.036	-3.630	-0.675	-3.680	-0.682
11	75.086	-3.640	-0.678	-3.640	-0.678
12	75.136	-3.630	-0.680	-3.620	-0.678
13	75.186	-3.620	-0.681	-3.610	-0.677
14	75.237	-3.610	-0.679	-3.590	-0.676
15	75.289	-3.600	-0.676	-3.580	-0.673
16	75.341	-3.580	-0.671	-3.570	-0.670
17	75.394	-3.570	-0.666	-3.560	-0.665
18	75.448	-3.550	-0.660	-3.550	-0.660
19	75.502	-3.540	-0.655	-3.540	-0.656
20	75.557	-3.520	-0.650	-3.530	-0.652
21	75.612	-3.510	-0.647	-3.520	-0.649
22	75.668	-3.490	-0.645	-3.510	-0.647
23	75.725	-3.480	-0.645	-3.490	-0.647
24	75.783	-3.480	-0.648	-3.470	-0.647
25	75.841	-3.480	-0.651	-3.440	-0.645
26	75.899	-3.460	-0.648	-3.430	-0.643
27	75.959	-3.430	-0.641	-3.440	-0.643
28	76.019	-3.400	-0.637	-3.440	-0.642
29	76.080	-3.400	-0.638	-3.420	-0.641
30	76.142	-3.410	-0.644	-3.380	-0.638
31	76.204	-3.420	-0.645	-3.350	-0.634
32	76.267	-3.380	-0.635	-3.360	-0.631
33	76.331	-3.330	-0.621	-3.370	-0.627
34	76.395	-3.310	-0.615	-3.370	-0.623
35	76.460	-3.310	-0.616	-3.340	-0.621
36	76.526	-3.330	-0.624	-3.290	-0.617
37	76.593	-3.320	-0.624	-3.280	-0.616
38	76.661	-3.280	-0.615	-3.290	-0.617
39	76.729	-3.270	-0.612	-3.280	-0.613
40	76.798	-3.250	-0.610	-3.260	-0.611
41	76.868	-3.250	-0.610	-3.240	-0.609
42	76.939	-3.240	-0.610	-3.220	-0.605
43	77.010	-3.220	-0.605	-3.220	-0.604
44	77.083	-3.200	-0.601	-3.210	-0.602
45	77.156	-3.190	-0.599	-3.190	-0.598
46	77.230	-3.160	-0.595	-3.180	-0.598
47	77.305	-3.150	-0.594	-3.170	-0.597

48	77.380	-3.150	-0.598	-3.140	-0.595
49	77.457	-3.150	-0.598	-3.120	-0.594
50	77.534	-3.130	-0.596	-3.100	-0.591
51	77.613	-3.110	-0.589	-3.090	-0.586
52	77.692	-3.080	-0.580	-3.090	-0.581
53	77.772	-3.050	-0.572	-3.090	-0.579
54	77.853	-3.040	-0.571	-3.070	-0.576
55	77.935	-3.060	-0.576	-3.030	-0.572
56	78.018	-3.040	-0.576	-3.010	-0.571
57	78.101	-3.000	-0.569	-3.020	-0.572
58	78.186	-2.990	-0.568	-3.000	-0.569
59	78.272	-2.990	-0.569	-2.970	-0.565
60	78.358	-2.970	-0.565	-2.960	-0.564
61	78.446	-2.960	-0.563	-2.940	-0.560
62	78.534	-2.930	-0.557	-2.940	-0.558
63	78.624	-2.920	-0.553	-2.920	-0.554
64	78.714	-2.920	-0.552	-2.890	-0.548
65	78.805	-2.880	-0.544	-2.900	-0.547
66	78.898	-2.850	-0.540	-2.900	-0.547
67	78.991	-2.870	-0.547	-2.840	-0.542
68	79.085	-2.860	-0.547	-2.820	-0.540
69	79.181	-2.820	-0.539	-2.830	-0.540
70	79.277	-2.800	-0.535	-2.810	-0.537
71	79.374	-2.790	-0.533	-2.800	-0.534
72	79.473	-2.780	-0.532	-2.780	-0.531
73	79.572	-2.770	-0.530	-2.750	-0.527
74	79.672	-2.740	-0.525	-2.740	-0.524
75	79.774	-2.720	-0.520	-2.730	-0.520
76	79.876	-2.710	-0.516	-2.710	-0.515
77	79.980	-2.690	-0.511	-2.700	-0.513
78	80.084	-2.670	-0.509	-2.680	-0.511
79	80.190	-2.670	-0.510	-2.650	-0.507
80	80.296	-2.650	-0.508	-2.630	-0.504
81	80.404	-2.630	-0.503	-2.620	-0.500
82	80.513	-2.610	-0.496	-2.610	-0.496
83	80.622	-2.570	-0.488	-2.610	-0.494
84	80.733	-2.560	-0.488	-2.590	-0.492
85	80.845	-2.570	-0.493	-2.540	-0.489
86	80.958	-2.560	-0.493	-2.520	-0.487
87	81.072	-2.530	-0.487	-2.520	-0.486
88	81.187	-2.500	-0.481	-2.510	-0.482
89	81.303	-2.480	-0.477	-2.490	-0.478
90	81.420	-2.480	-0.474	-2.460	-0.471
91	81.538	-2.460	-0.468	-2.440	-0.466
92	81.657	-2.420	-0.459	-2.440	-0.462
93	81.777	-2.400	-0.453	-2.430	-0.458
94	81.898	-2.380	-0.452	-2.410	-0.455
95	82.020	-2.380	-0.455	-2.370	-0.453
96	82.144	-2.380	-0.456	-2.340	-0.450
97	82.268	-2.350	-0.449	-2.330	-0.448
98	82.393	-2.310	-0.442	-2.330	-0.444
99	82.520	-2.300	-0.438	-2.300	-0.438
100	82.647	-2.290	-0.435	-2.270	-0.433
101	82.775	-2.260	-0.428	-2.270	-0.429
102	82.905	-2.230	-0.422	-2.260	-0.426
103	83.035	-2.230	-0.422	-2.220	-0.420

104	83.166	-2.210	-0.419	-2.200	-0.417
105	83.299	-2.180	-0.413	-2.190	-0.415
106	83.432	-2.180	-0.412	-2.160	-0.409
107	83.566	-2.160	-0.408	-2.130	-0.403
108	83.701	-2.120	-0.397	-2.130	-0.399
109	83.837	-2.090	-0.389	-2.130	-0.395
110	83.974	-2.090	-0.389	-2.090	-0.389
111	84.112	-2.080	-0.389	-2.050	-0.385
112	84.251	-2.050	-0.383	-2.050	-0.383
113	84.391	-2.030	-0.379	-2.020	-0.377
114	84.531	-2.010	-0.373	-2.000	-0.371
115	84.672	-1.970	-0.364	-2.000	-0.367
116	84.815	-1.950	-0.359	-1.980	-0.362
117	84.958	-1.950	-0.358	-1.940	-0.356
118	85.101	-1.930	-0.355	-1.910	-0.352
119	85.246	-1.890	-0.347	-1.910	-0.349
120	85.391	-1.880	-0.344	-1.880	-0.344
121	85.538	-1.870	-0.341	-1.840	-0.337
122	85.684	-1.840	-0.332	-1.840	-0.332
123	85.832	-1.810	-0.323	-1.830	-0.327
124	85.980	-1.800	-0.320	-1.790	-0.319
125	86.129	-1.780	-0.315	-1.770	-0.314
126	86.279	-1.750	-0.308	-1.760	-0.309
127	86.429	-1.730	-0.303	-1.730	-0.304
128	86.580	-1.710	-0.300	-1.710	-0.299
129	86.731	-1.690	-0.295	-1.680	-0.294
130	86.883	-1.660	-0.289	-1.670	-0.290
131	87.035	-1.650	-0.285	-1.640	-0.284
132	87.188	-1.630	-0.280	-1.610	-0.278
133	87.342	-1.600	-0.273	-1.590	-0.272
134	87.496	-1.580	-0.265	-1.570	-0.265
135	87.650	-1.550	-0.257	-1.560	-0.258
136	87.805	-1.530	-0.251	-1.530	-0.251
137	87.960	-1.510	-0.245	-1.510	-0.246
138	88.116	-1.480	-0.240	-1.490	-0.242
139	88.271	-1.470	-0.237	-1.460	-0.236
140	88.428	-1.450	-0.234	-1.430	-0.231
141	88.584	-1.420	-0.227	-1.410	-0.225
142	88.741	-1.390	-0.218	-1.390	-0.218
143	88.898	-1.370	-0.210	-1.370	-0.211
144	89.055	-1.340	-0.202	-1.360	-0.204
145	89.212	-1.320	-0.197	-1.320	-0.197
146	89.369	-1.310	-0.193	-1.290	-0.191
147	89.527	-1.280	-0.185	-1.280	-0.185
148	89.685	-1.250	-0.178	-1.260	-0.179
149	89.842	-1.230	-0.173	-1.230	-0.172
150	90.000	-1.210	-0.167	-1.200	-0.166
151	90.158	-1.180	-0.160	-1.180	-0.160
152	90.315	-1.150	-0.152	-1.170	-0.153
153	90.473	-1.140	-0.146	-1.140	-0.146
154	90.631	-1.120	-0.141	-1.110	-0.139
155	90.788	-1.090	-0.133	-1.090	-0.133
156	90.945	-1.060	-0.125	-1.070	-0.127
157	91.102	-1.040	-0.120	-1.040	-0.120
158	91.259	-1.020	-0.115	-1.020	-0.114
159	91.416	-0.997	-0.109	-0.989	-0.108

160	91.572	-0.977	-0.103	-0.961	-0.101
161	91.729	-0.948	-0.094	-0.942	-0.093
162	91.884	-0.918	-0.085	-0.924	-0.085
163	92.040	-0.895	-0.076	-0.899	-0.077
164	92.195	-0.868	-0.068	-0.878	-0.069
165	92.350	-0.836	-0.061	-0.862	-0.064
166	92.504	-0.808	-0.057	-0.841	-0.062
167	92.658	-0.810	-0.060	-0.791	-0.058
168	92.812	-0.815	-0.062	-0.737	-0.050
169	92.965	-0.762	-0.048	-0.742	-0.045
170	93.117	-0.710	-0.031	-0.745	-0.037
171	93.269	-0.695	-0.023	-0.712	-0.025
172	93.420	-0.676	-0.016	-0.682	-0.017
173	93.571	-0.652	-0.009	-0.657	-0.010
174	93.721	-0.629	-0.004	-0.631	-0.004
175	93.871	-0.608	0.002	-0.603	0.002
176	94.020	-0.583	0.008	-0.580	0.008
177	94.168	-0.554	0.015	-0.560	0.014
178	94.316	-0.532	0.021	-0.533	0.021
179	94.462	-0.513	0.026	-0.504	0.028
180	94.609	-0.484	0.034	-0.484	0.034
181	94.754	-0.458	0.041	-0.462	0.040
182	94.899	-0.437	0.047	-0.434	0.047
183	95.042	-0.412	0.054	-0.410	0.054
184	95.185	-0.384	0.061	-0.389	0.061
185	95.328	-0.360	0.068	-0.365	0.067
186	95.469	-0.339	0.074	-0.337	0.074
187	95.609	-0.314	0.080	-0.313	0.080
188	95.749	-0.289	0.086	-0.290	0.086
189	95.888	-0.267	0.093	-0.264	0.093
190	96.026	-0.241	0.100	-0.241	0.100
191	96.163	-0.214	0.106	-0.219	0.106
192	96.299	-0.191	0.113	-0.194	0.112
193	96.434	-0.169	0.118	-0.167	0.119
194	96.568	-0.145	0.125	-0.144	0.125
195	96.701	-0.120	0.131	-0.121	0.131
196	96.834	-0.096	0.137	-0.096	0.137
197	96.965	-0.072	0.143	-0.072	0.144
198	97.095	-0.048	0.150	-0.048	0.150
199	97.225	-0.024	0.156	-0.024	0.156
200	97.353	-0.012	0.160	-0.012	0.160

SUMMARY OF KEY STRESSES

SELF-WEIGHT LOADING CONSIDERATION

Table 6.3a Uniform Thickness, b/a=2.694

		Meridional stresses			Hoop stresses		
Y (m)	ϕ	$\sigma_{\phi in}$ (N/mm^2)	$\sigma_{\phi out}$ (N/mm^2)	Variance	$\sigma_{\theta in}$ (N/mm^2)	$\sigma_{\theta out}$ (N/mm^2)	Variance
0	74.56	-2.130	-2.380	-0.052	-0.323	-0.360	-0.008
5	74.94	-2.220	-2.180	0.020	-0.418	-0.411	0.003
90	90.00	-0.725	-0.724	0.011	-0.101	-0.101	0.002
106	94.12	-0.341	-0.338	0.011	0.006	0.007	0.001
120	97.36	-0.012	-0.012	0.010	0.095	0.095	0.002

Table 6.4a Uniform Thickness, b/a=2.2

		Meridional stresses			Hoop stresses		
Y (m)	ϕ	$\sigma_{\phi in}$ (N/mm^2)	$\sigma_{\phi out}$ (N/mm^2)	Variance	$\sigma_{\theta in}$ (N/mm^2)	$\sigma_{\theta out}$ (N/mm^2)	Variance
0	69.87	-1.890	-2.490	-0.122	-0.297	-0.386	-0.018
6	70.33	-2.150	-2.100	0.008	-0.571	-0.562	0.002
20	71.70	-1.950	-1.950	-0.002	-0.511	-0.510	0.000
90	90.00	-0.738	-0.732	-0.001	-0.153	-0.153	0.000
105	95.75	-0.369	-0.371	-0.002	0.001	0.001	0.000
120	100.65	-0.013	-0.012	-0.002	0.142	0.143	0.000

Table 6.5a Uniform Thickness, b/a=2.5

		Meridional stresses			Hoop stresses		
Y (m)	ϕ	$\sigma_{\phi in}$ (N/mm^2)	$\sigma_{\phi out}$ (N/mm^2)	Variance	$\sigma_{\theta in}$ (N/mm^2)	$\sigma_{\theta out}$ (N/mm^2)	Variance
0	72.92	-2.050	-2.410	-0.075	-0.314	-0.368	-0.011
6	73.39	-2.180	-2.150	0.003	-0.469	-0.464	0.001
15	74.21	-2.070	-2.030	0.005	-0.441	-0.435	0.001
90	90.00	-0.730	-0.725	-0.002	-0.117	-0.116	0.000
105	94.49	-0.366	-0.365	-0.002	0.000	0.000	0.000
120	98.45	-0.012	-0.012	-0.002	0.110	0.110	0.000

Table 6.6a Uniform Thickness, b/a=2.8

		Meridional stresses			Hoop stresses		
Y (m)	ϕ	$\sigma_{\phi in}$ (N/mm^2)	$\sigma_{\phi out}$ (N/mm^2)		$\sigma_{\theta in}$ (N/mm^2)	$\sigma_{\theta out}$ (N/mm^2)	Variance
0	75.37	-2.180	-2.370	-0.050	-0.328	-0.357	-0.008
6	75.83	-2.230	-2.190	0.008	-0.392	-0.385	0.001
90	90.00	-0.727	-0.719	0.000	-0.093	-0.092	0.000
105	93.59	-0.361	-0.365	-0.003	0.001	0.000	0.000
120	96.85	-0.012	-0.012	-0.002	0.088	0.088	0.000

SELF-WEIGHT LOADING CONSIDERATION

Table 6.7a, Uniform Thickness, b/a=2.694, $\phi_0=100^0$

Y (m)	ϕ	Meridional stresses			Hoop stresses		
		$\sigma_{\phi in}$ (N/mm^2)	$\sigma_{\phi out}$ (N/mm^2)	Variance	$\sigma_{\theta in}$ (N/mm^2)	$\sigma_{\theta out}$ (N/mm^2)	Variance
0	75.00	-2.300	-2.610	-0.050	-0.344	-0.391	-0.008
8	75.64	-2.370	-2.380	0.010	-0.411	-0.413	0.001
85	90.00	-1.090	-1.090	0.012	-0.153	-0.152	0.002
113	96.93	-0.391	-0.403	0.010	0.047	0.046	0.002
120	98.39	-0.221	-0.222	0.012	0.091	0.091	0.001
128.93	100.00	0.001	-0.025	0.007	0.133	0.129	0.002

Table 6.8a, Uniform Thickness, b/a=2.694, $\phi_0=95^0$

Y (m)	ϕ	Meridional stresses			Hoop stresses		
		$\sigma_{\phi in}$ (N/mm^2)	$\sigma_{\phi out}$ (N/mm^2)	Variance	$\sigma_{\theta in}$ (N/mm^2)	$\sigma_{\theta out}$ (N/mm^2)	Variance
0	75.00	-1.810	-2.210	-0.083	-0.271	-0.331	-0.013
6	75.45	-1.970	-1.910	0.032	-0.392	-0.382	0.005
85	90.00	-0.467	-0.466	0.017	-0.065	-0.065	0.003
95	92.61	-0.229	-0.229	0.017	0.001	0.001	0.003
104.9	95.00	-0.007	-0.007	0.017	0.062	0.063	0.002

Table 6.9a, Uniform Thickness, b/a=2.2, $\phi_0=100^0$

Y (m)	ϕ	Meridional stresses			Hoop stresses		
		$\sigma_{\phi in}$ (N/mm^2)	$\sigma_{\phi out}$ (N/mm^2)	Variance	$\sigma_{\theta in}$ (N/mm^2)	$\sigma_{\theta out}$ (N/mm^2)	Variance
0	75.00	-1.260	-1.950	-0.119	-0.189	-0.292	-0.018
6	76.06	-1.560	-1.490	0.033	-0.434	-0.423	0.005
7	76.29	-1.540	-1.490	0.029	-0.431	-0.424	0.004
49	90.00	-0.679	-0.674	0.020	-0.141	-0.140	0.003
63	95.39	-0.337	-0.339	0.018	0.002	0.002	0.003
76.943	100.00	-0.010	-0.009	0.019	0.132	0.133	0.003

Table 6.10a, Uniform Thickness, b/a=2.2, $\phi_0=95^0$

Y (m)	ϕ	Meridional stresses			Hoop stresses		
		$\sigma_{\phi in}$ (N/mm^2)	$\sigma_{\phi out}$ (N/mm^2)	Variance	$\sigma_{\theta in}$ (N/mm^2)	$\sigma_{\theta out}$ (N/mm^2)	Variance
0	75.00	-0.948	-1.640	-0.142	-0.143	-0.246	-0.021
6	76.06	-1.240	-1.170	0.049	-0.390	-0.379	0.007
8	76.51	-1.170	-1.170	0.031	-0.374	-0.374	0.005
56	92.74	-0.142	-0.141	0.031	0.005	0.005	0.005
61.11	95.00	-0.012	-0.011	0.031	0.060	0.060	0.005

SELF-WEIGHT LOADING CONSIDERATION

Table 6.7a, Uniform Thickness, b/a=2.694, $\phi_0=100^0$

Y (m)	ϕ	Meridional stresses			Hoop stresses		
		$\sigma_{\phi in}$ (N/mm^2)	$\sigma_{\phi out}$ (N/mm^2)	Variance	$\sigma_{\theta in}$ (N/mm^2)	$\sigma_{\theta out}$ (N/mm^2)	Variance
0	75.00	-2.300	-2.610	-0.050	-0.344	-0.391	-0.008
8	75.64	-2.370	-2.380	0.010	-0.411	-0.413	0.001
85	90.00	-1.090	-1.090	0.012	-0.153	-0.152	0.002
113	96.93	-0.391	-0.403	0.010	0.047	0.046	0.002
120	98.39	-0.221	-0.222	0.012	0.091	0.091	0.001
128.93	100.00	0.001	-0.025	0.007	0.133	0.129	0.002

Table 6.8a, Uniform Thickness, b/a=2.694, $\phi_0=95^0$

Y (m)	ϕ	Meridional stresses			Hoop stresses		
		$\sigma_{\phi in}$ (N/mm^2)	$\sigma_{\phi out}$ (N/mm^2)	Variance	$\sigma_{\theta in}$ (N/mm^2)	$\sigma_{\theta out}$ (N/mm^2)	Variance
0	75.00	-1.810	-2.210	-0.083	-0.271	-0.331	-0.013
6	75.45	-1.970	-1.910	0.032	-0.392	-0.382	0.005
85	90.00	-0.467	-0.466	0.017	-0.065	-0.065	0.003
95	92.61	-0.229	-0.229	0.017	0.001	0.001	0.003
104.9	95.00	-0.007	-0.007	0.017	0.062	0.063	0.002

Table 6.9a, Uniform Thickness, b/a=2.2, $\phi_0=100^0$

Y (m)	ϕ	Meridional stresses			Hoop stresses		
		$\sigma_{\phi in}$ (N/mm^2)	$\sigma_{\phi out}$ (N/mm^2)	Variance	$\sigma_{\theta in}$ (N/mm^2)	$\sigma_{\theta out}$ (N/mm^2)	Variance
0	75.00	-1.260	-1.950	-0.119	-0.189	-0.292	-0.018
6	76.06	-1.560	-1.490	0.033	-0.434	-0.423	0.005
7	76.29	-1.540	-1.490	0.029	-0.431	-0.424	0.004
49	90.00	-0.679	-0.674	0.020	-0.141	-0.140	0.003
63	95.39	-0.337	-0.339	0.018	0.002	0.002	0.003
76.943	100.00	-0.010	-0.009	0.019	0.132	0.133	0.003

Table 6.10a, Uniform Thickness, b/a=2.2, $\phi_0=95^0$

Y (m)	ϕ	Meridional stresses			Hoop stresses		
		$\sigma_{\phi in}$ (N/mm^2)	$\sigma_{\phi out}$ (N/mm^2)	Variance	$\sigma_{\theta in}$ (N/mm^2)	$\sigma_{\theta out}$ (N/mm^2)	Variance
0	75.00	-0.948	-1.640	-0.142	-0.143	-0.246	-0.021
6	76.06	-1.240	-1.170	0.049	-0.390	-0.379	0.007
8	76.51	-1.170	-1.170	0.031	-0.374	-0.374	0.005
56	92.74	-0.142	-0.141	0.031	0.005	0.005	0.005
61.11	95.00	-0.012	-0.011	0.031	0.060	0.060	0.005

Table 6.15a EFFECT ON OFFSET PARAMETER *A*=10m
Uniform Thickness, b/a=2.694

		Meridional stresses			Hoop stresses		
Y (m)	ϕ	$\sigma_{\phi in}$ (N/mm^2)	$\sigma_{\phi out}$ (N/mm^2)	Variance	$\sigma_{\theta in}$ (N/mm^2)	$\sigma_{\theta out}$ (N/mm^2)	Variance
0	74.56	-2.160	-2.610	-0.091	-0.333	-0.399	-0.013
12	75.55	-2.220	-2.220	0.022	-0.497	-0.496	0.004
90	90.00	-0.722	-0.719	0.023	-0.134	-0.134	0.003
105	93.88	-0.365	-0.358	0.024	0.000	0.001	0.003
120	97.36	-0.012	-0.012	0.022	0.125	0.125	0.003

Table 6.16a OFFSET PARAMETER *A*=20m

		Meridional stresses			Hoop stresses		
Y (m)	ϕ	$\sigma_{\phi in}$ (N/mm^2)	$\sigma_{\phi out}$ (N/mm^2)	Variance	$\sigma_{\theta in}$ (N/mm^2)	$\sigma_{\theta out}$ (N/mm^2)	Variance
0	74.56	-2.140	-2.810	-0.115	-0.334	-0.433	-0.017
7	75.11	-2.410	-2.330	0.035	-0.633	-0.621	0.005
12	75.55	-2.290	-2.290	0.019	-0.600	-0.600	0.003
90	90.00	-0.720	-0.716	0.020	-0.167	-0.166	0.003
105	93.88	-0.364	-0.357	0.021	0.000	0.001	0.003
120	97.36	-0.012	-0.012	0.019	0.154	0.154	0.003

Table 6.17a OFFSET PARAMETER *A*=40m

		Meridional stresses			Hoop stresses		
Y (m)	ϕ	$\sigma_{\phi in}$ (N/mm^2)	$\sigma_{\phi out}$ (N/mm^2)	Variance	$\sigma_{\theta in}$ (N/mm^2)	$\sigma_{\theta out}$ (N/mm^2)	Variance
0	74.56	-2.010	-3.160	-0.241	-0.321	-0.493	-0.036
7	75.11	-2.570	-2.370	0.097	-0.849	-0.819	0.015
90	90.00	-0.718	-0.712	0.048	-0.231	-0.231	0.007
105	93.88	-0.362	-0.356	0.048	0.001	0.003	0.007
120	97.36	-0.012	-0.012	0.047	0.213	0.214	0.007

Table 6.18a EFFECT ON SCALE, i.e. Scale Factor=0.5

		Meridional stresses			Hoop stresses		
Y (m)	ϕ	$\sigma_{\phi in}$ (N/mm^2)	$\sigma_{\phi out}$ (N/mm^2)	Variance	$\sigma_{\theta in}$ (N/mm^2)	$\sigma_{\theta out}$ (N/mm^2)	Variance
0	74.56	-1.069	-1.184	-0.024	-0.163	-0.179	-0.003
4	75.19	-1.093	-1.073	0.010	-0.206	-0.203	0.002
45	90.00	-0.362	-0.363	0.005	-0.049	-0.049	0.001
53	94.12	-0.169	-0.170	0.005	0.004	0.004	0.001
60	97.36	-0.012	-0.012	0.005	0.046	0.047	0.001

Table 6.19a EFFECT ON SCALE, i.e. Scale Factor=1.667

		Meridional stresses			Hoop stresses		
Y (m)	ϕ	$\sigma_{\phi in}$ (N/mm^2)	$\sigma_{\phi out}$ (N/mm^2)	Variance	$\sigma_{\theta in}$ (N/mm^2)	$\sigma_{\theta out}$ (N/mm^2)	Variance
0	74.57	-3.580	-3.950	-0.081	-0.540	-0.594	-0.012
6	74.84	-3.770	-3.640	0.044	-0.701	-0.682	0.006
150	90.00	-1.210	-1.200	0.014	-0.167	-0.166	0.002
175	93.87	-0.608	-0.603	0.012	0.002	0.002	0.002
200	97.35	-0.012	-0.012	0.011	0.160	0.160	0.002

APPENDIX A2

ABAQUS INPUT DECK

```
*HEADING
ANALYSE SELF-WEIGHT STRESS OF COOLING TOWER
*PREPRINT, ECHO=YES, HISTORY=YES, MODEL=YES
**----------------------------------------
*NODE, nset=tower
 95, 44.901, -90
 96, 44.625, -89
 97, 44.351, -88
 98, 44.078, -87
 99, 43.807, -86
100, 43.537, -85
101, 43.269, -84
102, 43.002, -83
103, 42.737, -82
104, 42.474, -81
105, 42.212, -80
106, 41.951, -79
107, 41.693, -78
108, 41.436, -77
109, 41.181, -76
110, 40.927, -75
111, 40.676, -74
112, 40.426, -73
113, 40.178, -72
114, 39.932, -71
115, 39.688, -70
116, 39.446, -69
117, 39.206, -68
118, 38.968, -67
119, 38.732, -66
120, 38.499, -65
121, 38.267, -64
122, 38.038, -63
123, 37.811, -62
124, 37.586, -61
125, 37.364, -60
126, 37.143, -59
127, 36.926, -58
128, 36.711, -57
129, 36.498, -56
130, 36.288, -55
131, 36.080, -54
132, 35.875, -53
133, 35.673, -52
134, 35.474, -51
135, 35.277, -50
```

136, 35.083, -49
137, 34.892, -48
138, 34.704, -47
139, 34.519, -46
140, 34.337, -45
141, 34.158, -44
142, 33.982, -43
143, 33.809, -42
144, 33.640, -41
145, 33.473, -40
146, 33.310, -39
147, 33.151, -38
148, 32.994, -37
149, 32.842, -36
150, 32.692, -35
151, 32.547, -34
152, 32.404, -33
153, 32.266, -32
154, 32.131, -31
155, 32.000, -30
156, 31.873, -29
157, 31.749, -28
158, 31.630, -27
159, 31.514, -26
160, 31.403, -25
161, 31.295, -24
162, 31.191, -23
163, 31.092, -22
164, 30.996, -21
165, 30.905, -20
166, 30.818, -19
167, 30.735, -18
168, 30.656, -17
169, 30.582, -16
170, 30.512, -15
171, 30.447, -14
172, 30.386, -13
173, 30.330, -12
174, 30.277, -11
175, 30.229, -10
176, 30.185, -9
177, 30.146, -8
178, 30.112, -7
179, 30.083, -6
180, 30.057, -5
181, 30.037, -4

```
182, 30.021, -3
183, 30.009, -2
184, 30.002, -1
185, 30.000, 0
186, 30.002, 1
187, 30.009, 2
188, 30.021, 3
189, 30.037, 4
190, 30.057, 5
191, 30.083, 6
192, 30.112, 7
193, 30.147, 8
194, 30.185, 9
195, 30.229, 10
196, 30.277, 11
197, 30.329, 12
198, 30.386, 13
199, 30.447, 14
200, 30.512, 15
201, 30.582, 16
202, 30.657, 17
203, 30.735, 18
204, 30.818, 19
205, 30.905, 20
206, 30.996, 21
207, 31.092, 22
208, 31.191, 23
209, 31.295, 24
210, 31.403, 25
211, 31.514, 26
212, 31.630, 27
213, 31.749, 28
214, 31.873, 29
215, 32.000, 30
**nset, nset=tester
*NODAL THICKNESS
tower, 0.150
*ELEMENT, TYPE=SAX1,elset=tower
1, 95, 96
*ELGEN, ELSET=tower
1, 120, 1, 1
**elset, elset=tester
**34,35
**----------------------------------------
*SHELL SECTION, ELSET=tower, MATERIAL=CONCRETE
0.150,
```

```
*MATERIAL, NAME=CONCRETE
*DENSITY
2400
*ELASTIC
28E9, 0.15
**----------------------------------------
**Constraints
*BOUNDARY
95, encastre
**OUTER-EXL, XSYMM
**OUTER-L, XSYMM
**
**Analysis steps
*STEP
*STATIC
1.0,1.0
*restart,write,overlay
*DLOAD
tower,grav,9.81,0,-1,0
*OUTPUT, FIELD, VARIABLE=PRESELECT, FREQ=1
*OUTPUT, HISTORY, FREQ=1
*ELEMENT OUTPUT,elset=tower
S,E
*EL PRINT,FREQ=1, ELSET=tower, position=averaged at nodes
s,
**FILE OUTPUT, NUMBER INTERVAL=10, TIME MARKS=YES
**EL FILE
*END STEP
**
```

APPENDIX A3

CONTOUR STRESS PLOTS

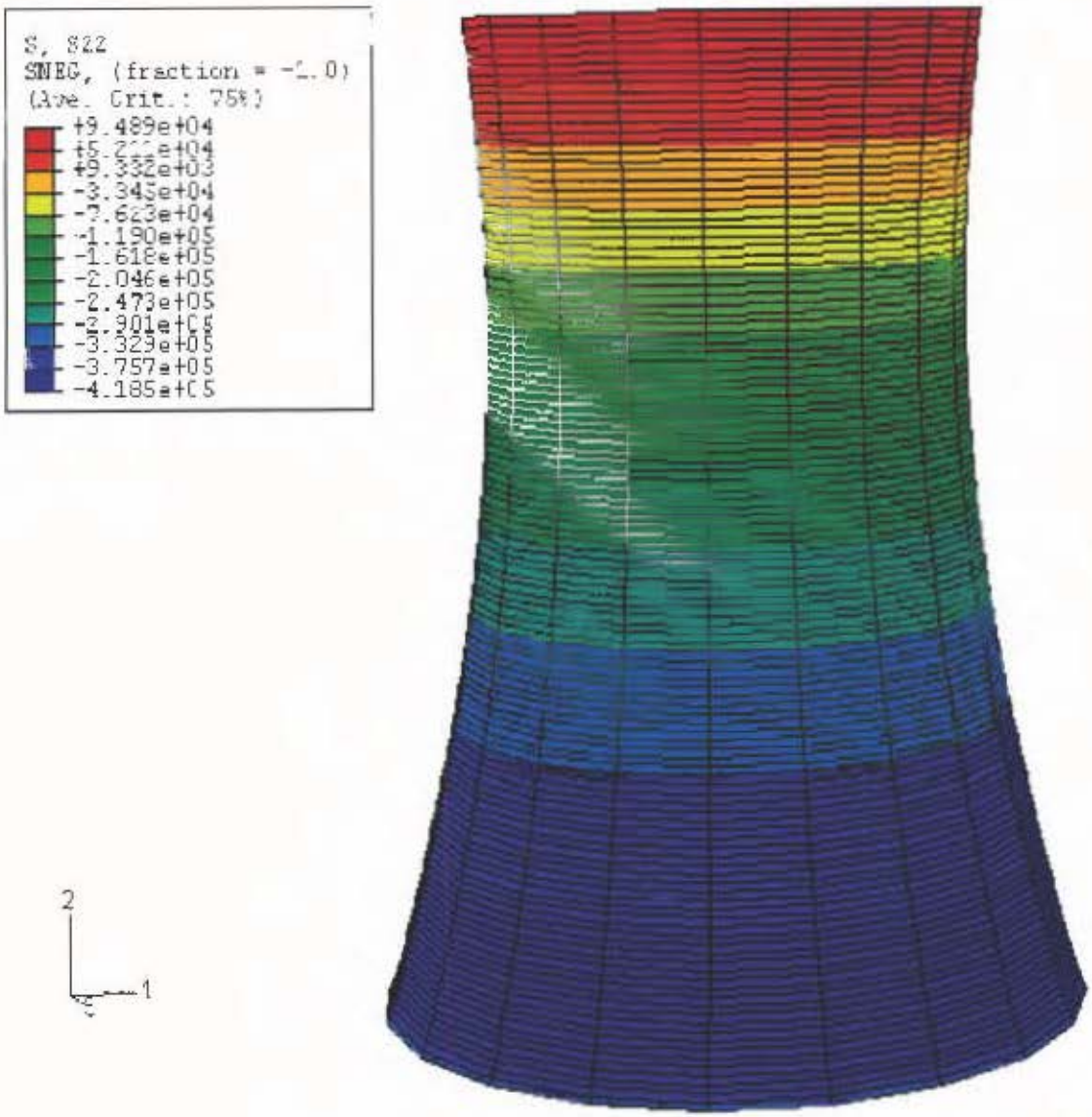

Fig. A3.1 Contour plot for hoop stress

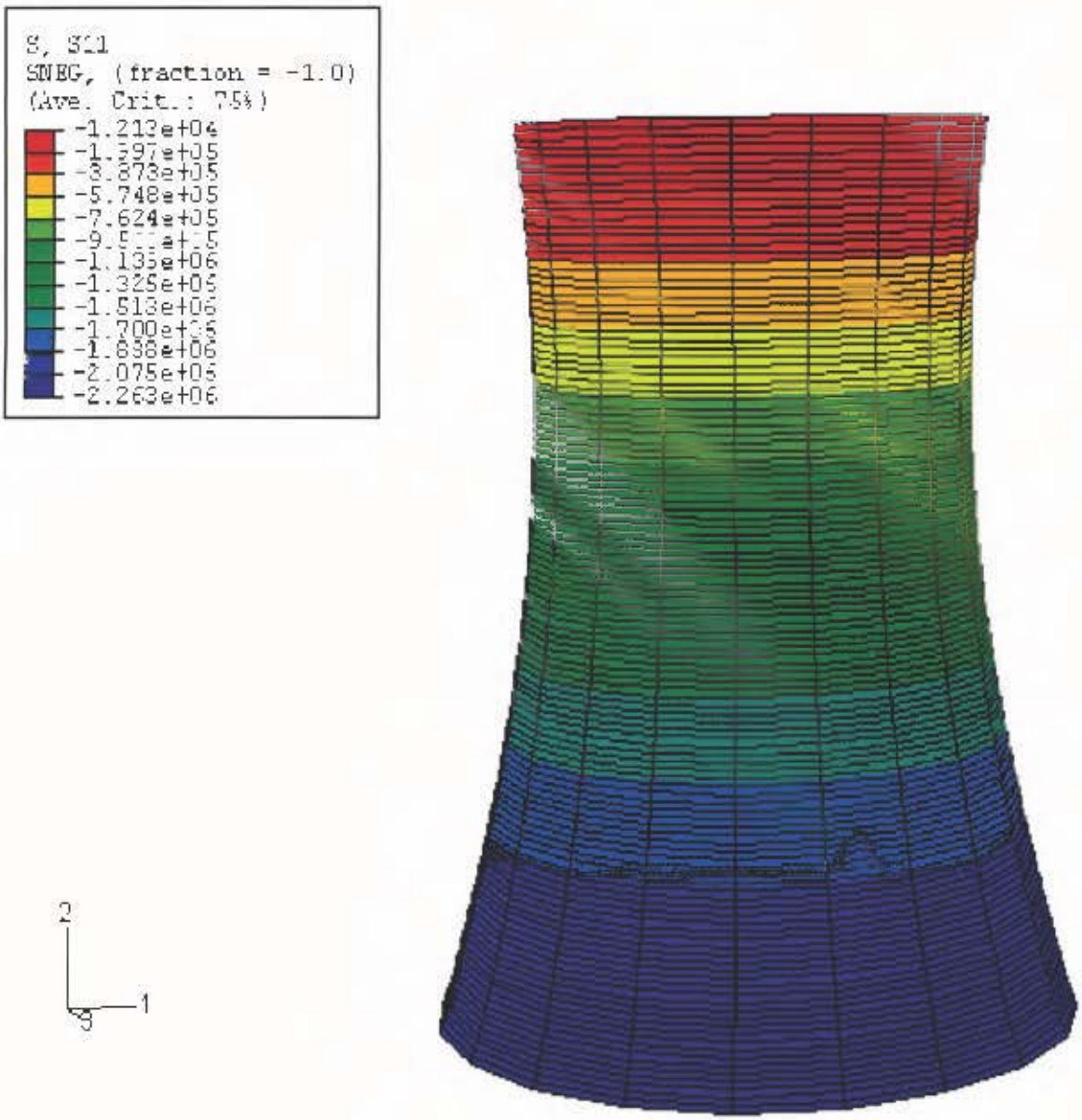

Fig. A3.2 Contour plot for meridional stress